ELECTRICAL AND COMPUTER ENGINEERING
DEPARTMENT

CLEMSON UNIVERSITY

CLEMSON, SC 29634-0915

IN-47-CR
1104

TR-051190-3570P

ANALYSIS AND IMPROVED DESIGN CONSIDERATIONS FOR AIRBORNE PULSE DOPPLER RADAR SIGNAL PROCESSING IN THE DETECTION OF HAZARDOUS WINDSHEAR

by

Jonggil Lee

Radar Systems Laboratory
Technical Report No. 12

Analysis and Improved Design Considerations for Airborne Pulse Doppler Radar Signal Processing in the Detection Of Hazardous Windshear

by

Jonggil Lee

Technical Report #12
May 11, 1990

Radar Systems Laboratory
Electrical and Computer Engineering Department
Clemson University
Clemson, SC 29634-0915

Windshear Detection Radar Signal Processing Studies
Grant NAG-1-928
National Aeronautics and Space Administration
Langley Research Center
Hampton, VA 23665

ABSTRACT

High resolution windspeed profile measurements are needed to provide reliable detection of hazardous low-altitude windshear with an airborne pulse Doppler radar. the system phase noise in a Doppler weather radar may degrade the spectrum moment estimation quality and the clutter cancellation capability which are important in windshear detection. Also the bias due to weather return Doppler spectrum skewness may cause large errors in pulse pair spectral parameter estimates. These effects are analyzed for the improvement of an airborne Doppler weather radar signal processing design. This dissertation also presents a method for the direct measurement of windspeed gradient using low pulse repitition frequency (PRF) radar. This spatial gradient is essential in obtaining the windshear hazard index. As an alternative the modified Prony method is suggested as a spectrum mode estimator for both the clutter and weather signal. Estimation of Doppler spectrum modes may provide the desired windshear hazard information without the need of any preliminary processing requirement such as clutter filtering. The results obtained by processing a NASA simulation model output support consideration of mode identification as one component of a windshear detection algorithm.

ACKNOWLEDGEMENTS

I would like to acknowledge my respect for and give special thanks to my advisor, Dr. Ernest G. Baxa, Jr., for his encouragement and immeasurable support. I also want to express my gratitude to Dr. C. W. Ulbrich, Dr. J. J. Komo, and Dr. R. W. Snelsire for their guidance and constructive review of the dissertation. Additionally, I would like to recognize the support of the National Aeronautics and Space Administration under grant No. NAG-1-928.

I would like to thank my parents for their unending support and sacrifice. Finally, I would like to express my appreciation to my wife for her unfaltering support.

TABLE OF CONTENTS

Table of Contents (Continued)

LIST OF TABLES

LIST OF FIGURES

List of Figures (Continued)

List of Figures (Continued)

CHAPTER I

INTRODUCTION

Doppler Weather Radar

Radar is considered to have a great potential as a remote sensing device, but ordinary radar can not see what the winds are doing. Only radars using the Doppler frequency shift can show the wind speed and its direction. These radars are called Doppler radars. Basically there are two different types of Doppler radars, i.e., a continuous wave (CW) Doppler radar and a pulse Doppler radar. The pulse Doppler radar has an advantage over the CW radar in that the detection performance is not limited by transmitter leakage or by signals reflected from nearby clutter or from the radome. The pulse Doppler radar avoids this difficulty since its receiver is turned off during transmission whereas the CW radar receiver is always on. Previous application of pulse Doppler radar techniques in mapping severe storm reflectivity and velocity structure has been very successful [1],[2]. Since Doppler radars have the capability of seeing dynamic structure of air in low reflectivity conditions [3], these radars are considered useful in the investigation of dry weather situations.

A pulse Doppler weather radar transmits a train of pulses and receives reflected signals as in phase (I) and quadrature phase (Q) components to differentiate receding or

approaching targets. Figure 1 shows a simplified Doppler radar diagram and Figure 2 illustrates the transmitted waveform and the demodulated return signal. Moving targets in the turbulent air illuminated by the radar will shift the transmitted frequency which is well known as the Doppler effect. This Doppler frequency shift which represents the time rate of phase change in the demodulated signal is determined as

$$f_d = \frac{2V_r}{\lambda}$$

where V_r is the radial velocity of target particles and λ is the wavelength of transmitted signal. As seen in Figure 2, the change in signal phase typically is extremely small within a pulse duration (e.g., $\tau \approx 1$ μsec, and weather target velocities on the order of tens of m/sec). Hence, target phase shifts are measured over an interpulse period T_s which means that the pulse Doppler radar behaves as a phase sampling device.

From the I,Q data, important information (i.e., mean velocity, spectrum width, reflectivity, etc.) can be extracted using the appropriate radar signal processing techniques. In coherent Doppler radar systems, the accuracy of such information depends on the system phase stability. By coherent it is meant that the phase of transmitted signal is preserved in the reference signal. As seen from Figure 1,

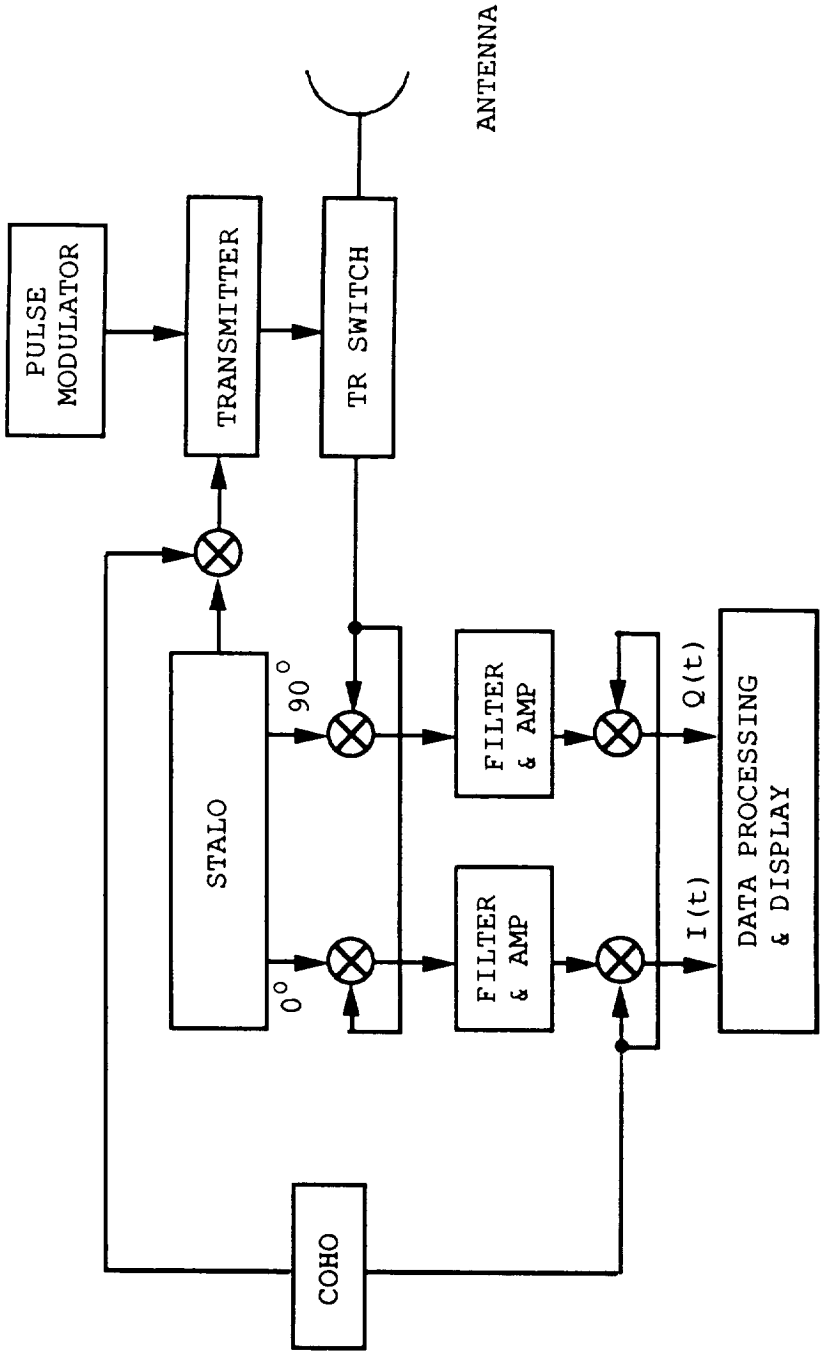

Figure 1. Simplified Block Diagram of a Doppler Radar

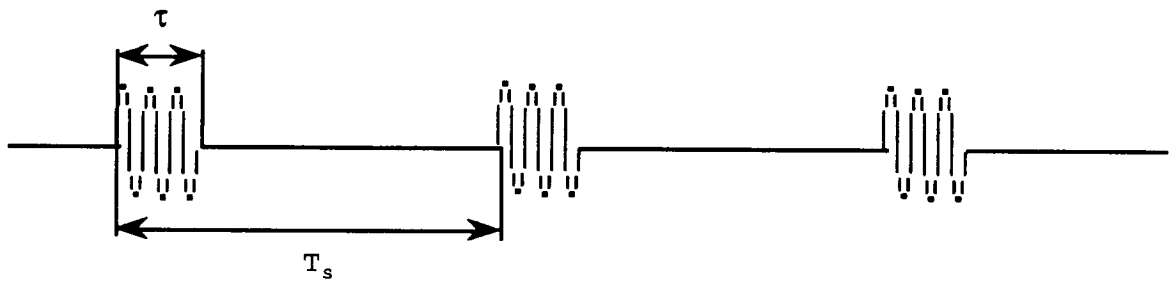

(a)

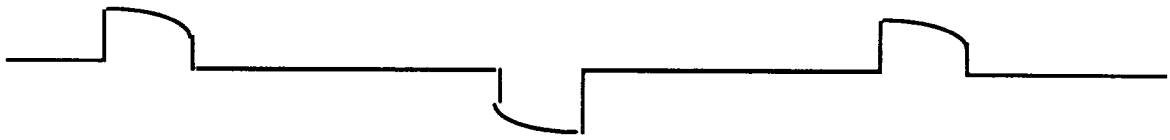

(b)

Figure 2. Doppler Weather Radar Signal

(a) Transmitted Pulse Train
(b) Demodulated Return Signal

usually two highly stable oscillators, i.e, stable local oscillator (STALO) and coherent oscillator (COHO), are needed in the heterodyne detection system to retain the phase coherence. Both oscillators are used to provide a transmitted and reference signal, but the stability problem of the COHO is not so serious compared with that of the STALO since the frequency range of the COHO is several orders of magnitude less than that of the STALO. Therefore it is considered that the STALO plays a major role in the pulse-to-pulse system phase stability problem. Of course, there may be many other factors increasing the system phase noise such as the mismatch problem in obtaining I, Q data [4]. Phase instability factors will degrade Doppler frequency resolution and the spectrum moment estimation quality. This phase noise effect may also severely limit the capability of clutter rejection filtering by spreading the clutter signal over the Doppler signal bandwidth as seen in Figure 3.

Although Doppler radar operation was successful in some other experimental cases [5],[6], future application of Doppler weather radar where higher spatial resolution is needed may require higher Doppler resolution and more accurate estimation of spectral moments [50],[51]. A fundamental problem is quantification of the effect of radar system phase noise on the performance of Doppler weather radar. However, it is really difficult to investigate all phase noise contributing factors separately in a radar system. Thus, a general systematic approach was developed in

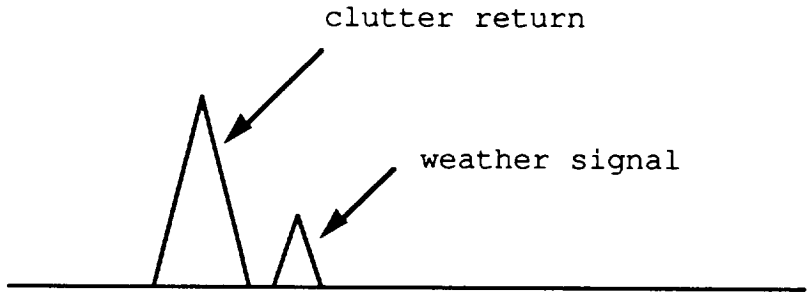

a return spectrum without phase noise

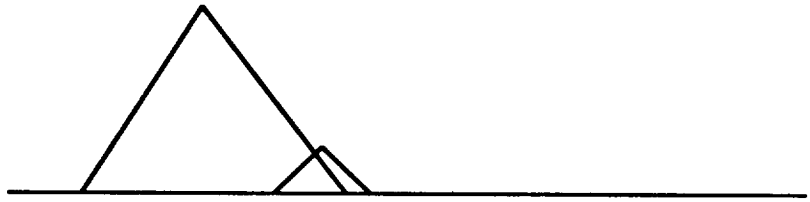

a return spectrum with phase noise

Figure 3. Comparison of Two Doppler Return Spectra Showing Phase Noise Effect

this dissertation to analyze the whole system phase noise effect.

Two popular methods used in radar signal processing for spectral moment estimation are the pulse pair method and the Discrete Fourier Transform (DFT) method. Modern spectral estimation techniques are considered to be much better than classical methods, but they may not be suitable for real time processing. The need to provide computed output as data are obtained from the radar may be essential in some applications such as airborne windshear detection when the look ahead time is limited by the ranging capability of the radar and may be on the order of tens of seconds at most. There are several methods which may be used in the estimation of weather spectral moments [7]. Among them, the most economical is generally considered to be the pulse pair estimator, often called a covariance estimator [8]. Especially in a weather radar system, this pulse pair algorithm is more widely accepted since it is simple to implement and fast enough to process huge amounts of data for real time mapping of the weather situation in an interested area. It is also shown in [52] that the performance of the pulse pair estimator is even better than that of the DFT estimator at low signal-to-noise (SNR) ratios and narrower widths. However, the DFT estimator has some advantages including the absence of bias due to nonsymmetric spectra and the feasibility of eliminating anomalous spectral powers. Also DFT based methods experience finite parameter estimation errors at very large spectral

widths which is not so with pulse pair processing where errors will increase exponentially as spectral widths increase. The other weakness in pulse pair estimation is that the algorithm may yield meaningless results in the case of a multimodal return spectrum while, for example, DFT processing will show all the modes in a return spectrum. In this dissertation these two popular estimators are reevaluated considering the system phase noise effect. Also, bias in the pulse pair estimation, introduced by a skewed spectrum, is analyzed. Alternatives for spectral parameter estimation which may be more robust in the presence of multi-modal spectra are also considered.

Windshear

One of the important potential applications of Doppler weather radar is in a windshear detection system. When the wind abruptly shifts its speed or direction, it can mean deadly difficulty for an airliner particularly at low altitudes such as on approach or take off. This dangerous windshear is frequently caused by microbursts. The term "microburst" was first used by Fujita [10] to describe a relatively small column of downward-rushing air when he was investigating the 1975 crash of an Eastern Airlines Boeing 727 at New York's Kennedy International Airport. Since then, an estimated 26 major aircraft accidents between 1964 and 1985 have been attributed to the microburst. Microbursts are sudden downdrafts of highly turbulent air that may cause very

hazardous windshear conditions. In their presence a plane can first encounter a sharp head wind, then an intense down draft, and finally a strong tail wind, all in a matter of seconds (see Figure 4). These resulting wind currents appear as if they are designed to cause airline crashes. To make matters worse, a recent study by Fujita indicates that microbursts are more common than previously thought and can be created by relatively small harmless-looking rain clouds, not just large thunderstorms. Therefore, it is really difficult to avoid these dangerous situations without any early warning system designed to detect windshear. However, conventional weather radars may not be appropriate for use in this kind of situation.

Since microbursts can occur within a very small geographical scale and the reflectivity of dry microbursts may be very weak, the weather radar for microburst detection, should have high sensitivity and high resolution of both range and Doppler frequency. Currently NASA is developing an airborne Doppler weather radar for the detection of microbursts, the number one killer of U.S. airline passengers. For the same purpose, the terminal Doppler weather radar (TDWR) is also now under development by Raytheon Co. for the Federal Aviation Administration (FAA). The second major function of TDWR is to improve air traffic management through forecasts of windshifts, precipitation and other weather related hazards. However, they need further improvement and verification to be used as a windshear

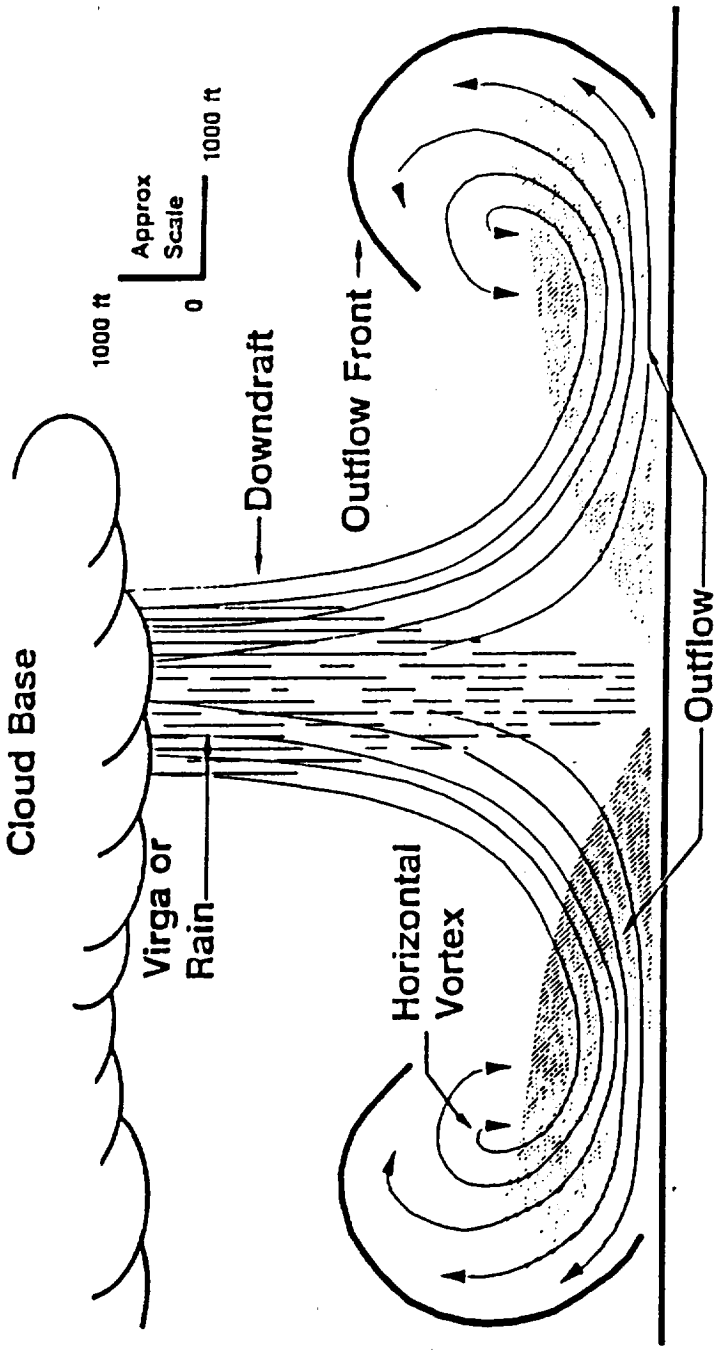

Figure 4. Symmetric Microburst

detection system since undetected microbursts may cause tragic accidents. The other weather radar called NEXRAD (next generation weather radar), which is just beginning to be deployed nationwide, may have the microburst-induced windshear detection capability, but its main purpose is to replace the non-Doppler meteorological radars of the National Weather Service. NEXRAD will operate in the 5-6 GHz frequency range and use a low pulse repetition frequency (PRF) to ensure the coverage of a longer range. It is developed as is TDWR, to have high resolution and sensitivity [51]. Therefore some NEXRAD radars with a suitable windshear detection algorithm will be used in the airport terminal areas on an interim basis until the TDWR is deployed.

In the detection of hazardous windshear conditions, reliable algorithms should be available to process the weather data obtained by a high precision Doppler radar. Considering a typical microburst characteristic, at least two methods are suggested. One is to compute the windshear hazard index which is represented in terms of spatial gradient of windspeed [11]. The other is to recognize the "S" curve characteristic associated with microbursts [12]. This "S" curve, showing mean windspeed versus range, develops as a strong downdraft induces an outburst of damaging winds on or near the ground. Usually this kind of information is obtained by estimating weather spectral moments through the DFT or the pulse pair method. Based upon these same basic concepts of

hazard detection, new techniques are developed and explained in this dissertation.

Of course, the reliability of any detection algorithm depends on the quality of original data collected by a weather radar. Therefore the system phase stability problem is one of the important issues in developing windshear detection radars. Although the airborne Doppler weather radar is considered to have good potential for providing the pilot information to help avoid the hazardous windshear conditions, it may be susceptible to phase noise. The period over which the radar return can be considered stationary limits the data analysis window in an airborne weather radar as compared to a ground based Doppler weather radar. Also since the radar platform is moving there may be less advance observation time as the aircraft approaches the area of windshear hazards. These limited data records may yield poor estimates of autocorrelation or power spectrum parameters which will be further degraded by system phase noise. Phase noise may be compounded in an airborne weather radar which is operating under look-down conditions. Since clutter power is typically much stronger than weather return power, increased clutter spectrum width due to any system phase instability will obscure the weak weather return signal making the clutter rejection inherently more difficult.

Windspeed Gradient and F-Factor

The phenomenon of windshear is associated with air turbulence and can generally be characterized by large spatial gradients of wind velocity (windspeed gradient). It seems feasible that the existence of a windshear condition may therefore be established on the basis of the measured wind velocity magnitude change within an airspace volume, given adequate spatial resolution of the measurements. With a typical pulse Doppler weather radar employed to remotely sense windspeed, the distribution of measured Doppler frequencies within each range cell is related to the reflecting particle motion within that range cell. The mean Doppler frequency of the return is a measure of the average windspeed within a range cell, while the spread of these frequencies is an indication of the turbulence within the range cell.

Bowles [11] defined a hazard index F which is represented as

$$F = \frac{W_x'}{g} - \frac{W_h}{v}$$

where W_x' is the rate of change of the horizontal component of windspeed, v is the relative speed of the aircraft, g is the acceleration due to gravity and W_h is the vertical component of windspeed. This F-Factor was derived considering aircraft energy balance for flight in spatially and temporally varying windfields. Positive values of F indicate a performance

decreasing situation while negative values mean the opposite. In [11], it is shown that the average F values of all investigated aircraft accidents exceeded 0.15 which may be considered as a threshold value. Although the vertical windspeed is needed in the computation of F value, the forward-looking airborne radar can only measure the radial windspeed along the flight path of the airplane. Therefore considering only the measurable term W_x, the radial component of F, F_R is given as

$$F_R = \frac{W_x'}{g} \cong \frac{v}{g} \frac{\Delta W_x}{\Delta R}$$

where ΔW_x is the change in radial velocity between range bins and ΔR is the distance between range bins. From this expression, it should be noted that F_R represents just the normalized value of windspeed gradient. Therefore, the direct measurement of windspeed gradient with low PRF radar may be very useful in the detection of hazardous windshear conditions.

Detection and False Alarm Probability

A reliable windshear detection system should alert a pilot when hazardous conditions exist, but nuisance alarms should be avoided by selecting a suitable statistic for detection. One fundamental problem is how to select the proper threshold value. A hazard index F-Factor has been suggested as appropriate [11]. Although a decision should be

based on both the detection and the false alarm probabilities along with risk factors associated with each possible outcome, it is difficult to compute those values since the probability distribution of F values must be known. If $P(F|H_1)$ and $P(F|H_0)$, the conditional probability distribution of F in the presence of a windshear hazard, H_1, and with no hazard, H_0, respectively, are known, a Nyman-Pearson criterion [13], for example, may be applied to set a threshold value which maximizes the probability of detection P_{DET} while constraining the false alarm rate P_{FA}. An optimum test, thresholding the likelihood ratio,

$$P(F|H_1)/P(F|H_0)=\Lambda(F) > \lambda$$

would indicate a windshear hazard alarm where P_{DET} and P_{FA} are given by

$$P_{DET} = \int_{\lambda}^{\infty} P(\Lambda|H_1)\ d\Lambda,\quad P_{FA} = \int_{\lambda}^{\infty} P(\Lambda|H_0)\ d\Lambda\ .$$

This likelihood ratio test is illustrated in Figure 5. In order to validate this test, numerous observations of microbursts should be made to estimate a reliable $P(F|H_1)$. This in turn can be used in determining a receiver operating characteristic curve which will show the relationship between the decision threshold value, P_{DET} and P_{FA}. An improved hazard index estimator has been suggested by Britt [14] using a

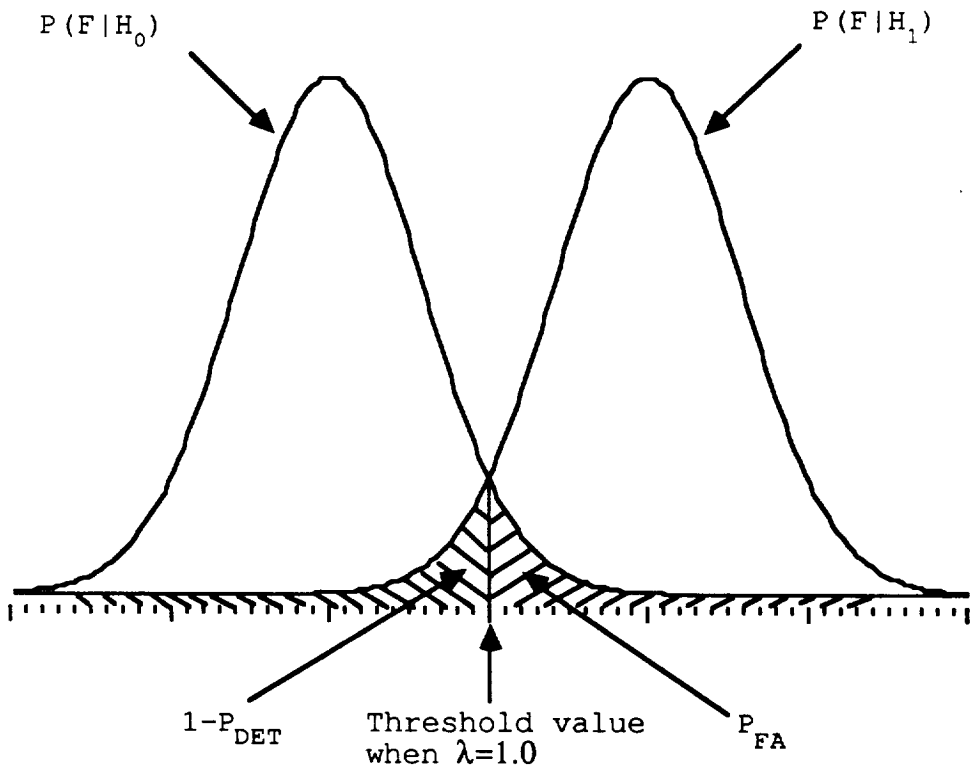

Figure 5. A Likelihood Ratio Test of Two Conditional Probability Density Functions

weighted least square technique to estimate windspeed gradient. This should provide a more reliable conditional probability distribution of F values with very little additional computation requirement. The basic component in the hazard index is the estimate of the spatial gradient of windspeed.

Problem Statement

Phase stability is a very important factor in obtaining accurate and reliable information in a coherent radar system. Since Doppler weather radar applications may impose severe requirements on phase stability, it is necessary to analyze the system phase instability problem which can be caused by a variety of sources, e.g., radar oscillators, complex sampling procedures, filtering and amplification, etc. [53],[54],[55]. Radar oscillator instability in a coherent radar has been previously analyzed, e.g, [15],[16], however, this work has been concerned primarily with a target detection radar system, not a weather radar system, and generally no analysis of the entire system phase noise effect is included. They have just considered one major phase noise source, i.e., STALO in relation with the performance of a single target detection radar. Therefore, in Chapter II of this dissertation, a general approach is developed to investigate the whole system phase noise effect. Two very popular weather signal processing algorithms, i.e., the DFT method and the pulse pair method, are analyzed considering phase noise.

Finally a benchmark laboratory test is proposed for the measurement of whole system phase noise in a pulse Doppler weather radar.

The commonly used pulse pair method is quite attractive when processing an enormous amount of weather radar data in real time since it is considered the fastest algorithm available. The original concept of the pulse pair algorithm was developed by Miller and Rochwarger [8]. Since then, it has been studied and analyzed by many researchers. The pulse pair method was derived and has been evaluated most often under the assumptions that the weather spectrum is symmetric and relatively narrow. With the turbulent situations associated with windshear, these assumptions may not be valid. Some observed weather spectra [17] show that nearly 25% are seriously skewed and can not be considered to be symmetric. This means that the pulse pair method may need reevaluation considering the skewness effect. Chapter III analyzes this effect using the skewed Gaussian spectrum model.

The poly-pulse pair method was originally suggested as a way of enhancing the accuracy of spectrum moment estimation, but this method may be also useful in reducing the bias errors of a skewed spectrum. Based on the similar concept, a new modified pulse pair mean estimator is developed in Chapter III where it shows an improvement over a conventional method by reducing the bias errors. In the symmetric spectrum, the mean and the mode are same. However, in the

case of a skewed spectrum, it may be questionable that the mean is a more representative value than the mode. Hence the difference between the mode and the true mean due to skewness effect is also presented in Chapter III.

Chapter IV presents a new method in the measurement of windspeed gradient. Since the windshear hazard index is computed from windspeed gradient, it may be considered the most important information in a windshear detection radar. Usually this information is obtained through the measurement of mean windspeed in each range cell. Because of the very strong wind involved with microbursts, a high PRF (pulse repitition frequency) radar is preferred to increase the Doppler spectrum range and thus the maximum unambiguous windspeed. This, however, results in an increased ambiguity in the range measurement. To overcome this difficulty, a new method is suggested for direct measurement of the windspeed gradient using a low PRF radar.

Another challenging problem arises in dry microburst cases where a very low signal-to-clutter ratio may cause meaningless results without efficient clutter filtering. In some situations where clutter and weather spectra are not well separated, it is difficult to remove the clutter without deteriorating the weather signal. Even though efficient clutter filtering can be done using algorithms developed recently [12],[18],[19], the additional computation requirements may be prohibitive in real time weather radar signal processing. A new approach described in Chapter V does

not need any preliminary processing such as clutter filtering. It applies a modified Prony method to estimate peak points of weather return spectra. These values may be used to recognize typical "S" curve characteristic associated with a windshear phenomenon. Using a NASA simulation model, some validating results are also shown in Chapter V. Overall conclusions and some recommendations for future work are presented in Chapter VI.

CHAPTER II

PHASE NOISE EFFECTS ON WEATHER SPECTRUM MOMENT ESTIMATION

Introduction

In the weather radar return the superimposed scattering of incident electromagnetic energy from many randomly distributed particles causes an unavoidable phase jitter effect which generally contributes to the spectrum width of the weather radar return signal. With a coherent pulse Doppler radar, this creates some ambiguity in determining a representative windspeed condition within a particular range cell. Any radar system phase instabilities may also contribute to this ambiguity and affect the Doppler frequency resolution as well as the dynamic range capability. There are many potential sources of system phase instability (phase noise or phase jitter) but a potential primary source is the stable local oscillator (commonly STALO) which provides transmitted and reference carriers within the radar. If the range time is adequate to decorrelate the STALO oscillator phase, any phase variation with time (jitter) may be adequate to contribute error in return Doppler spectral estimates. Furthermore, this may not be apparent when observing the weather return Doppler spectrum because of its inherent spread.

This chapter provides an analysis of the effect of pulse to pulse system phase jitter uncertainty on the pulse pair [29] and DFT based spectral moment estimates. More importantly a general analysis approach is developed which will allow for a quantitative assessment of the effect of the entire radar system phase noise. The approach can be used with an analytical model description of phase noise or with an actual measured system phase noise power spectrum. Intrapulse phase uncertainty is not considered here.

An analytical development of the Doppler spectrum using a Gaussian approximation for the phase jitter spectrum is presented first. Even though a power-law model is more appropriate in representing experimental results of a STALO phase noise spectrum [20], a Gaussian model is considered here for two reasons. First, it is reasonable to fit a Gaussian distribution to a major portion of a power-law phase noise spectrum particularly in the tails of the spectrum. Secondly, a Gaussian assumption provides mathematical tractability. It is recognized here that spectrum moment estimation error may depend upon the specific model of phase jitter noise. It is also true that the optimum model is not known. For example, considering an oscillator alone, even though many related papers have been published, none of them exactly describes all instability factors [21],[22],[23]. Therefore, the approach developed here is generalized to enable analysis of all types of phase jitter effects through numerical computation of the autocorrelation function from a

given measured or otherwise specified noise spectrum. This is particularly important because the analysis procedure can be used for any set of phase jitter power spectrum measurements that might be available or for any analytical spectrum function defined in terms of a set of values. The spectral mean and width as estimated by the pulse pair method and DFT method are analyzed analytically considering the effect of phase jitter. For the Gaussian model, the effect of phase jitter is computed for a particular phase jitter power level while allowing variation in both the weather spectrum width and the phase jitter spectrum width.

Gaussian Phase Noise

Any phase jitter occurring at the transmitter stage will spread the original sinusoidal signal spectrum. The stable local oscillator output is modelled as

$$V(t)= V_0 COS(\omega_c t +\Phi(t))$$

where $\Phi(t)$ is a phase jitter and the carrier is $\omega_c=2\pi f_c$. If one assumes that $\Phi(t)$ is a normal stationary process with zero mean and variance $\sigma^2= E[\Phi^2(t)]$, the spectral density of the transmitted signal is given by [24]

$$S_v(f)=\frac{v_0^2}{2} e^{-\sigma^2}\{\delta(f-f_c) +S_\phi(f-f_c) +\sum_{n=2}^{\infty}\frac{1}{n!}[S_\phi(f)^{n-1}*S_\phi(f)]_{f_c}\} \qquad (2.1)$$

where the first term inside the braces of (2.1) relates to the sinusoidal energy at f_c , the second term is the phase noise spectrum located at f_c and the last term includes n-1 convolutions of the phase noise spectrum with itself, followed by a translation around the carrier frequency f_c. As the mean intensity of phase noise becomes very small, the spectral density of phase jitter can be approximated by a Gaussian spectrum [25],[26]; i.e.

$$S_\phi(f)=W_0\exp\left\{\frac{-\omega^2}{\Delta\omega_c^2}\right\}$$

where the relationship between phase jitter width $\Delta\omega_c^2$ and the total phase jitter power σ^2 is represented by

$$\sigma^2=\int_{-\infty}^{\infty} s_\phi(f)\,df=\frac{\Delta\omega_c}{2\sqrt{\pi}}W_0 \quad .$$

With Gaussian phase noise , the spectral density of the transmitted signal from (2.1) can be obtained analytically as

$$S_v(f)=\frac{V_0^2}{2}e^{-\sigma^2}\left\{\delta(f-f_c)+\frac{2\sqrt{\pi}}{\Delta\omega_c}\sum_{n=1}^{\infty}\frac{\sigma^{2n}}{n!\sqrt{n}}\exp\left[\frac{-(\omega-\omega_c)^2}{n\,\Delta\omega_c^2}\right]\right\} \quad .$$

If σ is small(σ< 0.5 radians), which should be true in a high quality oscillator, $S_v(f)$ can be approximately given by

$$S_v(f)= \frac{V_0^2}{2} e^{-\sigma^2} \left\{ \delta(f-f_c) + \frac{2\sqrt{\pi}}{\Delta\omega_c} \sigma^2 \exp[\frac{-(\omega-\omega_c)^2}{\Delta\omega_c^2}] \right\} \quad . \qquad (2.2)$$

It can be noted that the theoretically exact description for the spectral density is [27]

$$S_v(f)= \frac{V_0^2}{2} \int_{-\infty}^{\infty} \exp(-\frac{\omega_c^2}{2} \tau^2 I^2(\tau)) \cos(\omega_c \tau) e^{-j\omega\tau} d\tau$$

where

$$I^2(\tau)= \frac{E\{[\phi(t_k+\tau)-\phi(t_k)]^2\}}{(\omega_c \tau)^2} \quad .$$

This theoretical expression would be useful if an approximation for the true variance $I^2(\tau)$ could be determined for all τ, but it is very difficult to obtain this experimentally except for a few discrete values of τ due to the requirement of very long observation time. Therefore, the approximation in (2.2) provides a realistic means of analyzing the effects of phase jitter in the Doppler radar.

The transmitted radar signal is scattered by many particles and the signal frequency will be shifted according to the particles' velocity which is the well known Doppler effect. Using the description given in (2.2), the scattered return signal can be approximated as

$$S_v(f)=\frac{V_0^2}{2}e^{-\sigma^2}C\{\frac{1}{\sqrt{2\pi}\,W}\exp(-\frac{(f-f_c-f_d)^2}{2W^2})+\sigma^2\frac{1}{\sqrt{2\pi(\Delta f_c^2/2+W^2)}}$$

$$\cdot\exp(-\frac{(f-f_c-f_d)^2}{2(\Delta f_c^2/2+W^2)})\} \qquad (2.3)$$

where W is the spectrum width with zero transmitter phase noise and C is a constant determined by the reflectivity of target particles and some other factors (see for example [28]). If the noise is small (σ small), the second term in (2.3) can be ignored and the typical Doppler return signal will have a purely Gaussian spectral shape. With this assumption the autocorrelation function of the return signal after demodulation will be

$$R(\tau)=\frac{v_0^2}{2}C\,\gamma(\sigma,w,\tau)\,e^{j\omega_d\tau}+N\,\delta_{\tau,0} \qquad (2.4)$$

where

$$\gamma(\sigma,w,\tau)= e^{-\sigma^2}\left\{ e^{-2\pi^2 w^2\tau^2} + \sigma^2 e^{-2\pi^2(w^2+\frac{\Delta f_c^2}{2})\tau^2} \right\} .$$

The additive white noise $N\delta_{\tau,0}$ is included in the signal model to represent the usual background noises [29]. The autocorrelation function shown in (2.4) is obtained under the assumption that no phase noise occurs at the receiver in the process of demodulation. However, in the interest of a more complete understanding of pulse pair estimation, the effect of phase jitter occurring at the receiver should be included.

In the pulse-pair method [30], a two-point estimate of the complex autocorrelation is based upon processing coherent returns from pairs of transmitted pulses. Assuming that the pulse pairs are separated by T_s and repeated with period T as illustrated in Figure 6, the complex time autocorrelation function of the complex received wave form z(t) at the lag value T_s is defined as

$$R(Ts)=E\{Z^*(iT)\, Z(iT+T_s)\} .$$

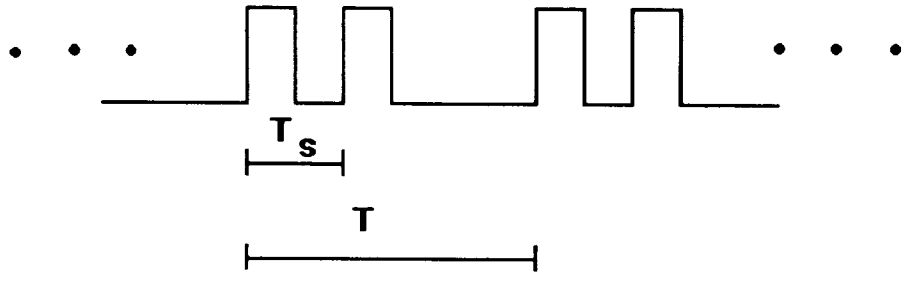

Figure 6. Pulse Pairs for the Estimate of Autocorrelation Function

Considering the phase deviations in the process of heterodyne demodulation designated by Φ_{iT} and Φ_{iT+Ts}, the autocorrelation function is

$$R(T_s)= R(T_s)\, E\{e^{-j\phi_{iT}}\, e^{j\phi_{iT+T_s}}\} \tag{2.5}$$

where, from (2.4),

$$R(T_s)= S\,\gamma(\sigma,w,T_s)\, e^{j\omega_d T_s} \quad , \quad S=\frac{v_0^2}{2}C \quad . \tag{2.6}$$

If one assumes that $\Phi_1=\Phi_{iT}$ and $\Phi_2=\Phi_{iT+Ts}$ and are, for example, normal random variables [20], then (2.5) can be rewritten as

$$R(T_s)= R(T_s)\,(2\pi\overline{\phi^2}\sqrt{1-\rho^2}\,)^{-1}\int_{-\infty}^{\infty}\int e^{-j\phi_1}e^{j\phi_2}\exp[-(\phi_1^2+\phi_2^2-2\rho(T_s)\phi_1\phi_2)$$

$$/(2\overline{\phi^2}(1-\rho^2))]\, d\phi_1 d\phi_2$$

where

$$\rho(T_s)= E[\phi_1\phi_2]\,/\,\overline{\phi^2} \qquad \text{and} \qquad E[\phi_1\phi_2]=\overline{\phi_1\phi_2} \quad .$$

The complex autocorrelation function can be further reduced to [31]

$$R(T_s) = R(T_s)\exp[-(\overline{\phi^2} - \overline{\phi_1\phi_2})]$$

$$= R(T_s)\exp\left[\int_{-\infty}^{\infty} S_\phi(f)(1-\cos\omega T_s)\,df\right] \quad . \qquad (2.7)$$

Similarly $S_\phi(f)$ can be assumed to have a Gaussian noise spectrum as described in the previous section since the same oscillator signal is fed into the receiver for heterodyning. With this assumption (2.7) will become

$$R(T_s) = R(T_s)\,\Psi(\sigma,T_s) + N\delta_{T_s,0} \qquad (2.8)$$

$$\Psi(\sigma,T_s) = \exp[-\sigma^2\{1-\exp(\frac{-\Delta\omega_c^2 T_s^2}{4})\}]$$

where $R(T_s)$ is given in (2.6) and σ is the r.m.s. phase noise. As seen from (2.8), this modified autocorrelation at lag value T_s is explicitly a function of the phase spectrum width $\Delta\omega_c$ and the total phase jitter power σ^2 with the additive white background noise also included.

General Approach by Numerical Computation

Using the system approach, the general complex autocorrelation function of the weather return signal in the

presence of phase noise can be obtained without full analytical representation of the phase noise spectrum. Again representing the weather return Doppler spectrum as Gaussian, modulation and demodulation procedures also can be represented by a simple mathematical form considering phase jitter as can be seen from the Figure 7. R_j and R_w are autocorrelation functions of phase jitter. R_j can represent the effect of phase instability in the radar system. R_w represents phase jitter due to particle scattering. Following the same procedure used in deriving (2.8) [26], these autocorrelation functions can be written as

$$R_j = E[e^{-j\phi(t)} e^{j\phi(t+T_s)}] = \exp(-\{\int_{-\infty}^{\infty} S_\phi(f)\, df - R_\phi(T_s)\})$$

$$R_w = e^{-2\pi^2 w^2 T_s^2}$$

C : attenuation constant

where

$$R_\phi(T_s) = \int_{-\infty}^{\infty} S_\phi(f)\, e^{j2\pi f T_s}\, df \quad . \qquad (2.9)$$

Since the exponential term in R_j represents the difference between phase noise power and the autocorrelation of phase noise at T_S, it can be shown that R_j goes to 1.0(no phase noise effect) as the phase noise spectrum becomes narrower.

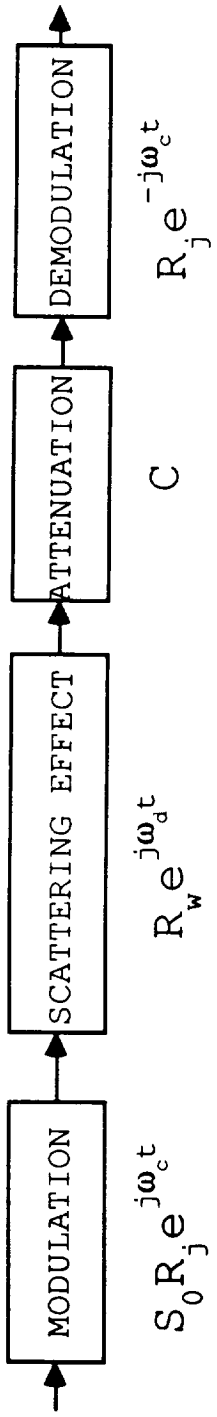

Figure 7. System Model of a Weather Radar Return

Considering statistical independence between these terms, the output complex autocorrelation function will be just the multiplication of all individual autocorrelation functions which is shown to be

$$R(T_s)= S \exp(-2\{\int_{-\infty}^{\infty} S_\phi(f)\, df - R_\phi(T_s)\})\, e^{-2\pi^2 w^2 T_s^2}\, e^{j\omega_d T_s} + N\delta_{T_s,0} \qquad (2.10)$$

As seen from (2.9), a closed form expression for $R_\phi(T_S)$ is generally not possible unless the phase noise spectrum is a known functional form, e.g., Gaussian. Therefore, some numerical method may be needed to determine R_j. An adaptive quadrature algorithm [32] is used here in the computation of these terms. The next section analyzes the effect of these modified autocorrelations on the quality of the pulse pair and DFT estimates.

Pulse Pair Estimation Errors

Modern radar oscillators are very stable with small phase noise power so that the effect of phase jitter in a return Doppler spectrum may not be apparent, even if it does have an effect on the pulse pair estimates. Figures 8, 9 and 10 illustrate this situation. In Figure 8 simulated return Doppler spectrum is shown with and without phase jitter. A zero mean normal signal return spectrum with unity total power and a width corresponding to 15% of the processing bandwidth is depicted along with the resulting spectrum

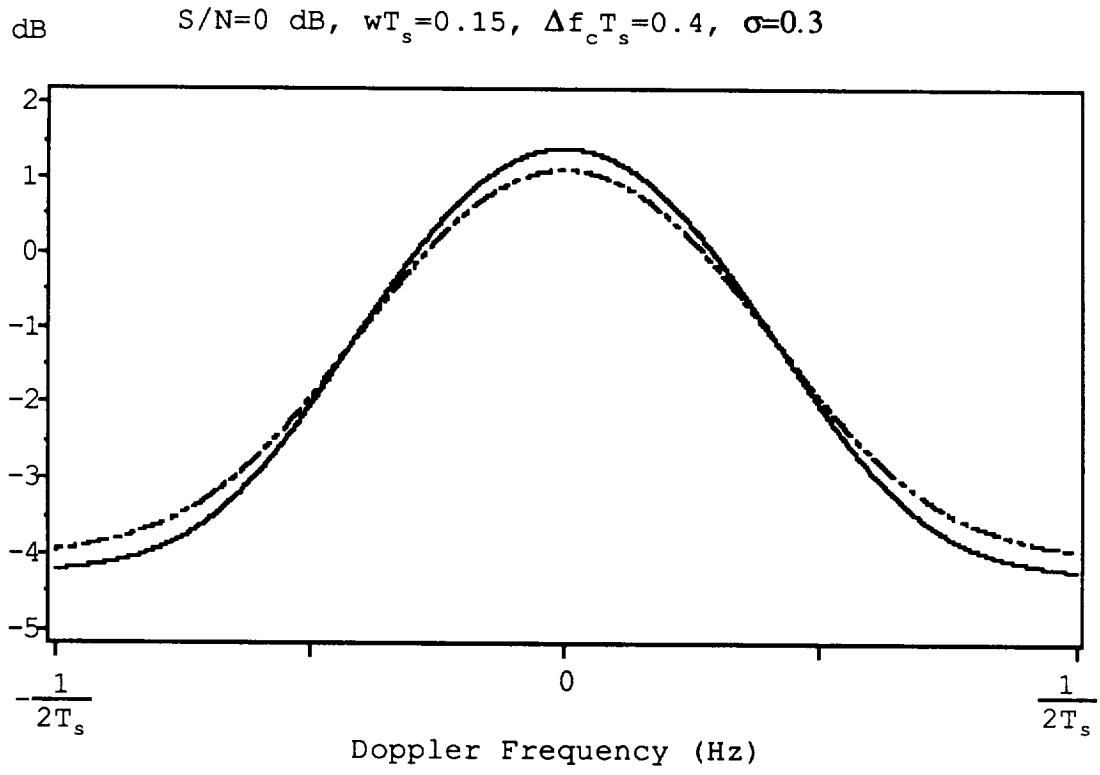

Figure 8. Example of Two Simulated Return Doppler Spectra Considering Phase Jitter Effect

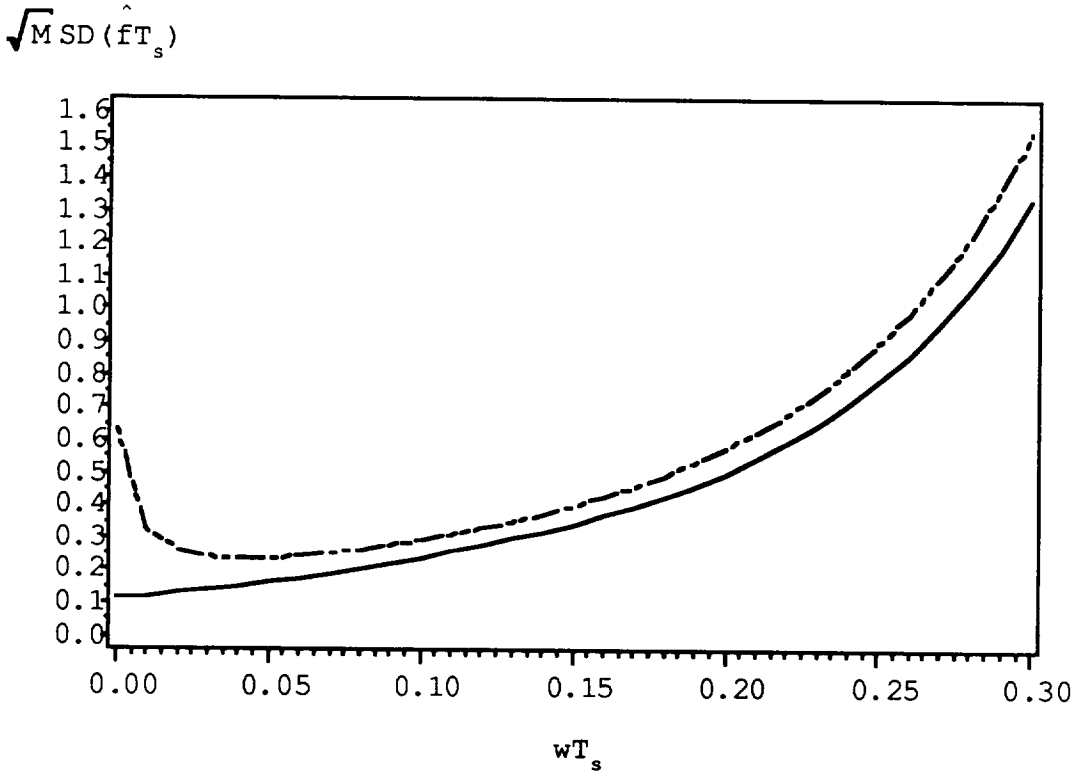

Figure 9. Error Standard Deviation of the Spectrum Mean Pulse-Pair Estimate for the Example in Figure 8

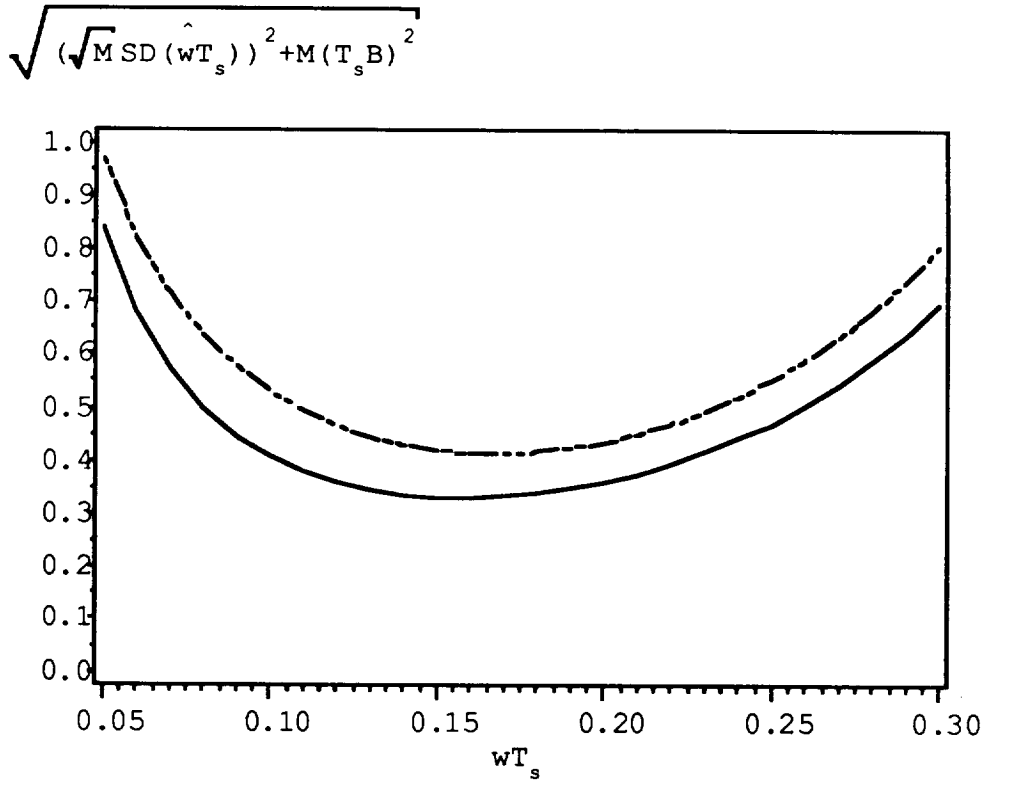

Figure 10. R.M.S. Error of the Spectrum Width Pulse Pair Estimate for the Example in Figure 8

contaminated with statistically independent phase noise having a total power level at 9% of the signal power and a width which is 28% of the processing bandwidth. This phase noise width is less than that of an inverse f type distribution with the same total phase noise power. There is little apparent difference between the two spectra depicted in Figure 8. Analyzing the standard deviation of the error of the pulse pair mean estimate for the situation depicted in Figure 8 (wT_s=0.30), however, shows in Figure 9 that the phase jitter causes more than a 15% increase. For other Doppler spectrum widths, this same phase jitter error can cause up to 50% increase in the error standard deviation without an apparent change in the spectrum. From Figure 10, the rms error of the pulse pair width estimate also can be significantly affected by this phase jitter, causing approximately 15% error for the Doppler return spectrum width considered. These results suggest that it may be useful to analyze and quantify the phase jitter effect on pulse pair estimation errors even when the effect on the Doppler spectrum is not apparent.

Consider estimation of the mean frequency with pulse pair processing [29]. The estimated return spectrum mean is defined by

$$\hat{f}_d = \frac{1}{2\pi T_s} \arg\left\{\hat{R}(T_s)\right\} \qquad (2.11)$$

where

$$\hat{R}(T_s) = \frac{1}{M}\sum_{i=0}^{M-1} Z^*(iT)\, Z(iT+T_s) \quad .$$

As seen from (2.9) and (2.11), the estimate of the mean frequency will not be dependent upon phase jitter because it does not affect arg{R(Ts)}, i.e., only the magnitude scaling is changed by phase jitter. Thus, according to this analysis, no bias will be introduced into the mean frequency estimate because of phase jitter.

The variance of the mean frequency estimate as previously published [30] is

$$\mathrm{VAR}(\hat{f}_d) = [8\pi^2 T_s^2 \beta^2(T_s)]^{-1} \left\{ M^{-2}[1-\beta^2(T_s)] \cdot \sum_{m=-(M-1)}^{M-1} \beta^2(mT)\,(M-|m|) \right.$$

$$\left. + \frac{N^2}{MS^2} + \frac{2N}{MS}[1-\beta(2T_s)\delta_{T-T_s,0} + \frac{\beta(2T_s)}{M}\delta_{T-T_s,0}] \right\} \quad . \qquad (2.12)$$

This expression can be rewritten considering phase jitter by replacing $\beta(T_s)$ with $\beta'(T_s)$ where

$$\beta'(T_s) = \gamma(\sigma, w, T_s)\, \psi(\sigma, T_s)$$

for the Gaussian spectral model and

$$\beta'(T_s)= \exp(-2\{\int_{-\infty}^{\infty} S_\phi(f)\, df - R_\phi(T_s)\})\, e^{-2\pi^2 w^2 T_s^2}$$

for the arbitrary spectral model. Here M is the number of sample pairs.

Analyzing the variance expression in (2.12), if the total phase jitter power σ^2 is held constant, one can investigate the effect of varying the spectral distribution of the phase jitter. The parameter Δf_c determines the shape of this spectral distribution. As Δf_c increases, the phase jitter spectrum is broadened. As can be seen from Figure 11, which is a plot of the mean frequency estimate standard deviation versus normalized Δf_c, when the phase jitter spectrum is broadened, an increase in the variance of the mean frequency estimate can be expected. Also from Figure 11, as the weather spectrum width W increases, this effect on the mean frequency estimate is more pronounced. Figure 12 is included to show the effect of phase noise through numerical computation from experimentally obtained phase noise data [34]. From Figure 12 it can be said that the Gaussian jitter spectrum model yields a maximum error bound in the estimation of mean frequency.

Considering the weather spectrum width estimate using the pulse pair method, the width estimation is independent of the mean frequency [9]. If the width is sufficiently smaller

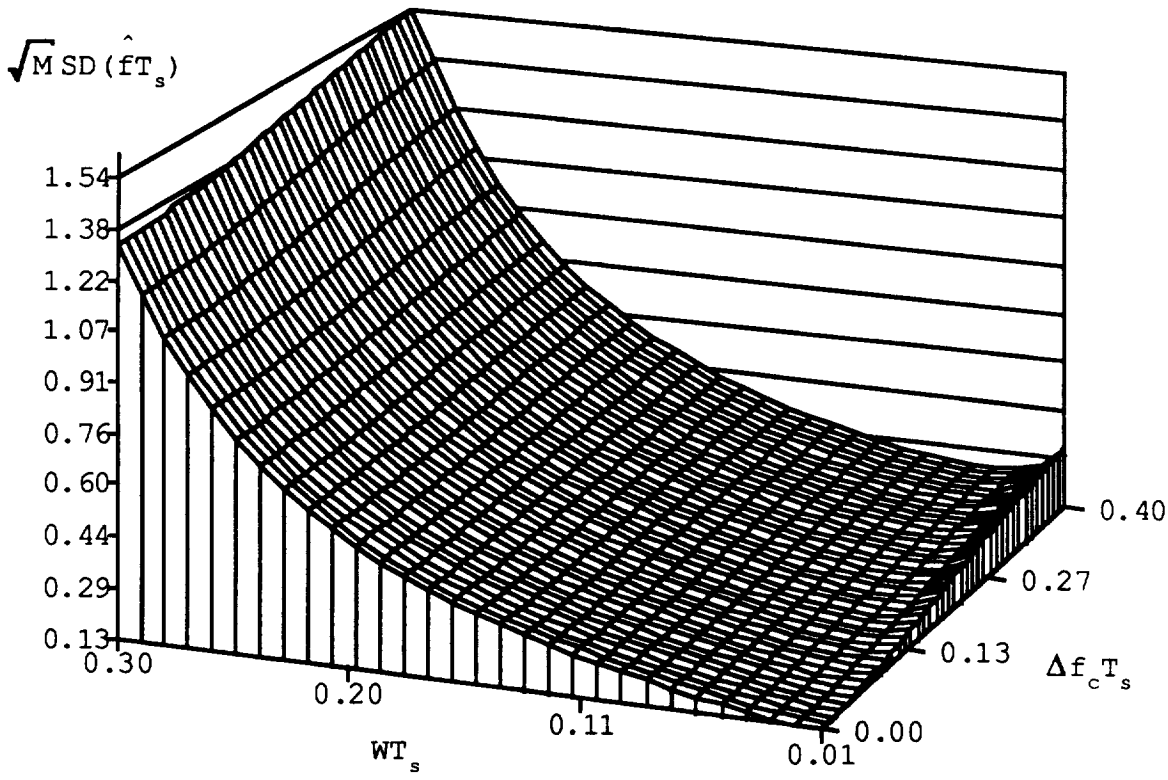

Figure 11. Error Standard Deviation of the Spectrum Mean Pulse Pair Estimate Considering STALO Phase Jitter

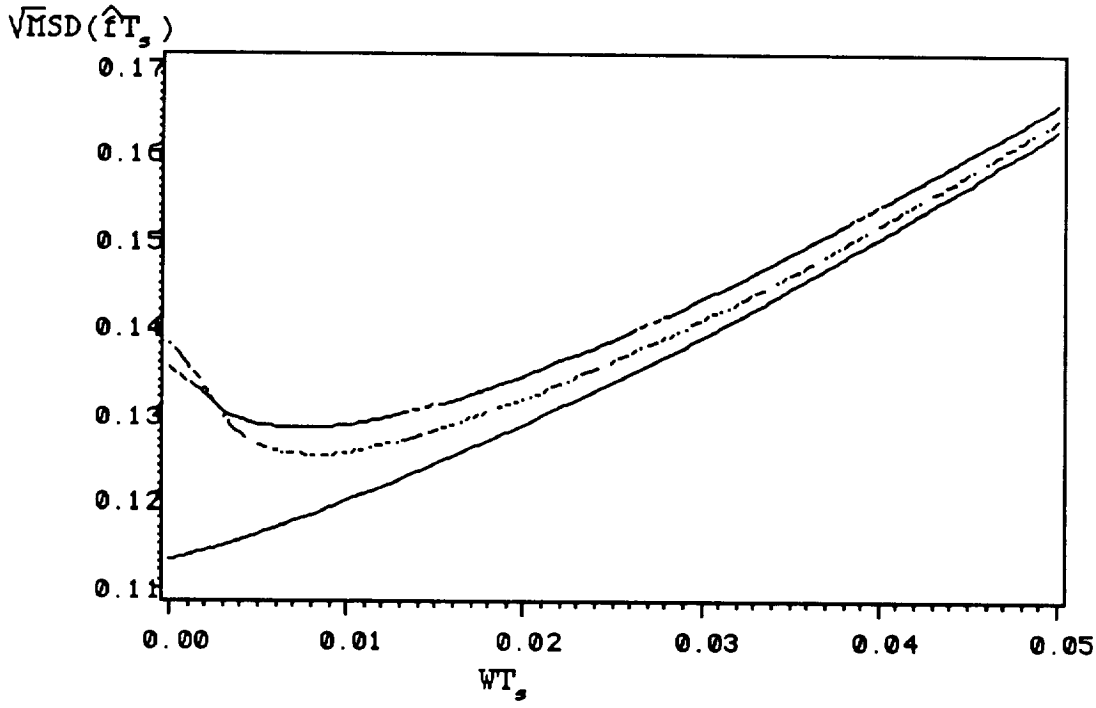

Figure 12. Comparison of Error Standard Deviation of the Spectrum Mean Pulse Pair Estimate

than the Nyquist interval, one form of the estimator which is not dependent upon spectrum shape is given by [9]

$$\hat{W}=\begin{cases}\dfrac{1}{\sqrt{2}\,\pi T_s}\left|1-\dfrac{\left|\hat{R}(T_s)\right|}{\hat{S}}\right|^{\frac{1}{2}} & \text{when } \left|\hat{R}(T_s)\right|<\hat{S} \\ \delta & \text{when } \left|\hat{R}(T_s)\right|\geq\hat{S}\end{cases} \tag{2.13}$$

where

$$\hat{S}=\frac{1}{L}\sum_{k=0}^{L-1}|Z_k|^2-N$$

and δ is an arbitrarily small number. With the introduction of phase jitter, this estimator becomes

$$\hat{W}'=\begin{cases}\dfrac{1}{\sqrt{2}\,\pi T_s}\left|1-\dfrac{\left|\hat{R}'(T_s)\right|}{\hat{S}}\right|^{\frac{1}{2}} & \text{when } \left|\hat{R}'(T_s)\right|<\hat{S} \text{ and} \\ \delta & \text{when } \left|\hat{R}'(T_s)\right|\geq\hat{S}\ .\end{cases} \tag{2.14}$$

where since $|\hat{R}'(T_s)|$ from (2.7) replaces $|\hat{R}(T_s)|$ in (2.13), the estimate of spectrum width is biased. Previous results for the asymptotically unbiased variance can now be extended to yield the variance of the width estimate as

$$\mathrm{VAR}(\hat{W}) = [32M\pi^4 (WT_s)^2 \beta^2(T_s) T_s^2]^{-1} \{ 2 \cdot [1-(1+\delta_{T-T_s,0})\beta^2(T_s) + \delta_{T-T_s,0}\beta^4(T_s)]\frac{N}{S} + [1+(1+\delta_{T-T_s,0})\beta^2(T_s)]\frac{N^2}{S^2} + \beta^2(T_s)\sum_{m=-(M-1)}^{M-1}\{2\beta^2(mT) + \beta^2(mT)\beta^2(T_s) + \beta(mT+T_s(1-\delta_{T-T_s,0})) - 4\beta(mT+T_s)\cdot\beta(mT)\beta^{-1}(T_s)\} \cdot (1-\frac{|m|}{M}) \}$$

where $\beta(T_s)$ given in a previously derived result [9] is replaced by $\beta'(T_s)$ as was done in (2.12). The variance of the width estimate may be increased by phase jitter, but does not completely describe the goodness of the width estimator, since phase noise will bias the width estimate of spectrum as seen from (2.14). Thus, in this situation the mean square error defined by

$$E\{(\hat{\theta}-\theta)^2\} = \mathrm{VAR}(\hat{\theta}) + B^2$$

where B is the bias of a biased estimation $\hat{\theta}$ of the parameter θ, will be a more representative measure of the effect of phase jitter on the pulse pair estimation of spectrum width. The bias term and the root mean square error of the width estimate are plotted in Figures 13 and 14 respectively. Figure 14 shows that the variance of width estimate is also increased due to phase jitter. In each case the normalized weather spectral width has been varied to illustrate its

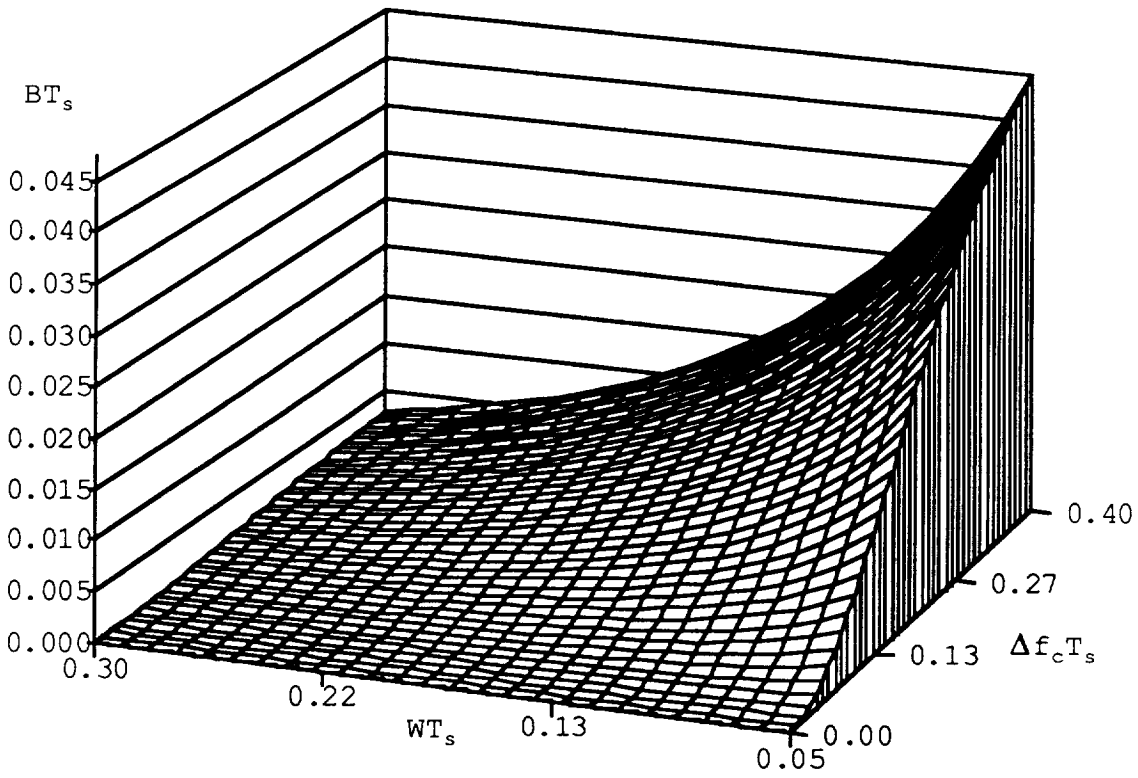

Figure 13. Bias of the Spectrum Width Pulse Pair Estimate Considering STALO Phase Jitter

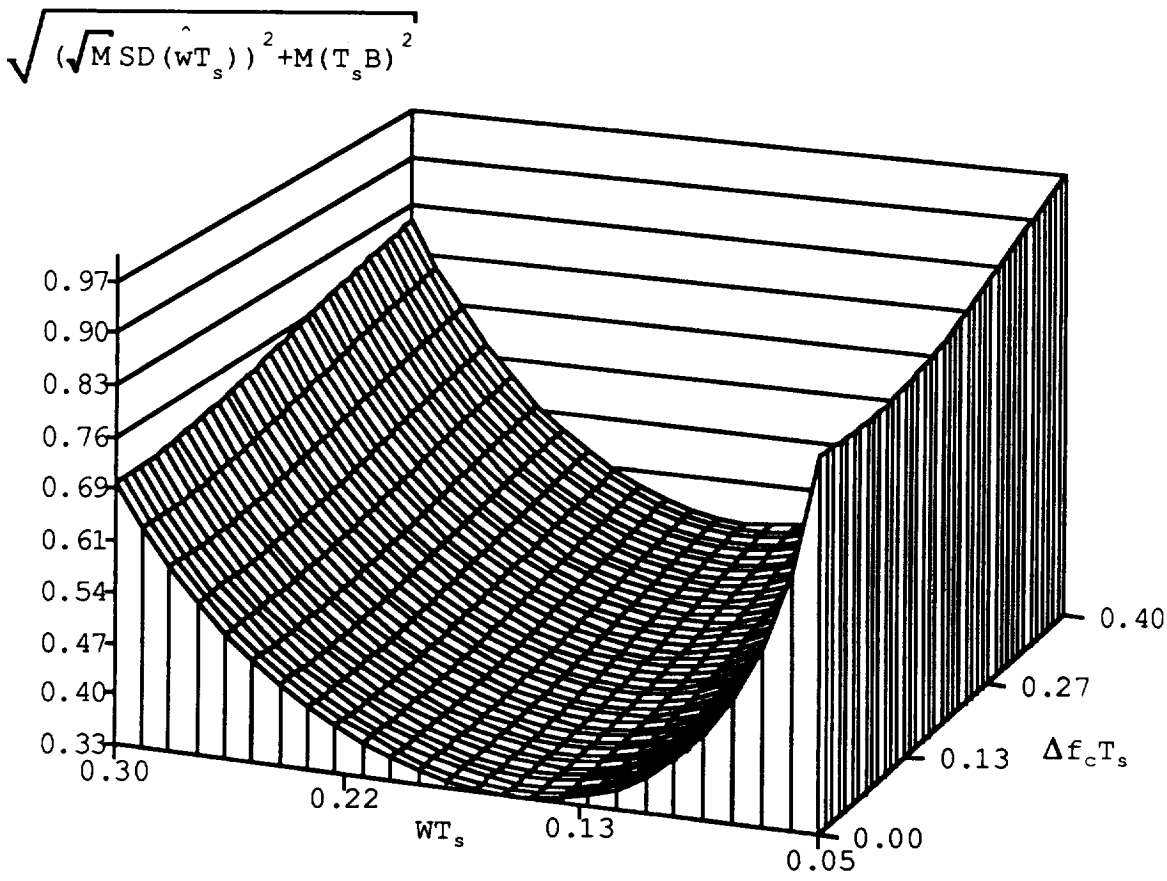

Figure 14. R.M.S. Error of the Spectrum Width Pulse Pair Estimate Considering STALO Phase Jitter

effect upon the estimation errors. As is seen in Figure 13, the bias in the width estimation is more sensitive to increasing phase jitter when the true normalized spectral width is small. This variation in sensitivity is less evident when considering the r.m.s. error in the width estimate in Figure 14. It should be noted that in each of Figures 11, 13 and 14 the curve for $\Delta f_c=0$ (no phase jitter) has been previously published [30].

DFT Estimation Errors

Consider the problem of calculating the mean frequency and the spectrum width from the DFT-derived spectral density. The most straightforward DFT spectrum estimates are simply the mean and width estimate of the derived spectral density $S(f_i)$ [7], i.e.,

$$\hat{f}=\frac{\sum_i f_i S(f_i)}{\sum_i S(f_i)} \quad \text{and} \quad \hat{w}^2=\frac{\sum_i (f_i-\hat{f})^2 S(f_i)}{\sum_i S(f_i)} \; .$$

These, of course, are parameter estimates of the composite signal-plus-noise spectrum. As it is well-known, these are not satisfactory estimates of signal parameters except for large signal-to-noise ratios. Therefore, some technique of removing the noise influence should be implemented. One method of noise suppression is to simply subtract the noise

spectral density $N(f_i)$ from the derived spectral density and calculate the estimates of the resulting spectrum, i.e,

$$\hat{f}=\frac{\sum_i f_i[S(f_i)-N(f_i)]}{\sum_i [S(f_i)-N(f_i)]} \quad ; \quad \hat{w}^2=\frac{\sum_i (f_i-\hat{f})^2[S(f_i)-N(f_i)]}{\sum_i [S(f_i)-N(f_i)]} \quad .$$

These estimates are unbiased by noise even for low signal-to-noise ratios. This method has been chosen here as the basis for evaluating the phase noise effect since the variance of both these estimates was derived earlier by Berger and Groginsky [33]. Another variation [7] to eliminate biases due to aliasing is useful for symmetric spectra, but it is not adopted in this analysis because no variance expression is available. Simulation results do, however, show similar estimation quality when compared to the method chosen here for further analysis.

Using previously derived variance expressions [33] and replacing the summations in the estimates with an integral over the Nyquist interval in each case, the mean frequency estimate variance can be expressed as

$$\text{var}(\hat{f}) = \frac{1}{MT_s^2}\left[T_s\int_{-\frac{1}{2T_s}}^{\frac{1}{2T_s}} f^2 S_n^2(f+f_m)\ df + 2\left(\frac{N}{S}\right)T_s^2\int_{-\frac{1}{2T_s}}^{\frac{1}{2T_s}} f^2 S_n(f+f_m)\ df + \frac{1}{12}\left(\frac{N}{S}\right)^2\right]$$

and the width estimate variance is

$$\text{var}(\hat{w}) = \frac{1}{MT_s^2}\left\{\frac{T_s}{4w^2}\int_{-\frac{1}{2T_s}}^{\frac{1}{2T_s}} [f^4+w^4-2w^2f^2]S_n^2(f+f_m)\ df + \frac{T_s^2}{2w^2}\left(\frac{N}{S}\right)\int_{-\frac{1}{2T_s}}^{\frac{1}{2T_s}} [f^4+w^4-2w^2f^2]S_n(f+f_m)\ df + \left(\frac{N}{S}\right)^2\left(\frac{1}{320w^2T_s^2}+\frac{w^2T_s^2}{4}-\frac{1}{24}\right)\right\}$$

where

f_m: the true mean frequency,

$S_n(f)$: the normalized power spectrum, i.e,

$S_n(f)=S(f_i)/S$ where $S=\sum S(f_i)$,

W: the true spectrum width and

N: a constant white noise power .

For a narrow Gaussian spectrum without phase noise, the variances can then be simplified to

$$\mathrm{var}(\hat{f}) = \frac{1}{MT_s^2}\left[\frac{wT_s}{4\sqrt{\pi}} + 2(wT_s)^2\left(\frac{N}{S}\right) + \frac{1}{12}\left(\frac{N}{S}\right)^2\right] \quad \text{and}$$

$$\mathrm{var}(\hat{w}) = \frac{1}{MT_s^2}\left[\frac{3wT_s}{32\sqrt{\pi}} + (wT_s)^2\left(\frac{N}{S}\right) + \left(\frac{1}{320w^2T_s^2} + \frac{w^2T_s^2}{4} - \frac{1}{24}\right)\left(\frac{N}{S}\right)^2\right] .$$

Unless the spectrum width is small compared to the Nyquist interval then zero mean assumption is needed to validate results. With the zero mean assumption, this analysis of the phase noise effect can validate the simplified derivations for other than very narrow spectra.

Considering Gaussian phase noise, The normalized spectrum $S_n(f)$ becomes

$$S_n(f) = e^{-2\sigma^2}\sum_{k=0}^{\infty}\frac{2^k\sigma^{2k}}{\sqrt{2\pi}\left(w^2+k\frac{\Delta f_c^2}{2}\right)^{\frac{1}{2}}\,k!}\exp\left(-\frac{f^2}{2\left(w^2+k\frac{\Delta f_c^2}{2}\right)}\right) \qquad (2.15)$$

where w is the width of the Gaussian spectrum without phase noise. Since the phase noise power is very small ($\sigma<0.5$) in quality oscillators, the normalized spectrum can be approximated very accurately by the first four terms, i.e.,

$$S_n(f) = e^{-2\sigma^2}\left[\frac{1}{\sqrt{2\pi}\,w}e^{\frac{f^2}{2w^2}} + \frac{2\sigma^2}{\sqrt{2\pi}\,(w^2+\Delta f_c^2/2)^{\frac{1}{2}}}e^{\frac{f^2}{2(w^2+\Delta f_c^2/2)}}\right.$$

$$+ \frac{2\sigma^4}{\sqrt{2\pi}\,(w^2+\Delta f_c^2)^{\frac{1}{2}}}e^{\frac{f^2}{2(w^2+\Delta f_c^2)}}$$

$$\left. + \frac{4\sigma^6}{3\sqrt{2\pi}\,(w^2+\frac{3}{2}\Delta f_c^2)^{\frac{1}{2}}}e^{\frac{f^2}{2(w^2+\frac{3}{2}\Delta f_c^2)}}\right] .$$

Using this spectrum expression, the variances were rederived and the results are given in Appendix A. From these expressions, one can investigate the effect of varying the spectral distribution of the phase jitter (parameter Δf_c) and also the effect of varying the phase noise power (parameter σ^2). Figure 15 shows that the standard deviation of the mean estimate is increased as $\Delta f_c T_s$ increases for the given phase noise power. From Figure 16, it also can be seen that broadening the phase noise spectrum increases the standard deviation of the width estimate.

Although a Gaussian phase noise assumption may be reasonable, and with this assumption a mathematically tractable analytic analysis is possible, the effect of phase noise may actually be dependent upon the specific noise model selected. For this reason, as in the previous section,

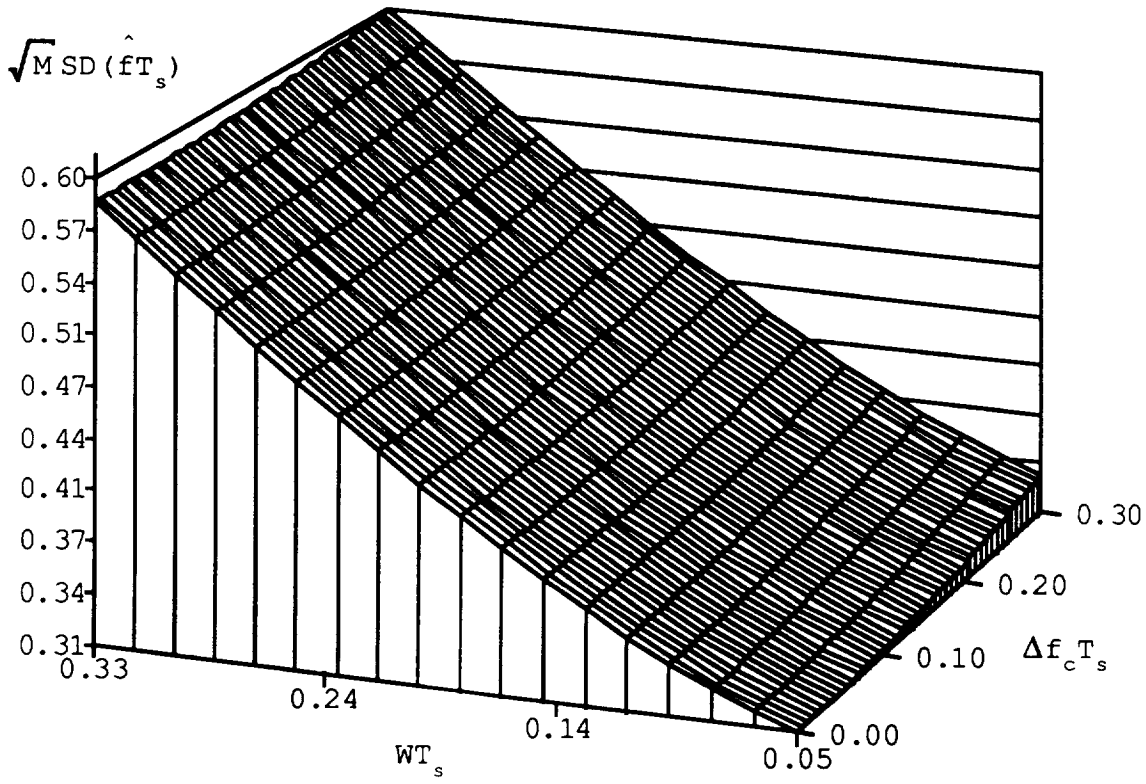

Figure 15. Error Standard Deviation of DFT Mean Estimate Considering Oscillator Phase Noise

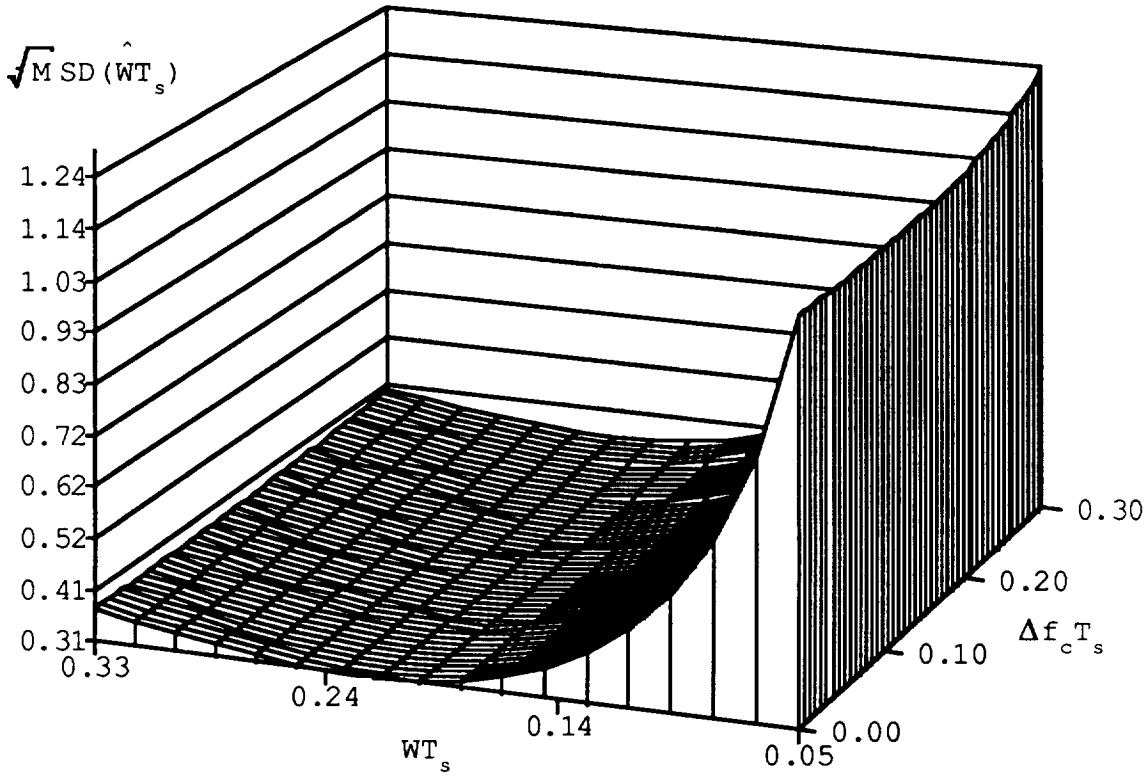

Figure 16. Error Standard Deviation of DFT Width Estimate Considering Oscillator Phase Noise

another approach was developed to analyze the effect of any given phase noise spectrum $S_\phi(f)$ which may be defined by interpolated experimental data or which may be some other kind of appropriate phase noise model. For the specific phase noise spectrum, $S_\phi(f)$, the procedure to obtain the variances of Gaussian Doppler spectrum with phase noise is described in Figure 17 using block diagrams. With this approach, published interpolated phase noise data [34] were processed to investigate DFT based spectral parameter estimation errors. As seen from Figure 18, the phase noise effect is almost negligible as might be expected, since the given phase noise spectrum is extremely narrow and contains very little power.

Limitation of Clutter Cancellation Capability

Ground clutter returns in an airborne Doppler weather radar are typically dominated by a very strong spectral power around the Doppler frequency corresponding to the aircraft ground speed. This is treated as the zero frequency reference in the discussions presented here. This ground clutter return is assumed to be from stationary structures on the ground and the ground itself. Additional clutter may also be present as return from moving objects (vehicles, etc.) on the ground. Without proper clutter cancellation, the spectrum moment estimates associated with the weather return may be so seriously biased that they do not provide reliable information for windshear detection [35]. It is considered that a 10 dB signal-to-clutter ratio (SCR) is needed for

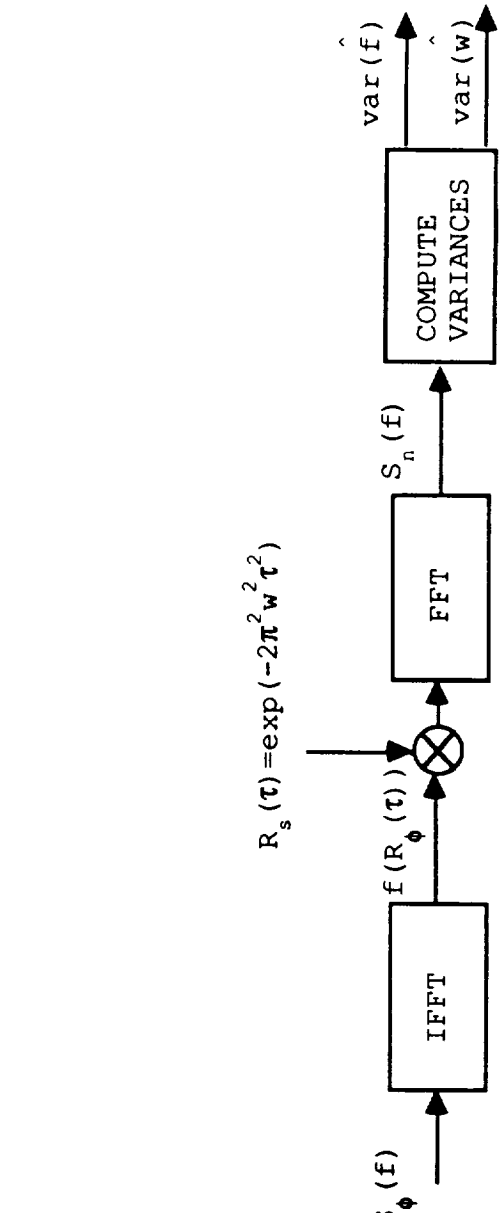

Figure 17. Computation Diagram

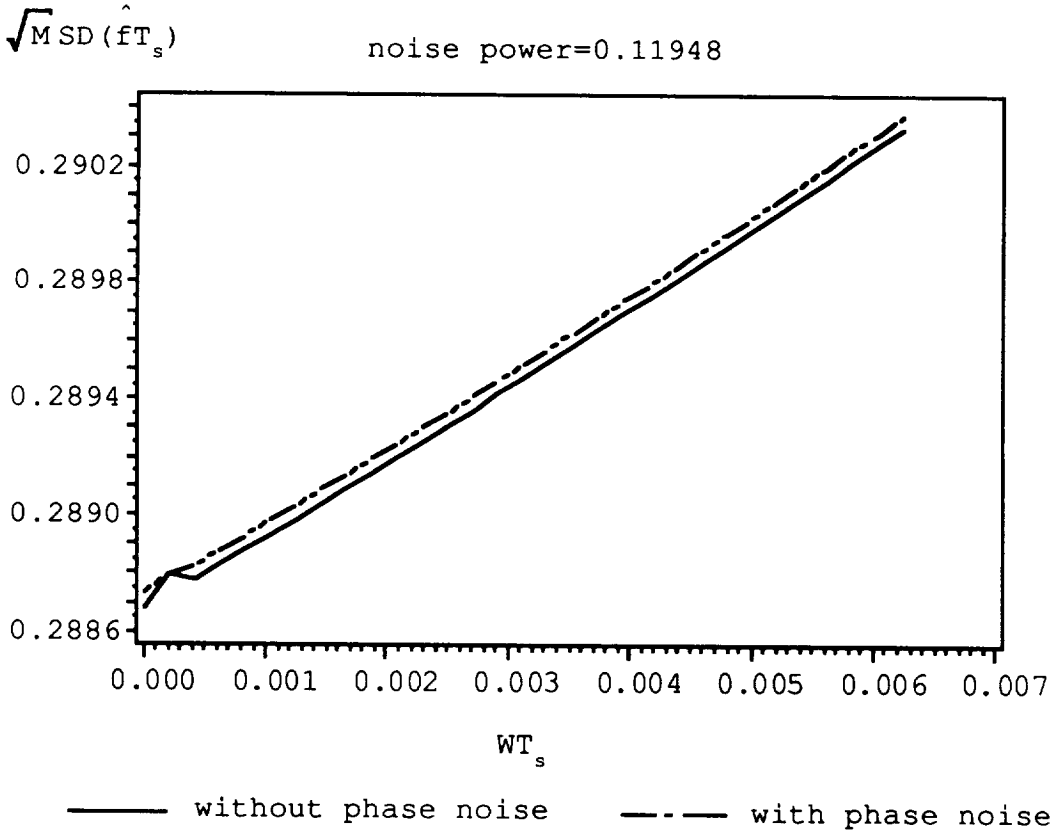

Figure 18. Comparison of Error Standard Deviation of the DFT Mean Estimate

accurate mean velocity estimation via a pulse pair processor while the spectrum width estimation may require 15 dB SCR [36]. This means that at least a 10 dB SCR should be achieved by filtering clutter power. Clutter power located around zero frequency can be removed very effectively using a high pass filter which attenuates low frequency powers to the desired level in a stopband region, but the width of stopband should be carefully selected to avoid elimination of low frequency weather signals. When the clutter spectrum is narrow, clutter cancellation can be done very successfully without degrading the weather spectrum. However, phase noise in a radar system will broaden the clutter spectrum making some portions of power spill into a pass band region limiting clutter cancellation capability. This may be a problem particularly in the case of a dry microburst situation where the weather signal is much weaker than the clutter return.

If it is assumed that the clutter and weather return spectra are both Gaussian, the return spectrum can be modeled as the sum of two normal functions

$$S(f) = \frac{C}{\sqrt{2\pi}\,W_c}\exp\left(-\frac{f^2}{2W_c^2}\right) + \frac{1}{\sqrt{2\pi}\,W_s}\exp\left(-\frac{(f-f_d)^2}{2W_s^2}\right) \qquad (2.16)$$

where $C = 10^{-(SCR/10)}$, f_d is the mean frequency of a weather return spectrum, the clutter is assumed to be zero mean, and W_c and W_s are the spectrum width of clutter and weather return

respectively. Considering the phase noise effect and using Equation (2.15), Equation (2.16) is rewritten as

$$S(f) = Ce^{-2\sigma^2}\sum_{k=0}^{\infty}\frac{2^k\sigma^{2k}}{\sqrt{2\pi}\,(W_c^2+k\frac{\Delta f_c^2}{2})^{1/2}}\exp\left(-\frac{f^2}{2(W_c^2+k\frac{\Delta f_c^2}{2},}\right)$$

$$+e^{-2\sigma^2}\sum_{k=0}^{\infty}\frac{2^k\sigma^{2k}}{\sqrt{2\pi}\,(W_s^2+k\frac{\Delta f_c^2}{2})^{1/2}}\exp\left(-\frac{(f-f_d)^2}{2(W_s^2+k\frac{\Delta f_c^2}{2})}\right) . \qquad (2.17)$$

Here, it should be noted that a Gaussian phase noise spectrum has been assumed. Since σ is usually very small as described before, Equation (2.17) can be approximated using the first four terms of the infinite summation. Considering the use of an ideal high pass filter having the stopband width of 2B and an attenuation value of ATT in dB is assumed, the SCR of the filtered return spectrum is represented by

$$SCR = 10\log_{10}\left(\frac{SR}{CR}\right)$$

where CR and SR can be expressed as

$$CR = Ce^{-2\sigma^2}\left[Q\left(\frac{B}{W_c}\right)+2\sigma^2Q\left(\frac{B}{W_1}\right)+2\sigma^4Q\left(\frac{B}{W_2}\right)+\frac{4}{3}\sigma^6Q\left(\frac{B}{W_3}\right)\right]$$

$$+10^{-ATT/10}Ce^{-2\sigma^2}\left[\left(1-Q\left(\frac{B}{W_c}\right)\right)+2\sigma^2\left(1-Q\left(\frac{B}{W_1}\right)\right)\right.$$

$$\left.+2\sigma^4\left(1-Q\left(\frac{B}{W_2}\right)\right)+\frac{4}{3}\sigma^6\left(1-Q\left(\frac{B}{W_3}\right)\right)\right]$$

where

$$W_k=(W_c^2+k\frac{\Delta f_c^2}{2})^{1/2},\quad Q(x)=2\int_x^{\infty}\frac{1}{\sqrt{2\pi}}e^{-\gamma^2/2}d\gamma \quad \text{and}$$

$$SR = e^{-2\sigma^2}[(1-P(\overset{B-f_d}{W_s}))+2\sigma^2(1-P(\overset{B-f_d}{Y_1}))+2\sigma^4(1-P(\overset{B-f_d}{Y_2}))+$$

$$\frac{4}{3}\sigma^6(1-P(\overset{B-f_d}{Y_3}))]+10^{-ATT/10}e^{-2\sigma^2}[P(\overset{B-f_d}{W_s})+2\sigma^2P(\overset{B-f_d}{Y_1})+$$

$$2\sigma^4P(\overset{B-f_d}{Y_2})+\frac{4}{3}\sigma^6P(\overset{B-f_d}{Y_3})]$$

where

$$Y_k=(W_s^2+k\frac{\Delta f_c^2}{2})^{1/2},\quad P(\frac{B-f_d}{z})=\int_{\frac{-B-f_d}{z}}^{\frac{B-f_d}{z}}\frac{1}{\sqrt{2\pi}}e^{-\gamma^2/2}\,d\gamma.$$

The resulting SCR figures after filtering the return spectrum are plotted for various values of f_d by changing phase noise power σ^2. It has been shown elsewhere [35] that the SCR of a filtered spectrum is decreased if the weather spectrum is not well separated from the stopband region. The emphasis here is placed upon the phase noise effect. It should be noted that the results are obtained assuming use of an ideal high pass filter and no aliasing effect in terms of the spectral representation. Figures 19 through 22 are obtained by

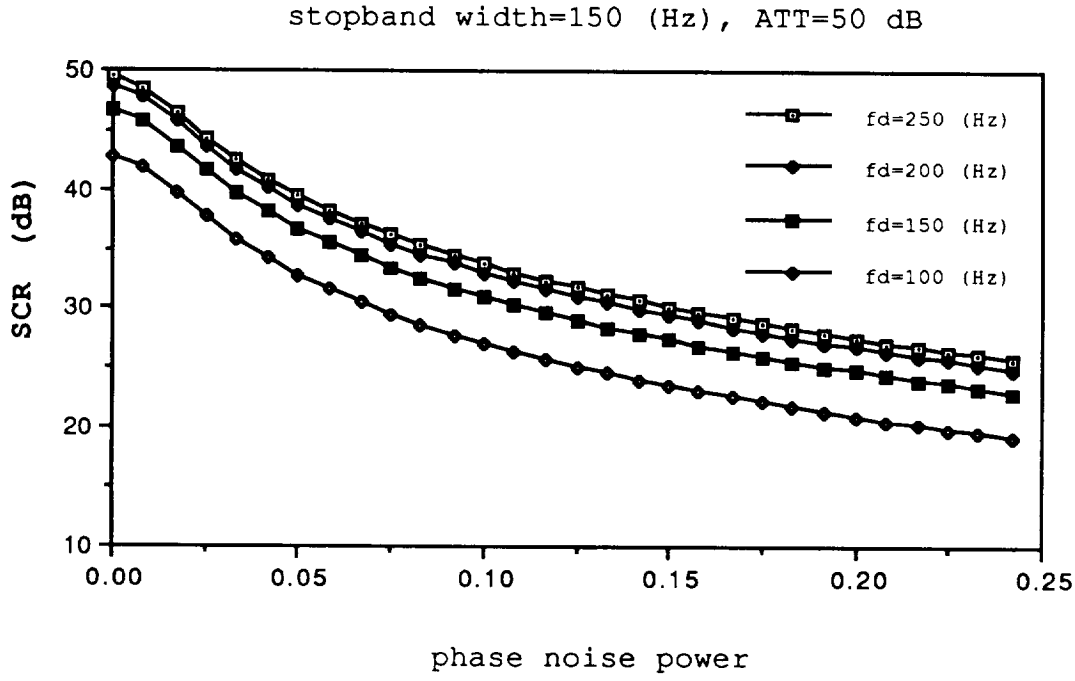

Figure 19. Phase Noise Effects on Clutter Filtering of 50 dB Stopband Attenuation for a Doppler Weather Return with 0 dB SCR

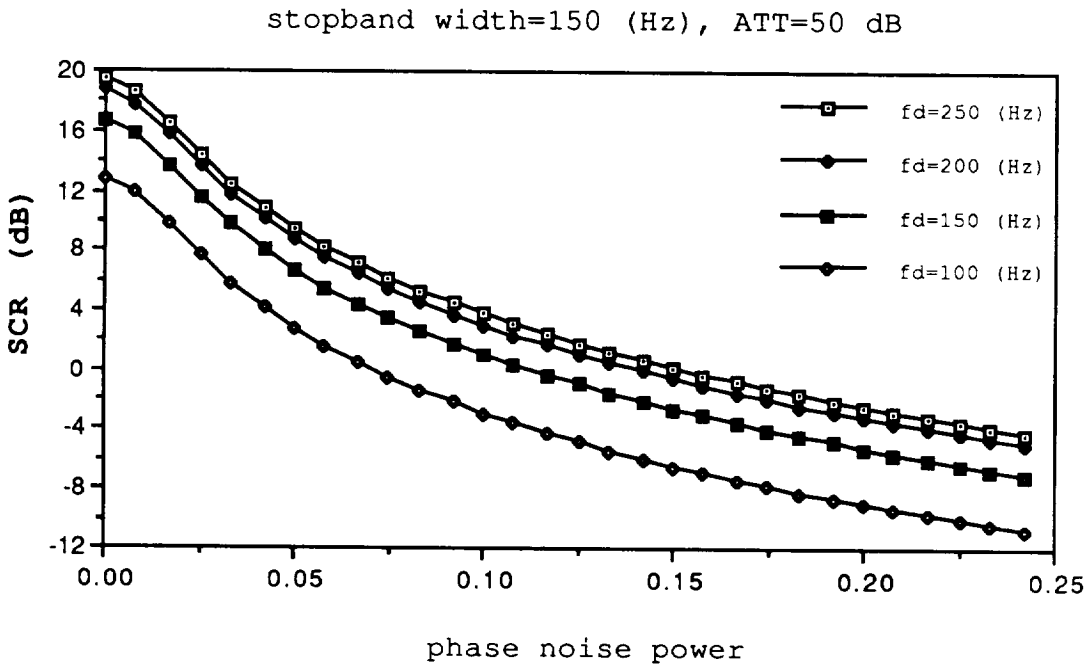

Figure 20. Phase Noise Effects on Clutter Filtering of 50 dB Stopband Attenuation for a Doppler Weather Return with -30 dB SCR

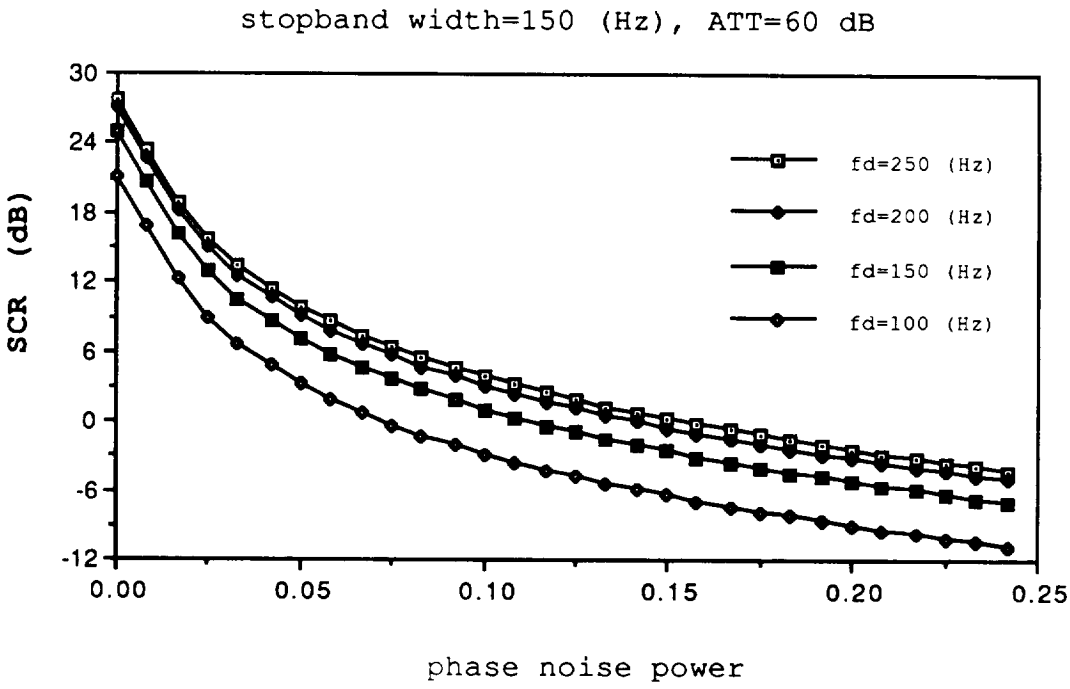

Figure 21. Phase Noise Effects on Clutter Filtering of 60 dB Stopband Attenuation for a Doppler Weather Return with -30 dB SCR

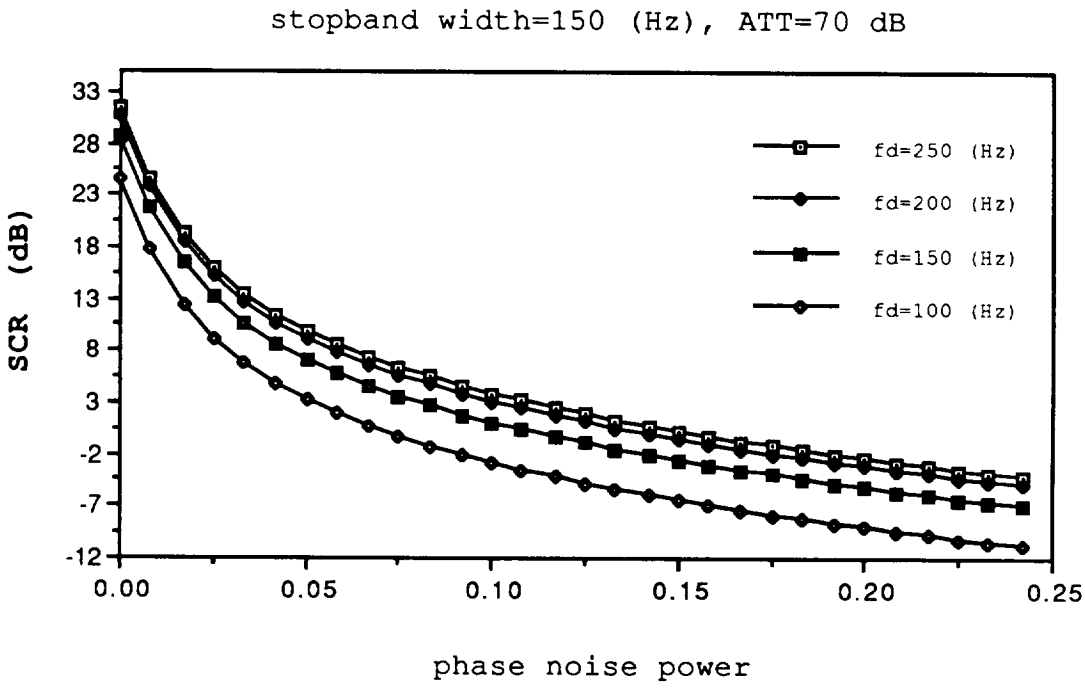

Figure 22. Phase Noise Effects on Clutter Filtering of 70 dB Stopband Attenuation for a Doppler Weather Return with -30 dB SCR

changing the attenuation value with the fixed stop band width of 150 Hz. All plots show that the SCR of a filtered spectrum is decreased as the phase noise power increases. The undesirable effect of clutter filtering resulting in some elimination of the weather signal power is also noticed. As expected, Figure 19 shows that phase noise is not a serious problem if the weather signal is strong or comparable to the clutter return. However, as can be seen from Figures 20 and 21, any small phase noise may seriously limit the clutter cancellation capability when the clutter power is much stronger than the weather signal. Even with the ideal high pass filter with 70 dB attenuation in the stopband, more than 10 dB SCR cannot be achieved if phase noise power exceeds 0.05, as shown in Figure 22.

Proposed Measurement of Radar System Phase Noise

It is desirable to determine the effect of phase jitter noise on the error in the pulse pair and DFT parameter estimates to understand the expected radar system performance. This section describes a procedure for the bench test of the radar to yield an estimate of the effective phase jitter power spectrum. For this purpose, the transmitted signal with some delay time is to be fed directly into the receiver. I,Q data would then be obtained to analyze phase jitter in the absence of a return Doppler signal. A return signal is not included in the procedure since just the pure

phase noise term is of interest. Figure 23 illustrates the setup.

It is anticipated that the stable local oscillator (STALO) will be a major potential contributor to phase jitter, even though it may be very small. The following analysis is based upon modelling the STALO phase as time varying. At the receiver illustrated in the Figure 23, the demodulated noise signal is

$$V_o(t) = I(t) + jQ(t) = e^{j(\phi(t) - \phi(t-t_d))}$$

where t_d is the delay line time (delay time is less than 25 μsec in the case of 7.5 km maximum detection range). Here, STALO oscillator phase jitter can affect the modulated signal at the transmitter and after a delay t_d can affect the demodulated signal. The interest here is in measurement of the effects of pulse to pulse phase jitter as will be observed at the receiver.

The autocorrelation of the receiver output $R_j(T_s, t_d)$ will be a function of both the transmitter/receiver delay time t_d and the pulse pair separation T_s. It can be expressed as

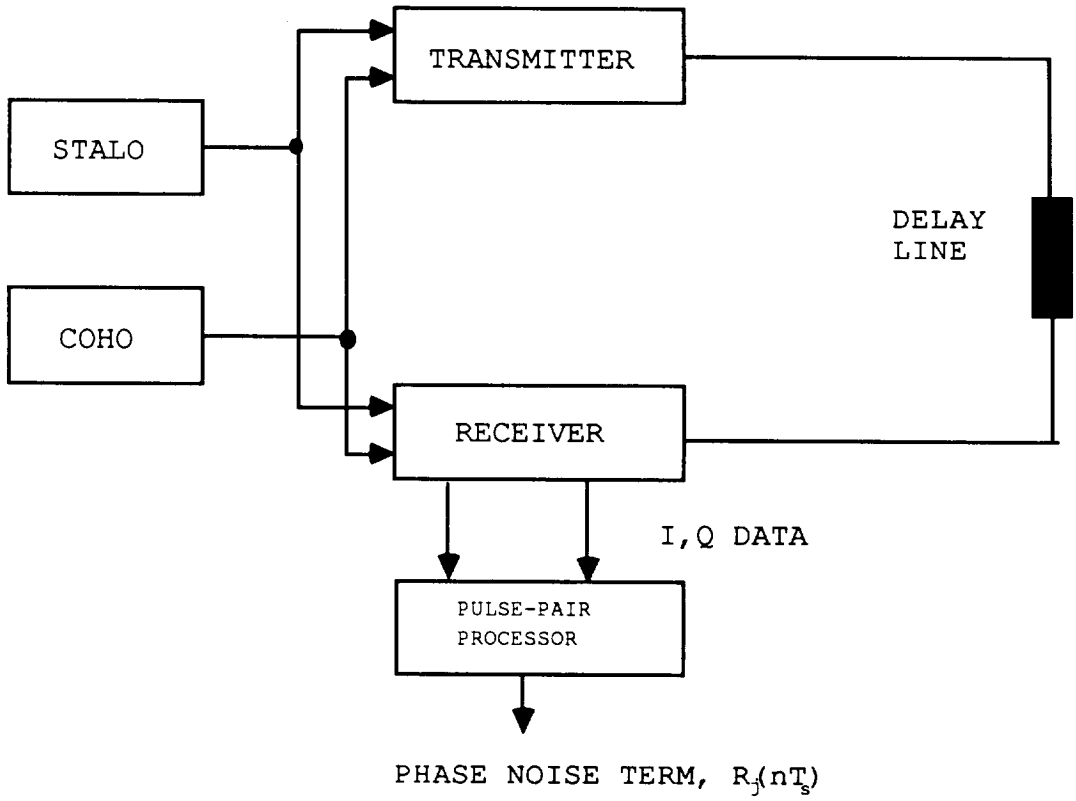

Figure 23. Diagram for the Laboratory Measurement

$$R_j(T_s,t_d)=E[V_0(t)V_0^*(t+T_s)]$$

$$=E[e^{j(\phi_1(t)-\phi_1(t-t_d))}\,e^{-j(\phi_1(t+T_s)-\phi_1(t+T_s-t_d))}]$$

$$=E[e^{j\phi_1(t)}\,e^{-j\phi_1(t+T_s)}\,e^{-j\phi_1(t-t_d)}\,e^{j\phi_1(t+T_s-t_d)}] \qquad (2.18)$$

where $\phi_1(t)$ represents the phase variation with time in the radar oscillator. With a PRF on the order of 3-4 kHz, the pulse separation is perhaps two orders of magnitude greater than t_d. It is expected that phase variations within the radar would be very slow such that the intra-pulse variation can be considered insignificant, but the delay time t_d may be long enough to experience a measurable phase variation. Thus if $t_d<1$ μsec the radar phase at the transmitter and at the receiver can be considered identical for each pulse and jitter present at the transmitter is exactly cancelled at the receiver, i.e., $R_j=1.0$. In the case of much longer t_d delays, $\phi_1(t)$ and $\phi_1(t-t_d)$ can be considered uncorrelated and the expression in (2.18) can be reduced to

$$R_j(T_s,\infty)=R_j(T_s)=E[e^{j\phi_1(t)}\,e^{-j\phi_1(t+T_s)}]E[e^{-j\phi_1(t-t_d)}\,e^{j\phi_1(t-t_d+T_s)}]$$

$$=\{E[e^{j\phi_1(t)}\,e^{-j\phi_1(t+T_s)}]\}^2$$

$$=\exp(-2\{\int_{-\infty}^{\infty}S_\phi(f)\,df-R_\phi(T_s)\}) \qquad (2.19)$$

using (2.10). Equation (2.19) represents the worst case that can be assumed since no phase cancellation occurs. With realistic delays, t_d, what actually will occur is probably $R_j(T_s)<R_j(T_s,t_d)<1.0$, since $R_j(T_s,t_d)$ would generally decrease as t_d increases.

The analytical result suggests that a practical measurement of $R_j(nT_s,t_d)$ may be possible using sampled I,Q data if the number of samples is very large , i.e.,

$$\hat{R}_j(nT_s) = \frac{1}{M}\sum_{i=0}^{M-1} V_o(iT)\,V_o^*(iT+nT_s)$$

where nT_s is the delay between pairs of pulses separated by n pulse repetition periods. Characterizing $R_j(nT_s,t_d)$ versus n for specific values of t_d will then delineate the phase jitter power spectrum due to the radar instabilities. The resulting measured complex autocorrelation could then be used in (2.12) and (2.13) to correctly specify the parameter estimation error for the actual system used.

Of course, it is expected that the measurement results will represent R_j as a composite of all system phase noises.

Summary

This chapter has developed a procedure for specifying the phase stability of a Doppler radar system through definition of the relationship between pulse to pulse phase error (phase jitter) and weather spectrum parameter

estimates. Both the pulse pair and DFT based estimators have been considered. The effect of phase jitter on post clutter rejection filtering signal to clutter ratio has also been analyzed. Finally a procedure for measuring the phase stability of a radar system has been proposed.

CHAPTER III

SPECTRUM SKEWNESS EFFECTS ON PULSE PAIR ESTIMATION

Introduction

The pulse pair estimator calculates the first two moments of the Doppler spectrum from estimates of the complex autocorrelation function at lag T_s. Goodness of this estimator is typically determined by examination of the bias and the variance of the moment estimates. To analyze the bias in the pulse pair estimates, consider the process autocorrelation function $R(T_s)$ expressed in terms of the true mean Doppler frequency f_d [28]:

$$R(T_s) = e^{j2\pi f_d T_s} \int_{\frac{-1}{2T_s}}^{\frac{1}{2T_s}} S'(f) e^{j2\pi f T_s} \, df \tag{3.1}$$

where $S'(f)$ is the zero-mean representation of the weather Doppler spectrum. Unbiasedness of pulse pair estimates is based on the assumption that a spectrum is symmetric or so narrow that the imaginary part of the integral in (3.1) can be considered as zero, i.e. [28],

$$\int_{\frac{-1}{2T_s}}^{\frac{1}{2T_s}} S'(f)\sin(2\pi f T_s)\, df = 0 \quad .$$

However, the weather return Doppler spectrum is often broad and not symmetric thus causing a bias. This bias effect is analyzed here using a skewed Gaussian spectrum model with various spectrum widths.

Analysis of Bias Errors

In this analysis, a skewed spectrum will be modelled as piecewise Gaussian with appropriate normalization, given by

$$S_n(f) = \frac{2}{1+p}\,\frac{1}{\sqrt{2\pi}\,w_1}\, e^{-\frac{f^2}{2w_1^2}} \qquad \text{when } f \leq 0$$

$$S_n(f) = \frac{2p}{1+p}\,\frac{1}{\sqrt{2\pi}\,w_2}\, e^{-\frac{f^2}{2w_2^2}} \qquad \text{when } f > 0 \qquad (3.2)$$

where the standard deviation ratio $p=w_1/w_2$ defines the degree of skewness, g, i.e. [37],

$$g = \frac{4\sqrt{2}}{\sqrt{\pi}}\left[(p^{-2}+1)^{-\frac{3}{2}} - (p^2+1)^{-\frac{3}{2}}\right] .$$

This skew parameter varies proportionally to skew from g=0 for no skew (p=1) to larger values, e.g., g=3.14 for a case which may be considered large skew (p=10). Figure 24 shows the relationship between the parameter, p and the degree of skewness, g. For a narrow Gaussian spectrum with symmetry, i.e., $w_1=w_2=w$, the integral in the autocorrelation function (3.1) can be reduced to one simple term, $\exp(-2\pi^2 w^2 T_s^2)$, but the results for the skewed spectrum model will include both a real term

$$a= \int_{-\frac{1}{2T_s}}^{\frac{1}{2T_s}} S_n(f)\cos(2\pi f T_s)\ df= \frac{2}{1+p}\ (\frac{1}{2}e^{-2\pi^2 w_1^2 T_s^2} + \frac{w_2}{2w_1}e^{-2\pi^2 w_2^2 T_s^2})$$

and an imaginary term

$$b= \frac{2}{1+p}\int_0^{\frac{1}{2T_s}}[\frac{1}{\sqrt{2\pi}\,w_1}(e^{-\frac{f^2}{2w_2^2}} - e^{-\frac{f^2}{2w_1^2}})]\sin(2\pi f T_s)\ df\ .$$

Using these terms, the bias in the pulse pair mean and width estimates can be represented by

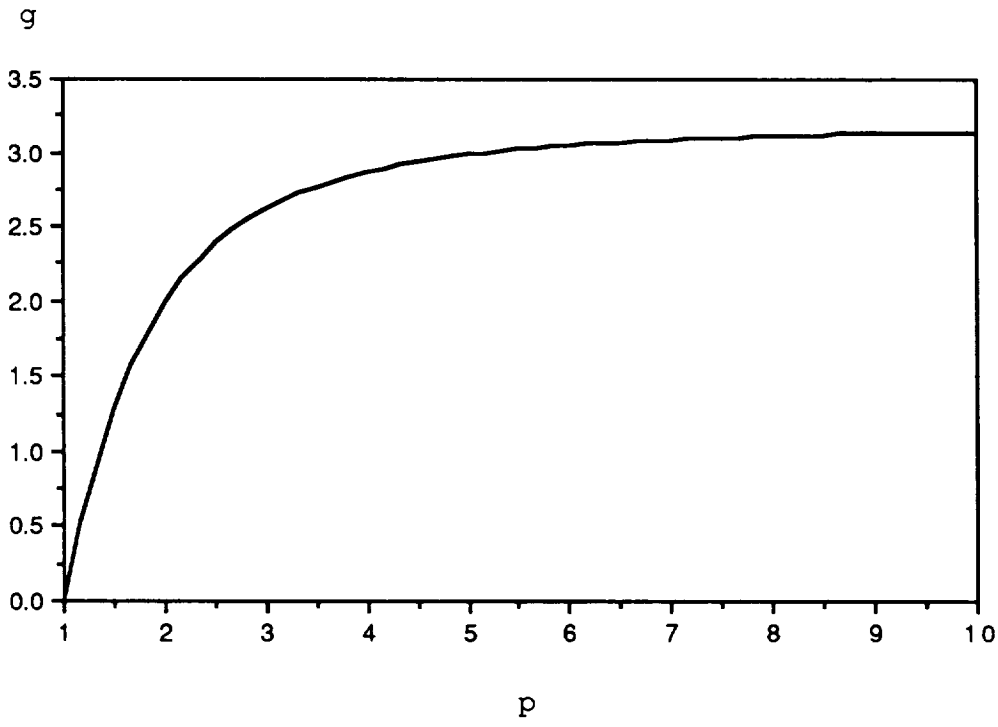

Figure 24. Relationship between the Parameter, p and the Degree of Skewness, g

$$\text{mean bias} = \left| \frac{1}{2\pi T_s} \tan^{-1}\left(\frac{b}{a}\right) - f_m \right|$$

$$\text{width bias} = \left| \left| \frac{1}{\sqrt{2}\,\pi T_s} \right| \ln\left(\frac{1}{\sqrt{a^2+b^2}}\right) \right|^{1/2} - W \Bigg| \qquad (3.3)$$

where true mean, f_m and true width, W are described from Equation (3.2) as

$$f_m = \int_{-\frac{1}{2T_s}}^{\frac{1}{2T_s}} f S_n(f)\, df = \frac{2}{1+p} \frac{1}{\sqrt{2\pi}} (pw_2 - w_1)$$

$$W^2 = \int_{-\frac{1}{2T_s}}^{\frac{1}{2T_s}} (f-f_m)^2 S_n(f)\, df = \frac{1}{1+p}(w_1^2 + pw_2^2) - f_m^2 \quad .$$

Estimate biases as given by Equation (3.3) are plotted as functions of the true width W and the skewness parameter g in Figures 25 and 26. In Figure 25 if there is no skew (g=0) tne pulse pair estimator is unbiased. As skew is increased there is a sharp increase in the bias. Once the skew parameter g>0, the percentage bias error is essentially independent of the specific value of skew but is strongly related to the spectrum width W. As seen, the bias error due to skewness is not negligible if the spectrum is broad. Figure 26 shows that

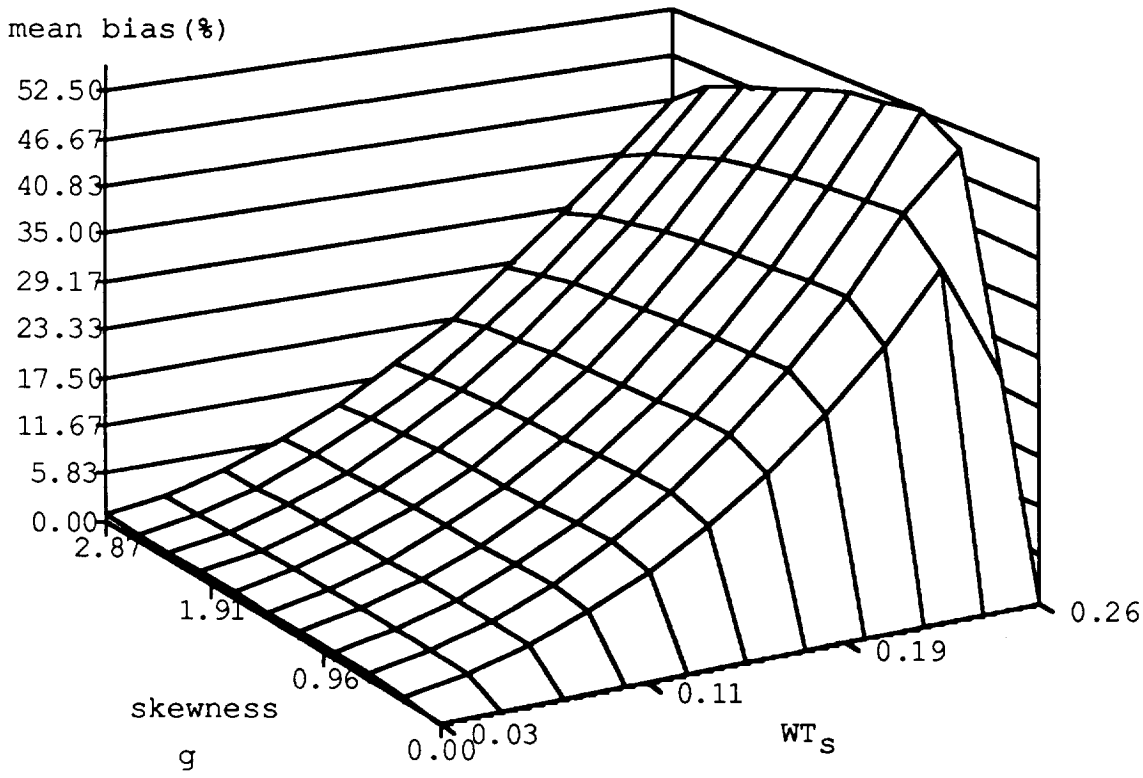

Figure 25. Mean Bias Error in Pulse Pair Estimates

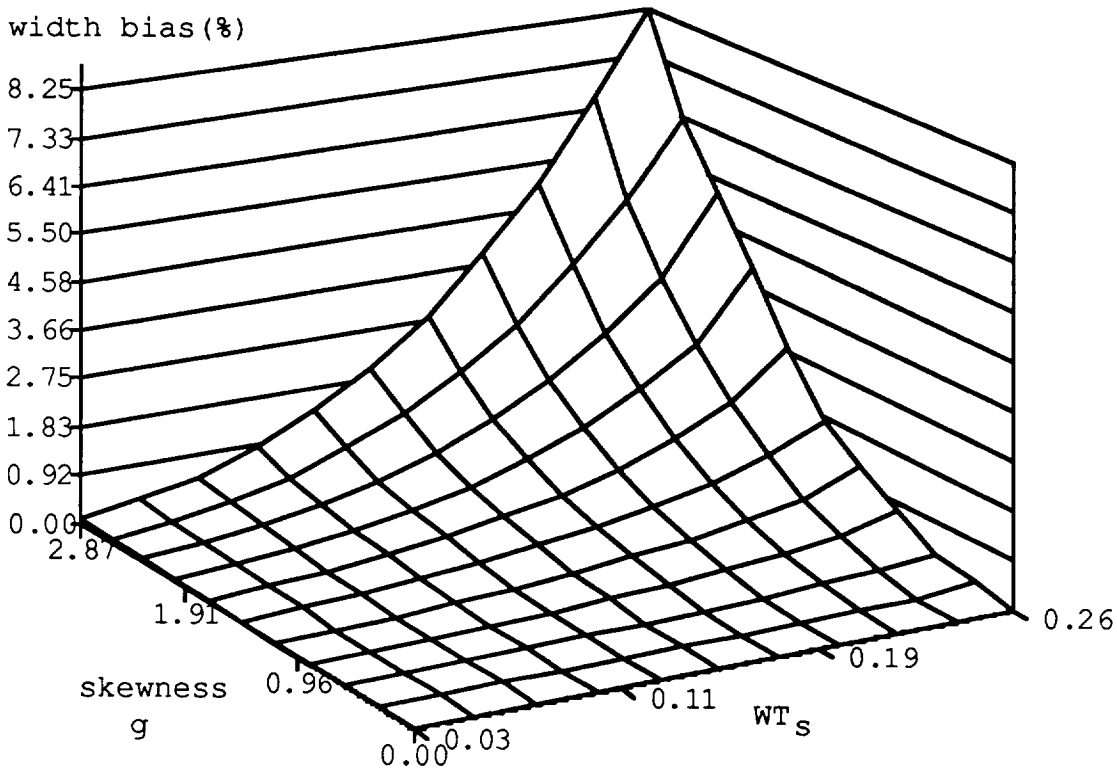

Figure 26. Width Bias Error in Pulse Pair Estimates

a broad spectrum with a large degree of skewness can degrade the quality of pulse pair width estimates, but it does not seem to be as serious compared to the pulse pair mean estimate error in Figure 25.

To get a more complete measure of the effect of skewness on the pulse pair mean estimate, Figure 27 compares the estimate r.m.s. error for the case of the skewed spectrum with that of a symmetric Gaussian spectrum having an equivalent width. As seen from Figure 27, the error caused by the skewness may seriously degrade the pulse pair estimation quality if the return Doppler spectrum width is 40% or more of the Nyquist bandwidth.

Poly-pulse pair Method

Since the pulse pair mean estimator bias is sensitive to skew, an alternative may be desirable. Therefore the poly-pulse pair method [38] is investigated here as a possible way of minimizing such errors. The pulse pair mean estimator algorithm uses the first lag of the complex autocorrelation estimate and is based on a linear approximation to the derivative of the phase function of the complex autocorrelation estimate, i.e.,

$$\hat{f} = \frac{1}{2\pi} \left. \frac{d\hat{\theta}(T_s)}{dT_s} \right|_{T_s=0} \cong \frac{1}{2\pi} \frac{\hat{\theta}(T_s)}{T_s}$$

$$\sqrt{(\sqrt{M}\,SD(\hat{f}T_s))^2+M(T_sB)^2}$$

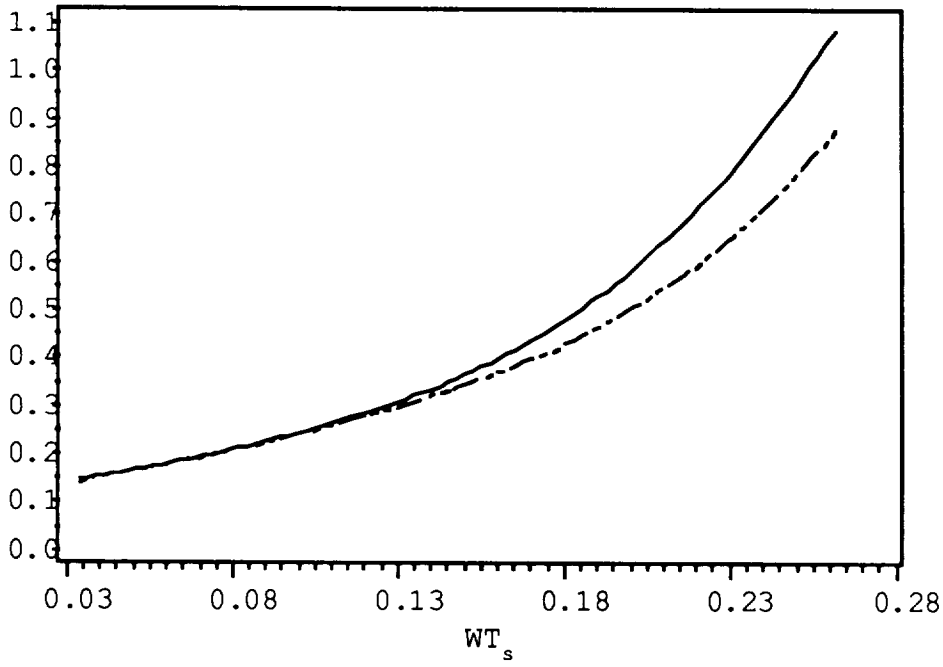

——— R.M.S. Error of Skewed Spectrum

------ R.M.S. Error (standard deviation) of Symmetric Spectrum with Equivalent width

Figure 27. R.M.S. Error of Skewed Gaussian Spectrum for a Certain Degree of Skewness (g=1.99)

where $\hat{\theta}(T_s)$ is the phase function. There will be no approximation error for a symmetric spectrum, but a large error can occur in a skewed spectrum since $\hat{\theta}(T_s)$ is no longer a linear function of T_s . An alternative which may reduce these errors is to approximate $\hat{\theta}(T_s)$ as a low order polynomial (greater than first order, n=1), i.e.,

$$\hat{\theta}(T_s) \cong \sum_{i=1,\text{odd}}^{n} a_i T_s^i \tag{3.4}$$

where $\theta(T_s)$ is an odd function of T_s [8]. An odd function representation is needed since $R(T_s)$ is the Fourier transform of a real valued spectrum. Then the mean estimate of a skewed spectrum will be

$$\hat{f} = \frac{1}{2\pi} \frac{d\hat{\theta}(T_s)}{dT_s} \Big|_{T_s=0} \cong \frac{1}{2\pi} \hat{a}_1 \ .$$

To estimate a_1 for a particular n>1, the complex autocorrelation function must be estimated for lags other than the first lag value T_S. This can be accomplished with the poly-pulse-pair method [38]. Figure 28 shows that the mean bias error for a spectrum skew of g=1.99 (p=2) can be significantly reduced over a range of spectrum widths using the poly-pulse-pair method. To more completely evaluate the poly-pulse-pair method the variance of these estimates should be compared to the conventional pulse pair method (n=1).

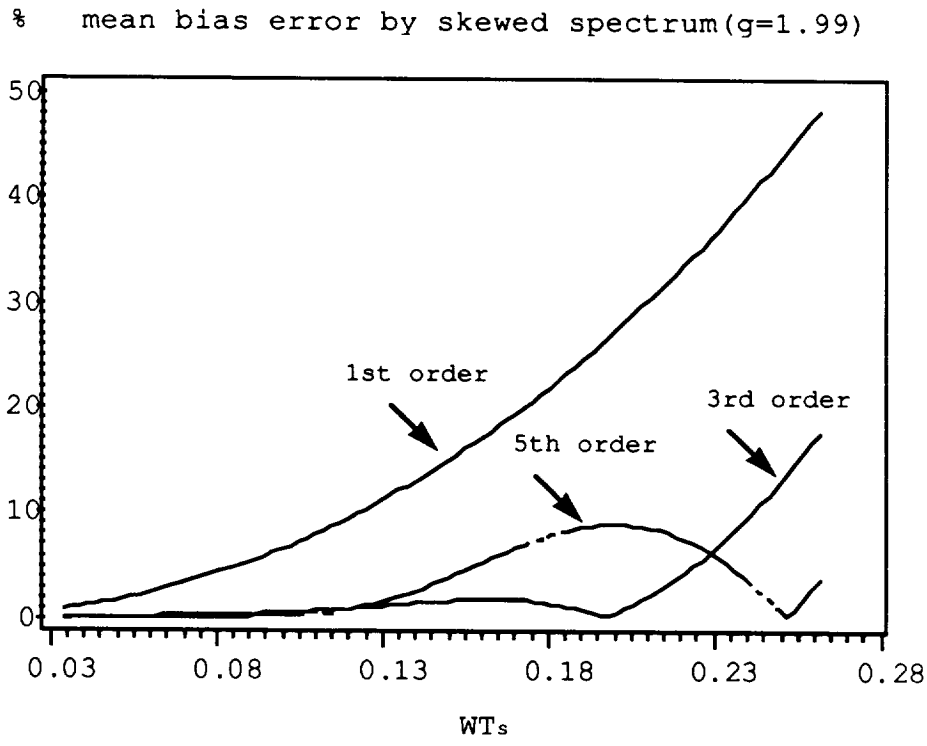

Figure 28. Performance Comparison between Poly-pulse Pair and Conventional Method

Considering a third order polynomial model in Equation (3.4), i.e.,

$$\hat{\theta}(T_s) = \hat{a}_3 T_s^3 + \hat{a}_1 T_s$$

the poly-pulse-pair mean estimate variance can be shown to be

$$\text{var}'(\hat{f}) = \text{var}(\hat{f}) - \frac{T_s^2}{2\pi^2} E\left[\hat{a}_3\hat{a}_1 - a_3 a_1\right] - \frac{T_s^4}{4\pi^2} E\left[\left(a_3 - \hat{a}_3\right)^2\right]$$

where $\text{var}(\hat{f})$ is the variance of the conventional pulse pair method. The first term may be positive or negative and the second term will actually reduce the pulse pair estimate variance. In any case, since the pulse interval T_s is generally very small, the higher order terms may be ignored to yield

$$\text{var}'(\hat{f}) \cong \text{var}(\hat{f}) \ .$$

From these results, it appears that the poly-pulse-pair method can improve the quality of mean estimates by reducing bias errors in a skewed spectrum.

Mode versus Mean Estimation

In the pulse Doppler radar signal processor, when estimating the "average" windspeed in a given range cell, there may be a question as to whether "average" should be the statistical mean or the statistical mode (most probable

value). The pulse pair algorithm will estimate the statistical mean. In the symmetric case the mean and the mode are the same. However, with skewness in the spectrum this is not true as seen in Figure 29 which shows that these two values can differ very largely due to the increased skewness and spectrum width. Figure 30 illustrates the difference between the mode of the skewed spectrum and the pulse pair mean as a function of skew and spectrum width. As the spectrum width increases, this difference is more sensitive to spectrum skew. Therefore, the pulse pair mean estimate tends not to be a good mode estimator for broad spectra. The idea of a mode estimator is developed further in Chapter V. A new approach of characterizing a summary statistic of windspeed within a range cell is presented using a classical harmonic decomposition technique. This indicates potential for overcoming the biased mean estimation problem with a skewed spectrum.

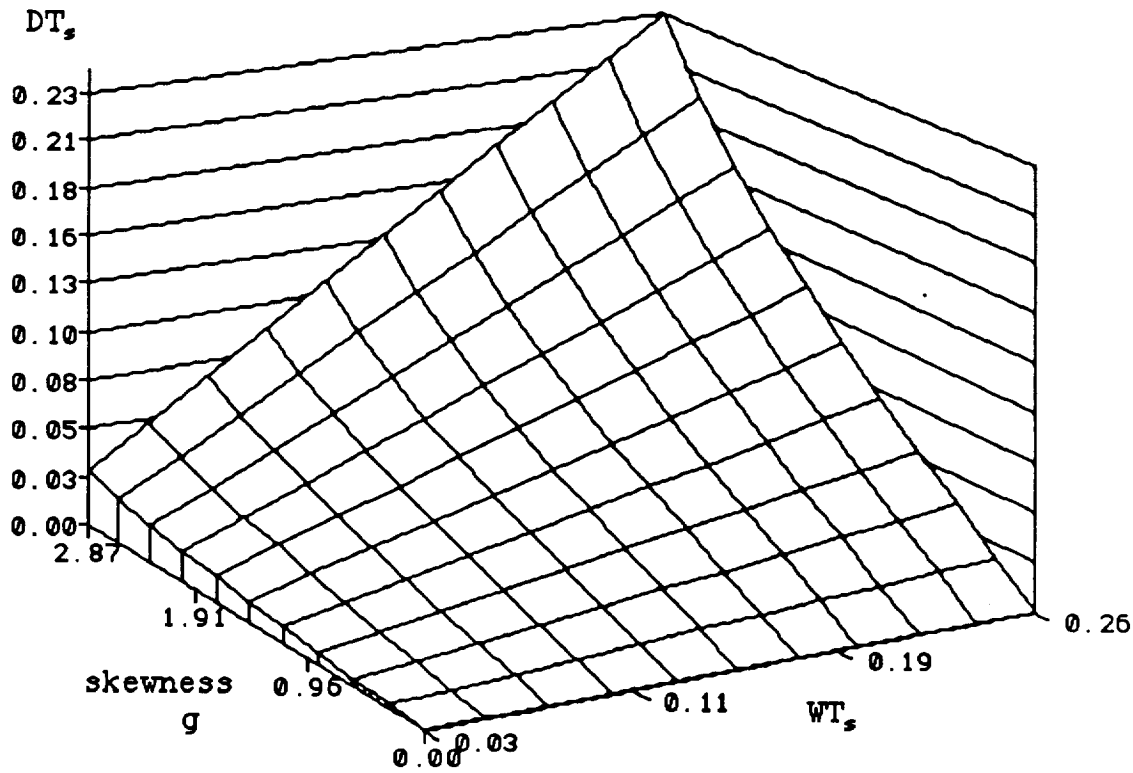

Figure 29. Normalized Difference Value between True Mean and Mode of Skewed Spectrum

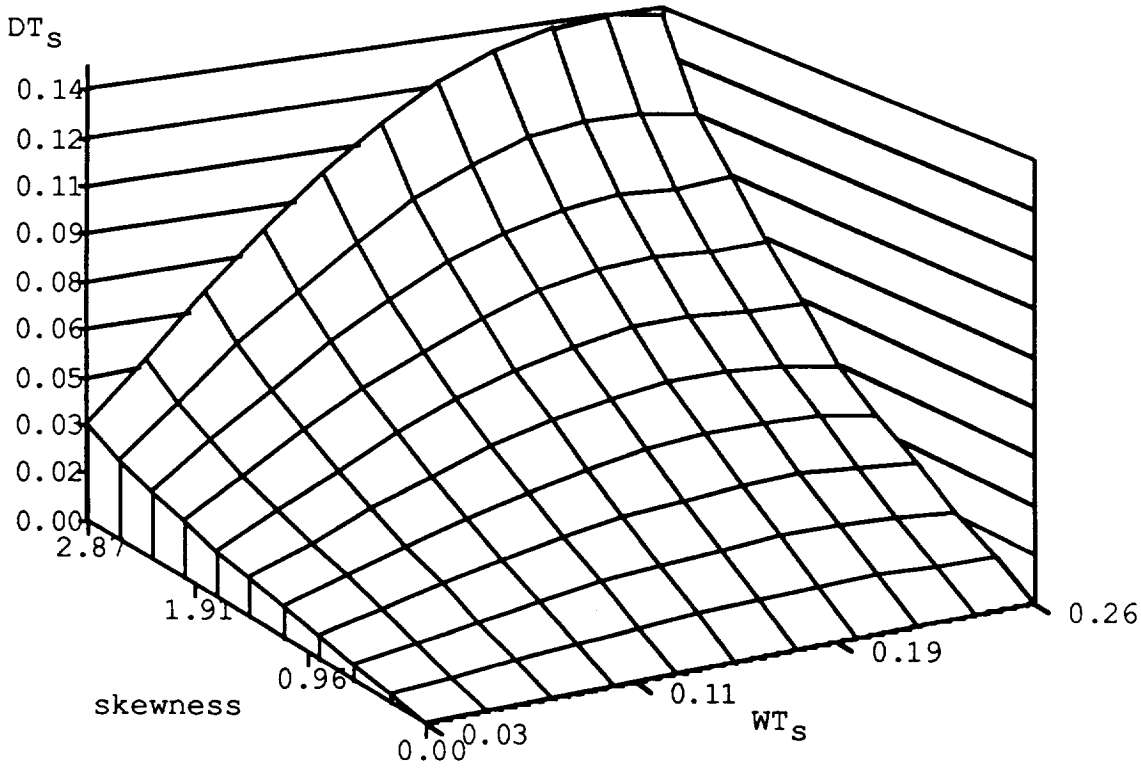

Figure 30. Normalized Difference Value between Pulse Pair Mean Estimate and Mode of Skewed Spectrum

CHAPTER IV

THE MEASUREMENT OF WINDSPEED GRADIENT WITH LOW PRF RADAR

Introduction

A satisfactory airborne radar sensor for the detection of windshear must possess good ranging capability, both in terms of maximum useable range and range resolution. Otherwise the look ahead range will be too short to provide adequate lead time warning of a windshear condition or a hazardous windshear will not be resolved. This suggests a low to medium PRF radar. On the other hand, a capability for unambiguously measuring large Doppler frequencies associated with high windspeed conditions would normally require a higher PRF radar. With adequate range resolution capability, one approach to estimating the change in windspeed throughout a region is to use the difference in mean Doppler from range cell to range cell as a first order estimate of the spatial wind velocity gradient. With this approach, it may not be necessary to estimate large absolute windspeeds in any particular range cell, but only the difference in average windspeeds between range cells, i.e., the windspeed gradient. The magnitude of the windspeed gradient determined from adjacent range cells should be substantially less than the absolute mean windspeed in any given range cell, even for high turbulence environments.

Thus, it appears that it may be possible to relax the PRF requirement for large unambiguous Doppler measurement, allowing a lower PRF to be used to measure the windspeed gradient. This would inherently allow good ranging capability without compromising the value of the system for detecting windshear. The discussion which follows develops this premise by illustrating the effect of measuring Doppler difference frequency with a reduced PRF. Simulated I and Q data are used to investigate the validity of this technique. It is anticipated that many hazardous windshear conditions can be detected with a reduced PRF if this technique is indeed proved to be valid. Relatively simple modification of the signal processing associated with conventional weather radar operating at reduced PRF could enable implementation of the technique.

Aliasing Effect

With a given PRF, unambiguous Doppler measurement is possible within a ± 0.5 PRF range of frequencies. In meteorological measurements where a much wider range of Doppler return frequencies is likely when high windspeed conditions exist, the radar return Doppler which exceeds the PRF/2 magnitude is aliased as a lower frequency. Thus, for highly turbulent conditions where the spread of Doppler frequencies is very high and significant aliasing can take place, the ratio of the peak magnitude of the return at the "mean" Doppler frequency to the level of the return at other

frequencies may be significantly degraded by aliasing. Obviously, reducing the PRF would further degrade this "signal-to-noise" ratio and may reduce the ability to locate the peak magnitude of the estimated spectrum of the return. Of course a reduced PRF directly reduces the signal-to-noise ratio in a given range cell simply because for a fixed observation time the number of signal returns is reduced.

Of perhaps even more significance is the effect of aliasing on the measurement of spectral width of the Doppler return. If the reduced PRF Nyquist interval is inadequate to unambiguously represent the breadth of Doppler frequencies present, there can be no way of estimating this width. Coupled with a reduced signal-to-noise ratio, the ability to detect turbulent windspeed conditions within a range cell with reduced PRF radar appears futile. However, the utility of low PRF in measuring large scale windspeed gradients between range cells may not be so limited.

To evaluate the effect of aliasing, two different scenarios will be examined. In each situation an assumed return with a postulated spectrum will be represented as an I/Q data sequence. This sequence will be examined with DFT processing at a rate associated with a high PRF weather radar processor. The sequence will then be decimated and reprocessed at a rate which would correspond to a reduced PRF. The decimation process not only reduces the number of data samples, but also produces the same data that would have been obtained had a reduced PRF radar been employed.

The first situation includes analysis of a pure complex sinusoid with no added noise. The complex sinusoid represents a specular signal with a one-sided bandwidth. Aliasing with a sinusoid signal does not affect the signal-to-noise ratio but only the frequency estimate of the sinusoid itself. The second situation examined involves an analysis of a simulated weather signal which has a Gaussian frequency spectrum typical of weather returns. This particular type signal is degraded by aliasing quite dramatically when considering the reduced PRF system. However, a useful range of mean Doppler difference can be preserved within the available sampling bandwidth.

Analysis of a Pure Sinusoid

Consider a situation corresponding to a noiseless specular pulse Doppler radar return present in two adjacent range cells. Fourier analysis of a record of sampled values will yield a spectral estimate which is corrupted by spectral leakage associated with the limited observation record and aliasing associated with the limited sampling rate [39]. In the radar situation the data record is limited by the observation time within a range cell and the sampling rate is just the PRF. Using the complex Discrete Fourier Transform (DFT), two complex sinusoids with a difference frequency less than the unambiguous processing frequency range (Nyquist bandwidth) have been analyzed. Using a sampling frequency (PRF) of 250 Hz, Figure 31 illustrates the difference in the

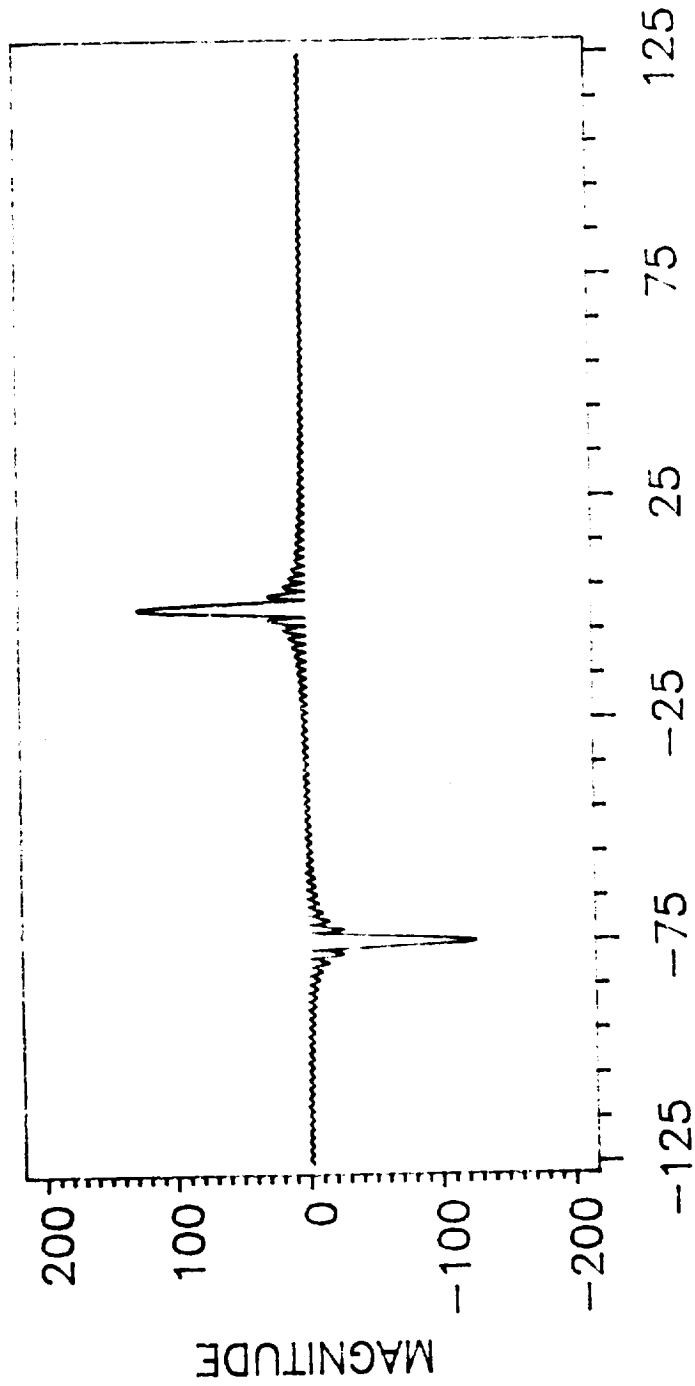

Figure 31. The Frequency Difference of Aliased Complex Sinusoids between 500 Hz and 425 Hz

magnitude of a DFT processed sinusoid at 500 Hz which aliased to 0 Hz and a 425 Hz sinusoid which aliased to -75 Hz. Even though both of these signals are undersampled and the original frequencies are not preserved, the difference frequency between the two sinusoids is clearly evident.

Theoretically, the aliasing effect on a pure sinusoid does not deteriorate the signal-to-noise ratio. It only relocates the peak and prevents unambiguous identification of the actual frequency. However, with spectral leakage associated with the DFT, there is some deterioration of signal-to-noise ratio in the sense that the leakage power is aliased within the processing bandwidth, resulting in a reduced peak to leakage power ratio. This leakage power is effectively cancelled out in the difference processing associated with Figure 31. As a result, any frequency difference which is less in magnitude than one-half the PRF is preserved and can be detected and estimated as the frequency difference between the positive peak and the negative peak.

Based upon this analysis it appears that if the radar return from adjacent range cells is specular the Doppler difference is preserved and easily recognized even though an absolute Doppler measurement is lost through aliasing. Of course, these signals are not representative of weather radar returns in turbulent wind environments. These signals have been used simply to illustrate the concept. The next section

begins a discussion of this approach using more representative Doppler spectra.

Analysis of a Simulated Weather Signal

Power Spectrum Simulation and Generation of I and Q Data

A Gaussian power spectrum can be represented by

$$G_k=\frac{1}{\sqrt{2\pi}\,\sigma}\exp\left[\frac{-(f_k-f_m)^2}{2\sigma^2}\right] .$$

G_k is a spectral coefficient corresponding to f_k; f_m and σ are the desired mean frequency and standard deviation respectively. The frequency dependent signal power density can now be defined as $S_k=C\cdot G_k$ where C is a signal-to-noise power scaling constant given by

$$C = \frac{10^{(SNR/10)}}{\sum_k G_k}$$

where SNR is the signal-to-noise ratio in dB. Defining the receiver's white noise power per discrete frequency, N_k, as the reciprocal of the number of spectral coefficients, i.e. ($\Sigma N_k=1$), the power spectrum can be given by

$$P_k=-\ln(X_k)\,.\,(S_k+N_k)$$

where X_k is a uniformly distributed random variable over the interval (0,1). For this simulation, normalization is performed in the frequency domain with $P_{kn}=P_k/P_t$. In order to transform the power spectrum into the time domain, the real and imaginary components of spectrum were obtained from

$$A_k=P_{kn}\cos(2\pi y_k),\ B_k=P_{kn}\sin(2\pi y_k)$$

where y_k is a uniformly distributed random variable over the interval(0,1). From these, we can obtain the in-phase and quadrature components through

$$I(i)+jQ(i)=\sum_{k=1}^{m}(A_k+jB_k)\exp(j2\pi ki/m)$$

where m should be larger than 30 to avoid any aliasing in the time domain [40].

In this particular spectral model the peak of the spectrum represents the strongest Doppler return from within the range cell and is interpreted as the mean windspeed within that cell. The variance of the Doppler spectrum is a measure of the distribution of windspeeds within the cell and will be larger in the presence of turbulence. A less turbulent condition would have a spectrum which is more peaked and which more closely resembles the specular situation discussed in the previous section.

The investigation here is concerned with the ability to measure the difference between spectral peaks when these modelled spectra are subjected to aliasing and differenced. The next subsection analyzes this further.

Typical Weather Radar Signals

A data record consisting of 1024 sample points of a representative power spectrum were simulated and I,Q data were obtained from that power spectrum. The simulated signals are assumed to be obtained with a high PRF radar without any serious signal aliasing problems. To analyze the effect of low PRF, one fourth of the simulated signal data were taken (which means one fourth of the original PRF) and processed using the DFT in the same way as the complex sinusoids in Figure 31. Figure 32 is a processed simulated typical weather radar return signal corresponding to a PRF of 2000 Hz and Figures 33 through 35 are aliased versions of this type signal as might be obtained with a low PRF of 500 Hz. A different mean frequency is associated with each of these Figures varying from 300 to 475 Hz to illustrate the effects of peak relocation by aliasing and reduced peak to background ratio associated with spectral leakage. Various spectrum magnitude differences are plotted in Figures 36 through 38 with a Nyquist interval associated with the reduced PRF. In each case the aliased spectral peaks are evident in the difference with the background level between peaks effectively cancelled. The original difference between

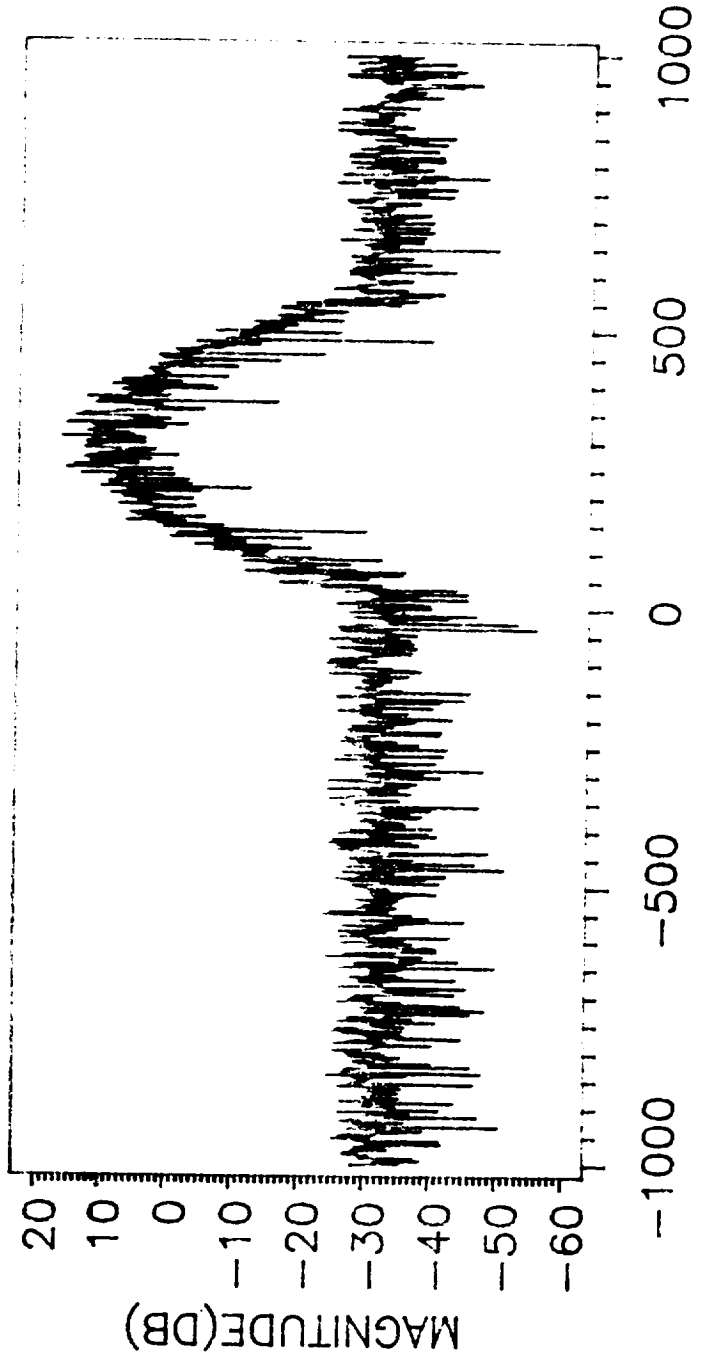

Figure 32. The DFT Result of Simulated Weather Radar Signal (mean freq.=+300 Hz, S/N=30 dB, sigma=0.0625*300, PRF= 2000 Hz)

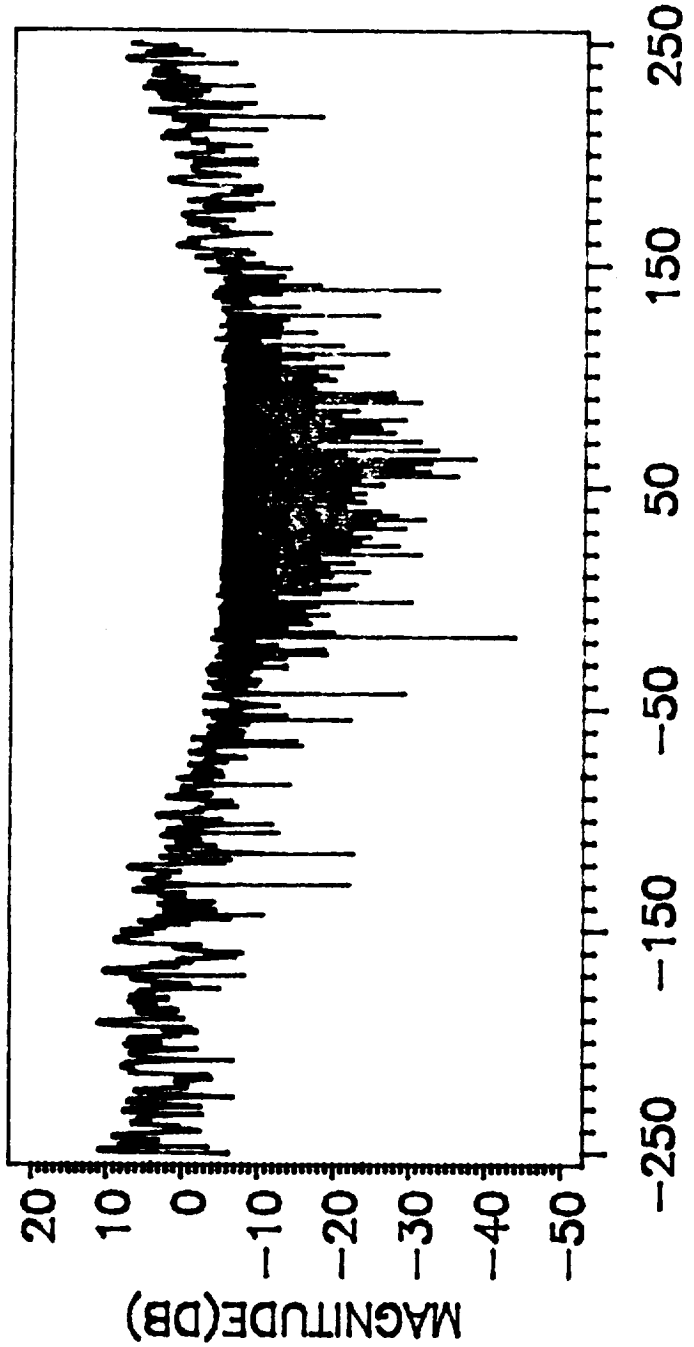

Figure 33. The Aliased DFT Result of Simulated Weather Radar Signal due to Low PRF (mean freq.=+300 Hz, PRF=500 Hz)

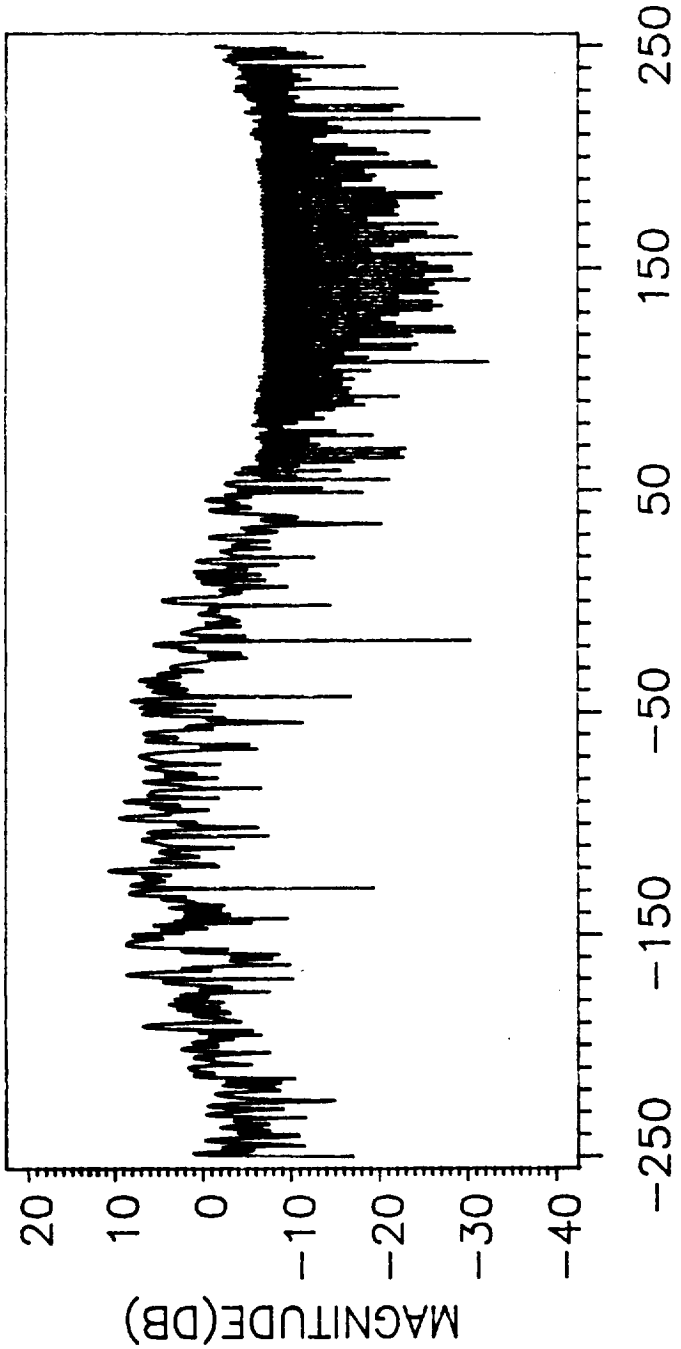

Figure 34. The Aliased Weather Signal with the Mean Frequency of +400 Hz (PRF=500 Hz)

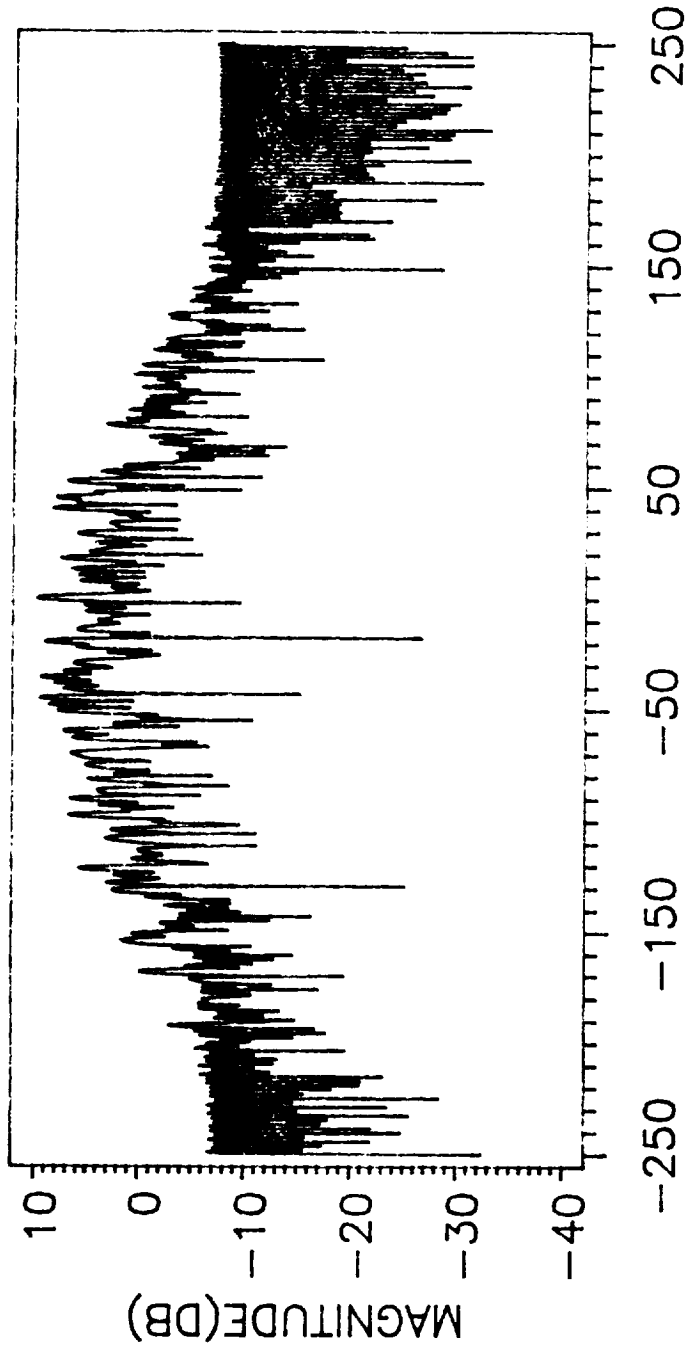

Figure 35. The Aliased Weather Signal with the Mean Frequency of +475 Hz (PRF=500 Hz)

spectral mean values is preserved and can be observed as the frequency difference between the maximum peak magnitude and the minimum peak magnitude on these plots. In Figure 36 this difference appears to be between a maximum peak at approximately -25 Hz and a minimum peak at approximately -200 Hz yielding a difference of 175 Hz which is the difference between the peaks of the unaliased spectra at 475 Hz and 300 Hz. The ambiguity problem arises in Figure 37 in that the Nyquist bandwidth is inadequate to represent the mean difference frequency and this figure shows the peaks of the aliased spectra at 100 Hz and -100 Hz corresponding to the actual peaks at 100 Hz and 400 Hz. The true difference frequency magnitude is larger than PRF/2, thus it is wrongly interpreted as a 200 Hz difference. A true frequency difference of 200 Hz between two aliased peaks at -100 Hz and 200 Hz is shown in Figure 38.

These examples are intended to represent computed differences in the spectral estimate of one range cell and that of an adjacent range cell. It appears that the detection of mean windspeed changes between adjoining range cells through low PRF radar is quite possible though signal peaks are not as well defined as in the case of noiseless signals.

Discussions and Problems

Based upon this analysis it can be readily seen that reduced PRF introduces aliasing and the peak to background ratio (SNR) will decrease accordingly, thus circumventing the

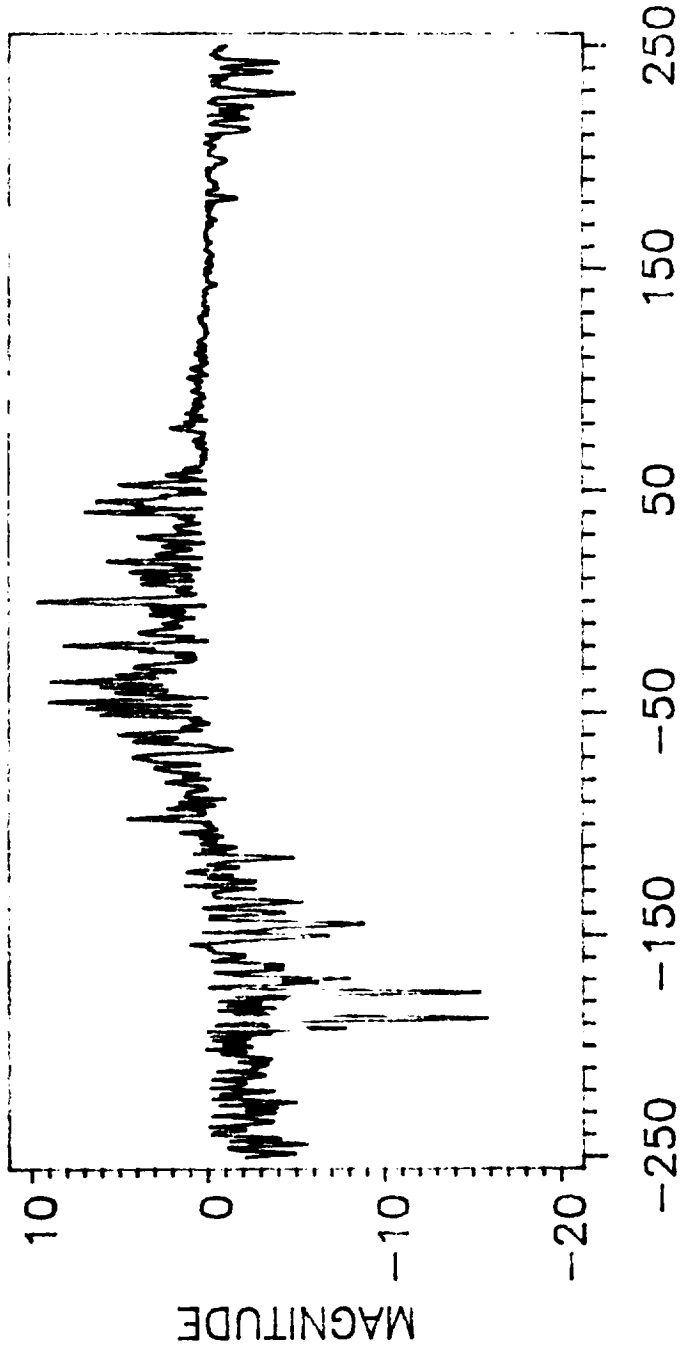

Figure 36. The Frequency Difference of Aliased Weather Signals between 475 Hz and 300 Hz

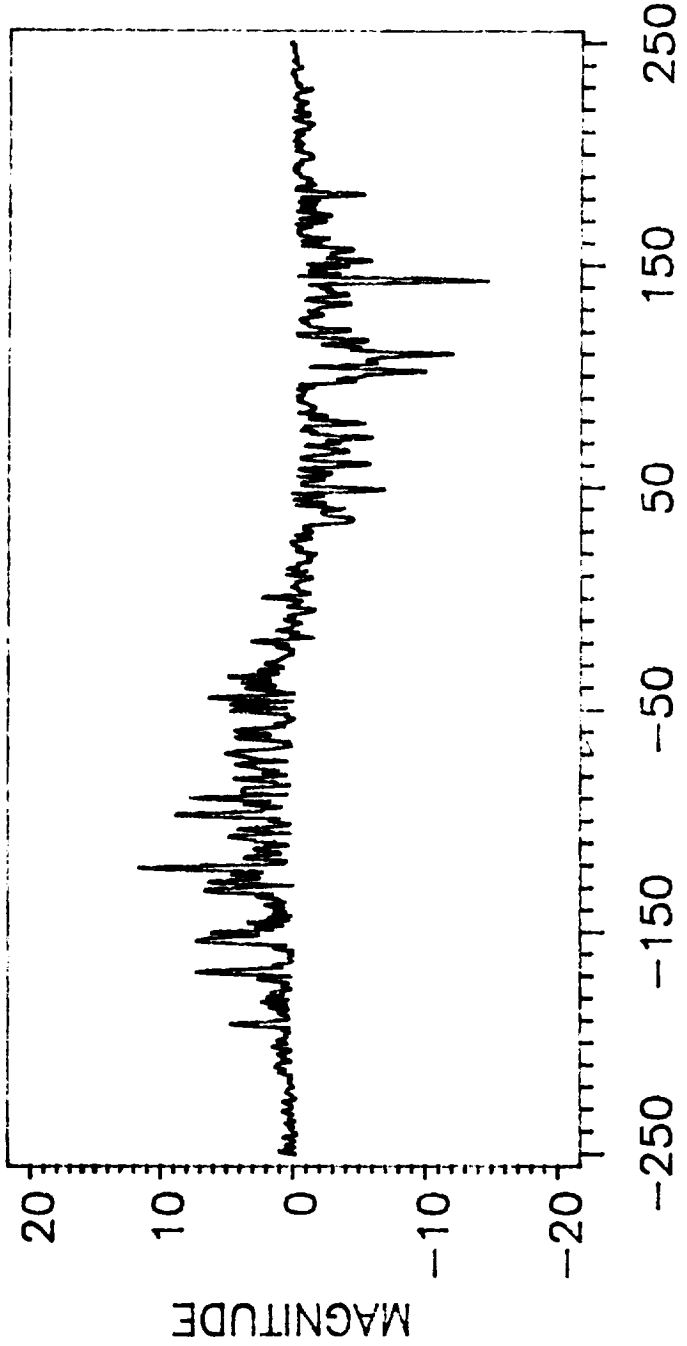

Figure 37. The Frequency Difference of Aliased Weather Signals between 400 Hz and 100 Hz

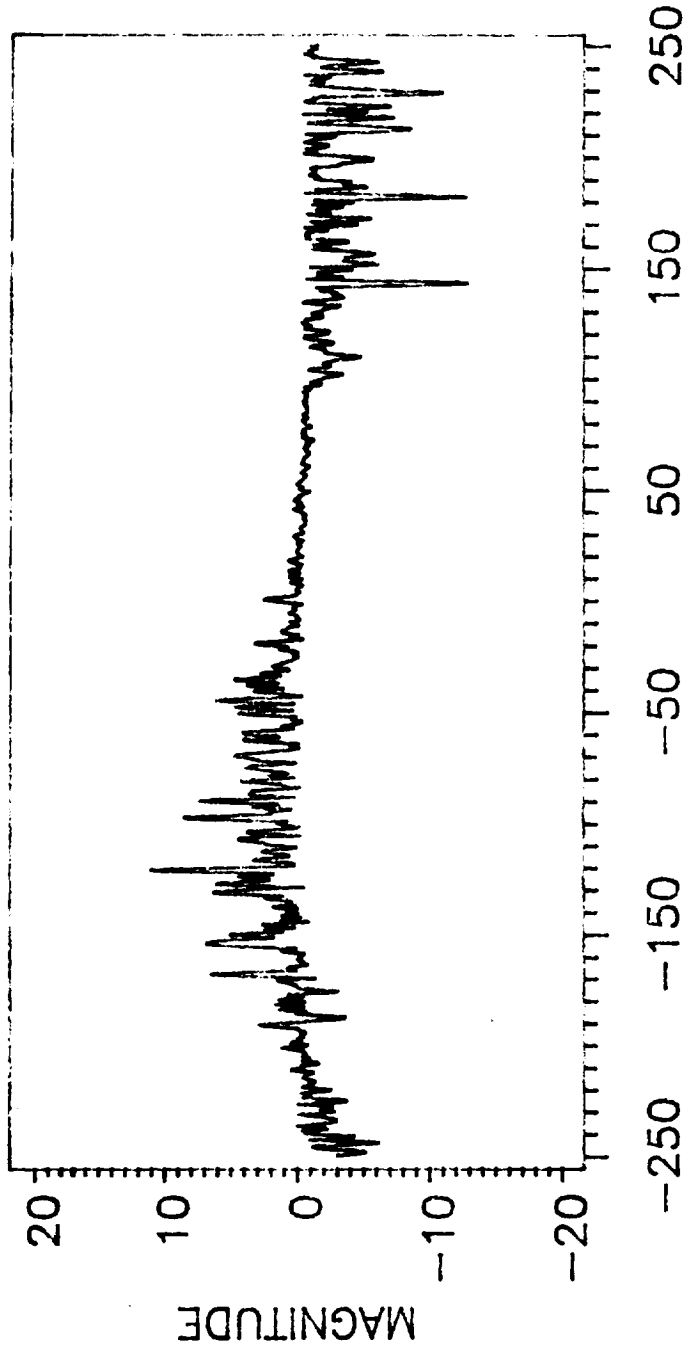

Figure 38. The Frequency Difference of Aliased Weather Signals between 400 Hz and 200 Hz

accurate estimation of mean frequency and spectrum width. Comparison of Figures 32 and 33 shows that the simulated weather signal of a low PRF radar is more contaminated with the background noise due to aliasing of high frequency components.

In spite of this aliasing problem, it appears that the mean frequency difference between aliased spectra can be preserved and detected because the peak location of the Gaussian spectrum is changed in a predictable way and the broader band incoherent background power level tends to cancel out. It can be noted that a difference in mean frequency larger than PRF/2 causes ambiguities. This demonstration suggests that the DFT magnitude difference of low PRF radar signals between range cells can overcome the difficulties of decreased SNR by aliasing and present the velocity gradient rather clearly.

In evaluating the utility of pulse Doppler weather radar for detection of windshear from an airborne platform the motivation for low PRF was stated earlier as a desire for large unambiguous range capability. Even though the analysis presented here tends to support the premise that windspeed gradient can be estimated within the Nyquist bandwidth associated with low PRF, other problems may be predominant. Turbulent wind conditions within a range resolution cell can cause a radar return which has a quite broad spectrum with a very small mode. Figure 39 illustrates the effect of aliasing a simulated weather spectrum which does not have a well

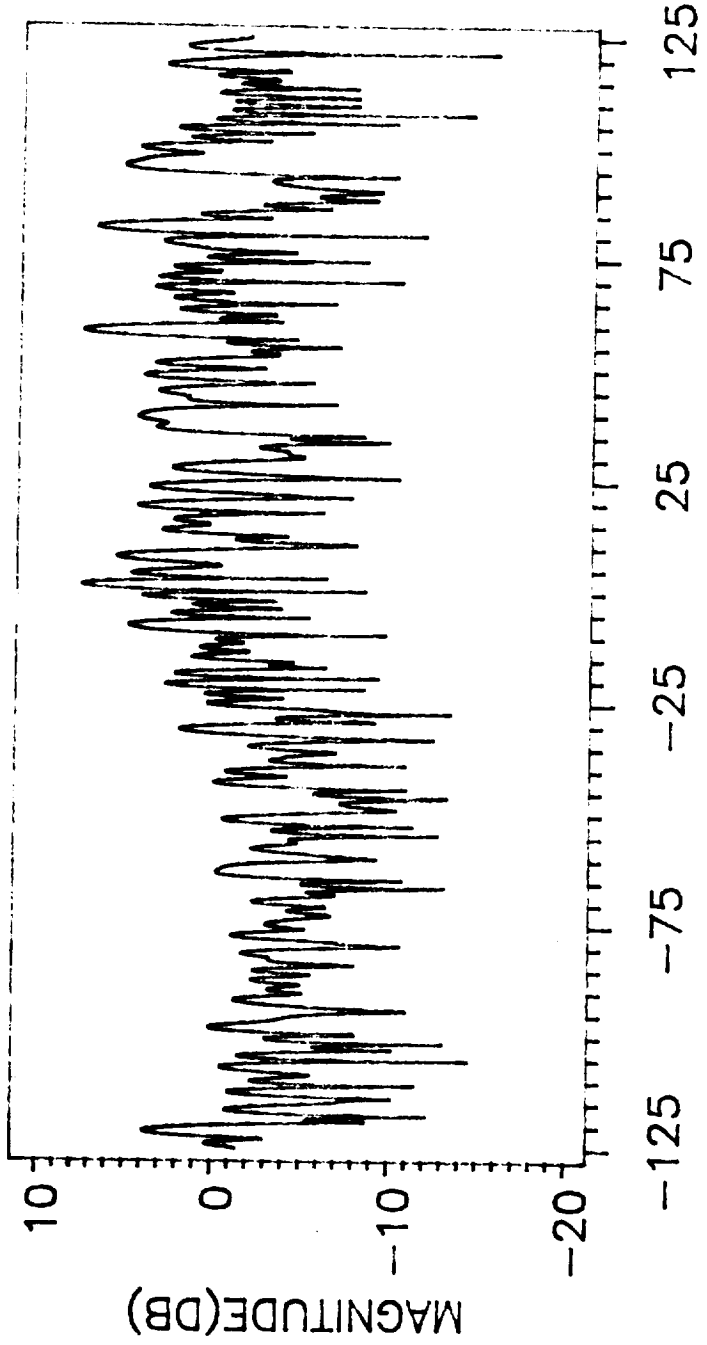

Figure 39. The Aliased Signal Obtained with PRF=250 Hz
(mean freq.=300 Hz, S/N=30 dB, width=18.75 Hz)

recognized peak. The peak to background level ratio is so low that the mean of the spectrum can no longer be identified in Figure 39. As shown in Figure 40 the difference between two such spectra yields a result which appears useless for estimating windspeed gradient.

Another consideration with low PRF radar is that the total magnitude of the return may be small in a turbulent situation and any reduction in return signal level because of a limited number of returns in a processing interval will cause the signal-to-noise ratio to be much too low for any practical use. Finally, a problem with the use of radar on an airborne platform in the neighborhood of urban airports is the clutter environment. High clutter levels may create a signal to clutter level ratio which precludes the use of a low PRF. Therefore, even though the analysis presented in this chapter supports the idea that a reduced Nyquist interval may be adequate for estimating windspeed gradients associated with windshear, it should not be concluded that simply reducing the weather radar PRF is the best means of improving the ranging capability of a weather radar.

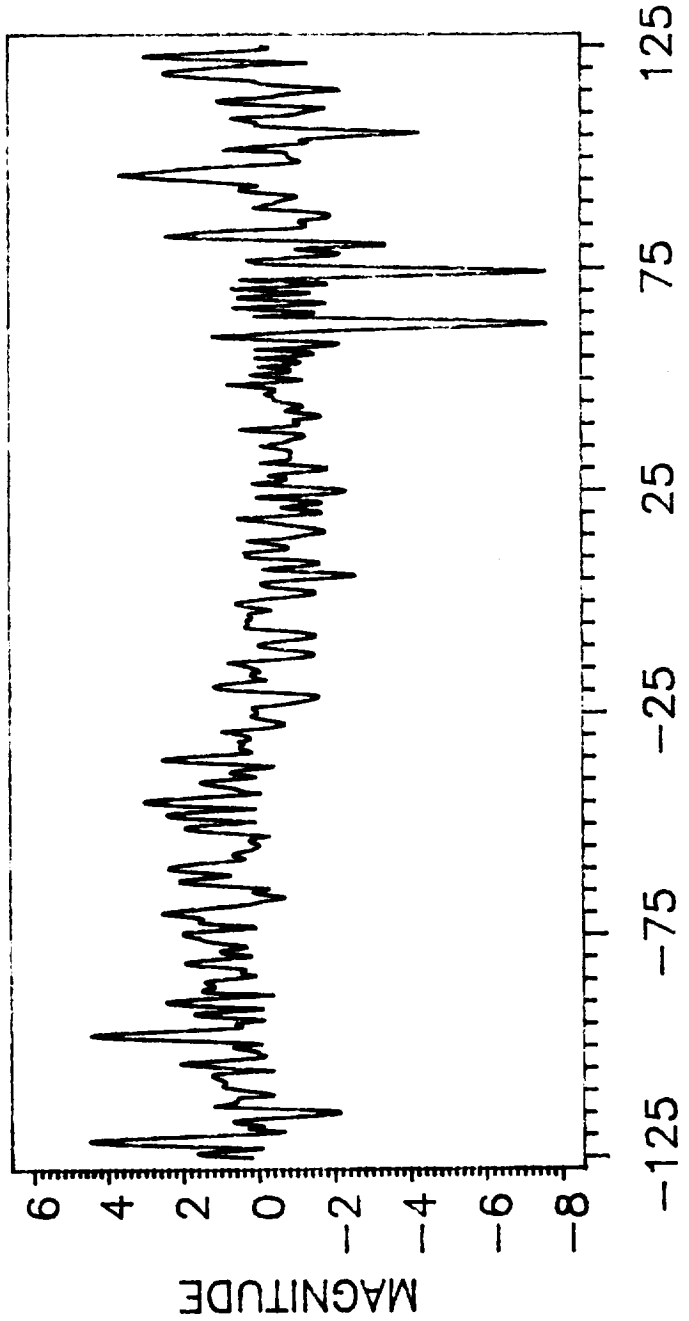

Figure 40. The Frequency Difference Plot of Aliased Weather Signals Obtained with PRF=250 Hz (f1=400 Hz, f2=300 Hz)

CHAPTER V

NEW APPROACH IN THE DETECTION OF HAZARDOUS WINDSHEAR CONDITIONS

Introduction

The aviational hazard often caused by microbursts can frequently be identified from a Doppler radar return by an S curve characteristic which describes mean windspeed changes along the radar range radial. The mean value of the weather return spectrum is generally considered as representing the windspeed in each range cell. However, based upon the results from Chapter III, in the skewed spectrum case or with the multimodal return spectrum, the modes of spectrum may provide more reliable information than the statistical mean for the purpose of windshear detection. Therefore, the mode estimation technique using the modified Prony method is presented in this Chapter. Also this mode estimator may be useful in recognizing the windshear hazard without the need for clutter rejection filtering.

As has been noted earlier, one of the more popular methods of estimating mean Doppler or mean wind speed within a range resolution cell is the pulse pair estimation technique. This is computationally much more efficient than DFT based methods although spectrum parameter estimates involving the DFT are generally considered to be more robust. With an airborne Doppler radar wet microburst return, where

signal-to-clutter ratio is large enough, the simple pulse pair estimator, for example, generally yields a very accurate estimate of mean wind velocity in each range cell. However, difficulties arise in a dry microburst case since a very low signal-to-clutter ratio may seriously bias the mean velocity estimates without effective and efficient clutter filtering. To make matters worse, the removal of clutter may not be an easy task though several methods have proven to be useful [45],[18],[19]. It has been shown [45] that efficient clutter suppression can be done using an auto-regressive least squares method, but mean estimates from clutter-only range cells often fluctuate randomly, because there remain only weak background noise signals after filtration. This can also occur when the weather return spectrum falls largely within the clutter filter notch and is mostly removed with clutter rejection processing. Another problem is that radar system phase noise may limit the clutter rejection capability yielding a too low signal-to-clutter ratio in the filtered spectrum thus causing an inaccurate estimation of the mean velocity as explained in Chapter II.

An alternate approach to identifying the presence of a weather return is to locate strong peak points in the spectrum which may well represent the velocity spectrum modes of wind and clutter signals in each range cell. These peak values may be adequate to identify the microburst S curve signature and detect a hazardous windshear condition. This new approach is particularly attractive since it does not

require processing to estimate the entire spectrum but only involves finding a few peak points of the spectrum. The modified Prony method [46] is investigated here to find strong peak points of simulated weather spectra that include microburst and static clutter signals.

Modified Prony Method

The modified Prony method [46] involves approximating a complex data sequence by a model consisting of undamped complex sinusoids. It is similar to Pisarenko Harmonic Decomposition (PHD) method [47], but the Prony algorithm is generally better than PHD procedure since it needs neither autocorrelation lags nor a more computationally complex eigen equation solution. The Prony method requires only the solution of two sets of simultaneous linear equations and a polynomial rooting. It is summarized briefly in the following:

1. Find the coefficients of a complex polynomial minimizing the squared smoothing error.
2. Root a complex polynomial to determine frequencies.
3. Solve for the amplitude of each frequency.

The 2p component Prony model is represented as

$$\hat{x}(n)=\sum_{k=1}^{2p} h_k Z_k^{n-1} \tag{5.1}$$

where $h_k=A_k\exp(j\theta_k)$ and $Z_k=\exp(j2\pi f_k T)$. The polynomial constructed with roots that are the Z_k of Equation (5.1) has the form

$$\phi(Z)=\prod_{k=1}^{2p}(Z-Z_k)=\sum_{k=0}^{2p}a[k]Z^{2p-k}$$

where $a[0]=1$ by definition. Due to the unit modulus property $Z_k^{-1}=Z_k^*$, it can be shown that the conjugate property $a[k]=a[2p]a^*[2p-k]$ for $k=0$ to $k=2p$ must exist between the coefficients. Therefore, the homogeneous linear difference equation that has Equation (5.1) as its solution is

$$a[2p]x[n-p]+\sum_{k=1}^{p}(a[2p-k]x[n-p+k]+a[2p]a[k]x[n-p+k])=0 \quad (5.2)$$

for $2p+1\leq n\leq N$, where N is the number of given data points. A more convenient form of (5.2) can be obtained which yields the conjugate symmetric difference equation

$$x[n-p]+\sum_{k=1}^{p}(g_{2p}[k]x[n-p+k]+g_{2p}^*[k]x[n-p-k])=0$$

where $g_{2p}[k]=a[2p-k]/a[2p]$ and $g_{2p}^*=a[k]$. Since N usually exceeds the minimum number needed to fit a model of 2p, i.e., $N\geq 2p+1$, the squared smoothing error given by

$$\rho_{2p}=\sum_{n=p+1}^{N-p}\left|e_{2p}(n)\right|^2$$

is minimized based on the measured complex data samples where

$$e_{2p}(n)=x[n]+\sum_{k=1}^{p}(g_{2p}[k]x[n+k]+g_{2p}^{*}[k]x[n-k])\ .$$

Setting the complex derivatives of ρ_{2p} with respect to $g_{2p}[1]$ through $g_{2p}[p]$ to zero yields

$$\mathbf{R}_{2p}\mathbf{g}_{2p}=\begin{bmatrix}\mathbf{0}_p\\ 2\rho_{2p}\\ \mathbf{0}_p\end{bmatrix} \tag{5.3}$$

where

$$\mathbf{g}_{2p}^{T}=[g_{2p}[p],\ldots,g_{2p}[1],1,g_{2p}^{*}[1],\ldots,g_{2p}^{*}[p]]$$

and $\mathbf{0}_p$ is a p×1 all zero vector. $\mathbf{R}_{2p}$ can be expressed as

$$\mathbf{R}_{2p}=\sum_{n=2p+1}^{N}[\mathbf{x}_{2p}^{*}[n]\mathbf{x}_{2p}^{T}[n]+\mathbf{J}\mathbf{x}_{2p}[n]\mathbf{x}_{2p}^{H}[n]\mathbf{J}]$$

where $\mathbf{J}$ is a (2p+1)×(2p+1) reflection matrix and H means complex conjugate transposition. Here $\mathbf{x}_{2p}[n]$ is defined as

$$\mathbf{x}_{2p}^{T}[n]=[x[n],\ldots,x[n-p+1],x[n-p],x[n-p-1],\ldots,x[n-2p]].$$

The fast algorithm to solve the symmetric covariance normal Equation (5.3) was developed by Marple [48].

After solving for a[1] through a[2p], the roots of the complex polynomial, Z_k, can be obtained using the polynomial factoring algorithm. Then, h_k in Equation (5.1) is computed minimizing the squared error with respect to each of the h_k parameters, i.e.,

$$\mathbf{h}= [\mathbf{Z}^{H}\mathbf{Z}]^{-1}\mathbf{Z}^{H}\mathbf{x}$$

where

$$\mathbf{Z}=\begin{bmatrix} 1 & 1 & \ldots & 1 \\ z_1 & z_2 & \ldots & z_{2p} \\ . & . & \ldots & . \\ . & . & \ldots & . \\ z_1^{N-1} & z_2^{N-1} & \ldots & z_{2p}^{N-1} \end{bmatrix}, \quad \mathbf{h}=\begin{bmatrix} h_1 \\ h_2 \\ . \\ . \\ h_{2p} \end{bmatrix}, \quad \mathbf{x}=\begin{bmatrix} x[1] \\ x[2] \\ . \\ . \\ x[N] \end{bmatrix}.$$

Performance and Computational Complexity

A second order Prony model was used here to find peak points of simulated weather spectra. This data set had been previously analyzed using adaptive clutter rejection filtering and pulse pair mean estimation [45]. Marple's programs [46] were slightly modified to avoid numerical ill-conditioning in some cases. A 512 point complex data sequence from each range cell was processed. Some typical DFT spectrum

plots are shown in Figures 41 through 44 with the Prony method peak estimates also indicated. As seen in Figures 41,42 and 43, the Prony method is able to locate spectrum peak points. However, Figure 44 shows somewhat inaccurately estimated peak points because of the presence of strong clutter power and the closeness of weather and clutter spectral peaks.

In order to check the usefulness of this new approach for detection of windshear, data from 40 contiguous range cells which include a dry microburst with clutter were processed and peak velocity points were plotted versus range. The resulting Figure 45 clearly shows the S curve characteristic around the range cell 27.

Another important consideration with any algorithm is computational complexity which must not prohibit real time processing. Some comparisons with other spectrum estimation methods are made in Table 1. Of course, the Prony method is computationally much more complicated than other classical spectrum estimation techniques as the model order increases, but as it can be seen from Table 1, the second order Prony model used here requires less computation than the DFT method. Therefore, the modified Prony method may be useful as a component of a windshear detection algorithm.

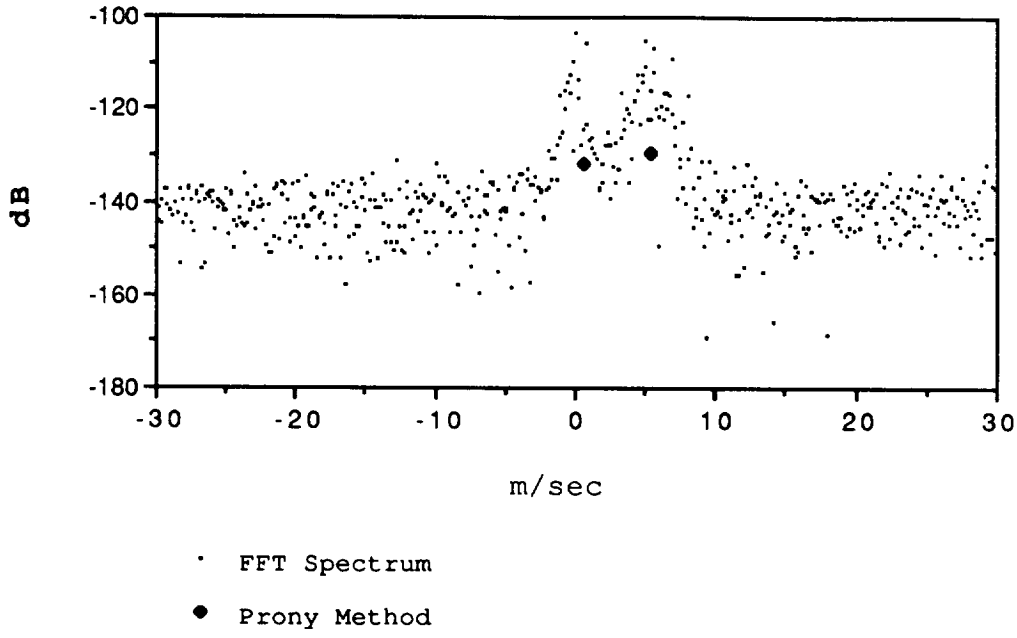

Figure 41. Mode Estimates Shown in Simulated Weather Spectrum of Range Cell 24

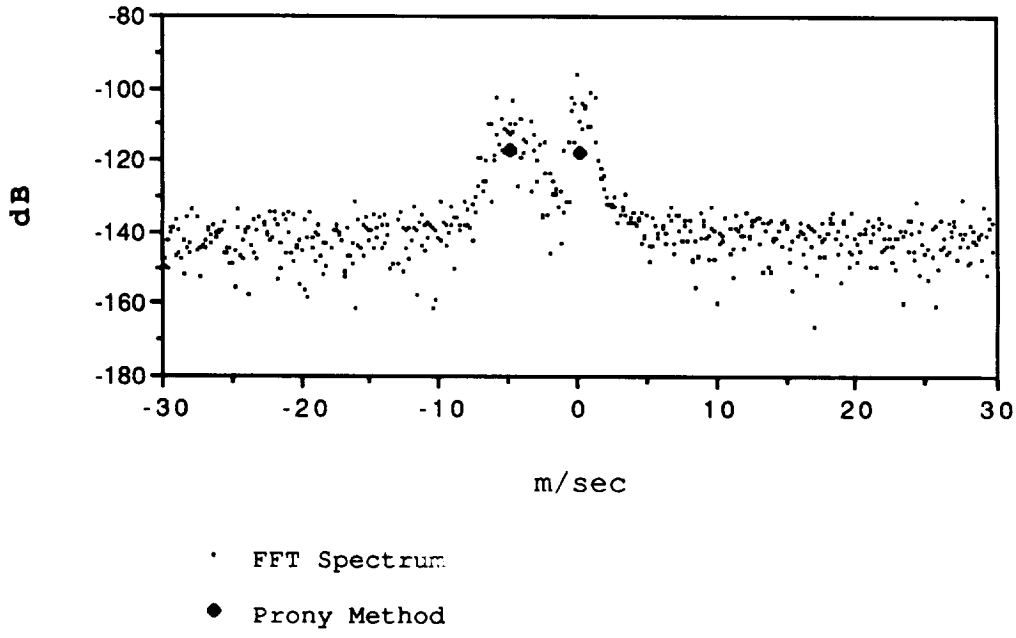

Figure 42. Mode Estimates Shown in Simulated Weather Spectrum of Range Cell 29

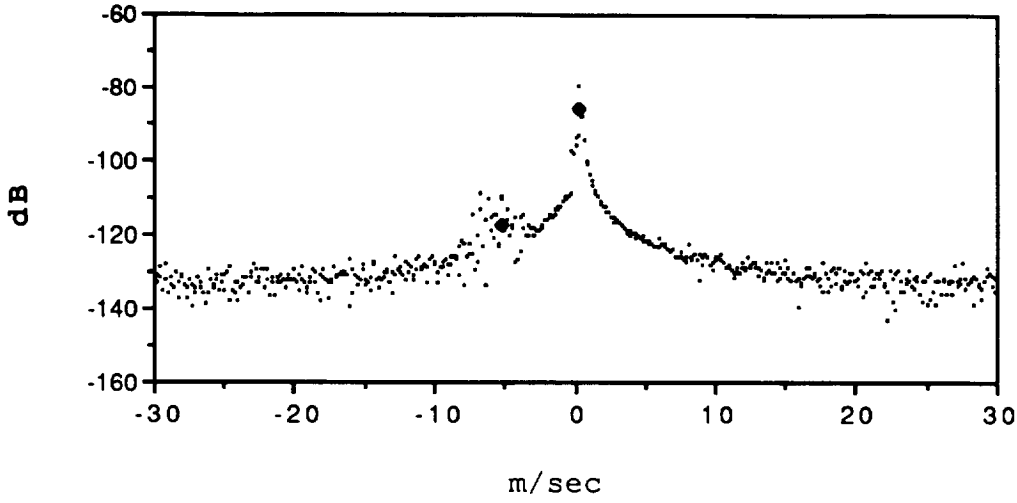

Figure 43. Mode Estimates Shown in Simulated Weather Spectrum of Range Cell 30

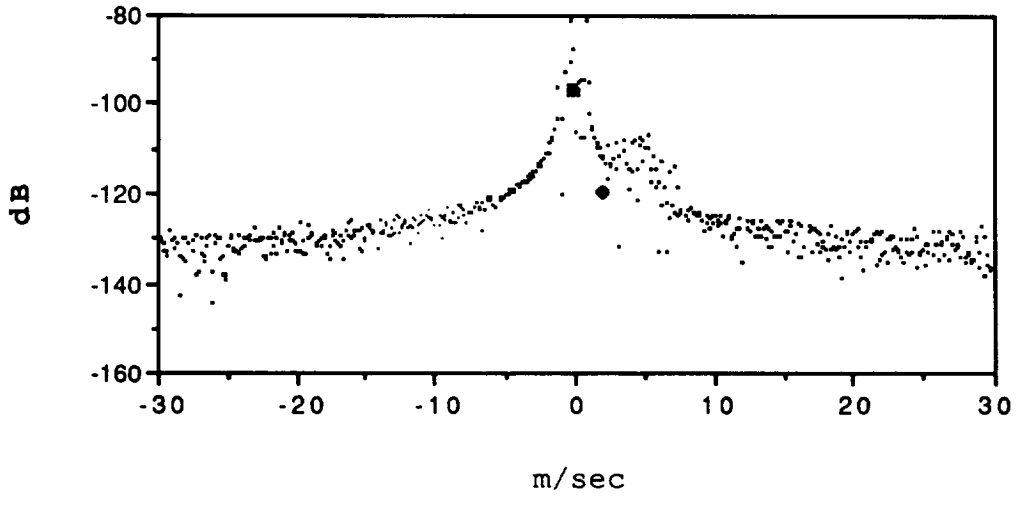

Figure 44. Mode Estimates Shown in Simulated Weather Spectrum of Range Cell 25

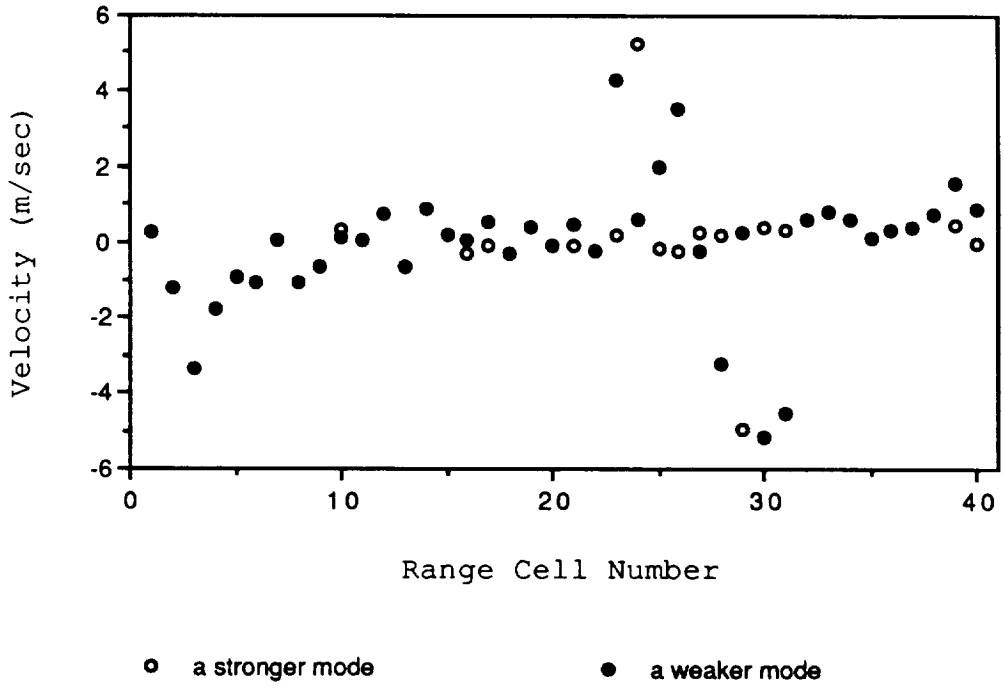

Figure 45. Estimated Spectrum Modes of Simulated Weather Data in All Range Cells

Table I. Comparison of Computational Complexity Where N=512

(f(p) means that the required number of computations depends on the algorithm used for a polynomial rooting)

method	computation requirement	approximate number of calculations for a reasonable model order
FFT	$N\log_2 N$	4700 complex adds/mults
AR LSQ	$2NP+P^2$	10500 complex adds/mults for p=10
Prony	$2NP+18P^2+P^3+f(P)$	2300 complex adds/mults for p=2

CHAPTER VI

CONCLUSIONS AND RECOMMENDATIONS FOR FUTURE WORK

Chapter II of this dissertation has presented a method of evaluating the effect of pulse Doppler radar phase instabilities (jitter) on the estimation of return signal Doppler spectrum parameters using the pulse pair and DFT algorithms. Phase instabilities are modeled as statistically independent from the radar return itself. This phase jitter model can in fact represent a cumulative effect from various sources within the radar transmitter/receiver. As seen from the results presented, phase jitter is not expected to cause any bias error in the pulse pair and DFT mean estimates. However, it can cause an increase in the variance of the mean estimate and is essentially independent of the radar return spectrum width. On the other hand it has been confirmed there is significant increase in the bias of the pulse pair width estimate particularly with more narrow return Doppler spectrum widths. Some increase in the variance of the pulse pair width estimate with increasing phase jitter is also noted. It is also confirmed on the basis of these results that the phase jitter effect on pulse pair estimation is negligible if T_s is small enough and most of phase noise spectrum power is concentrated around the carrier frequency.

However, if these conditions are not satisfied, any phase jitter can cause significant estimation errors.

Comparing the results of DFT estimation with the pulse pair estimation case, it can be said that DFT estimates are relatively immune to phase jitter since the DFT estimate errors are much smaller than the comparable results using pulse pair estimates. This result may be anticipated because it is well-known that DFT estimate variances increase much more slowly, as the normalized spectrum width WT_s increases, than the exponential increase associated with the pulse pair method. One example was shown using actual phase jitter data to demonstrate the general approach for evaluating the system performance with arbitrary phase jitter spectral data.

A significant contribution of this work is the development of a technique whereby radar phase instability measurements can actually be incorporated into an analytical evaluation of pulse pair and DFT estimation quality by using appropriate numerical techniques. This precludes the necessity to rely on any particular notion of a closed form distribution for the phase jitter spectrum. Radar system phase stability design specifications can now be quantitatively determined based on the desired quality for spectrum parameter estimates.

The phase jitter analysis is based upon earlier published results for pulse pair spectrum parameter estimates which, in many cases, have been derived through a series of simplifying assumptions. These assumptions may limit

application of the results to weather spectra which are narrow with respect to the Nyquist processing interval and which are Gaussian, or at least symmetric, as well as situations where a large signal-to-noise ratio exists. The pulse pair estimator variance expressions presented here were derived using perturbation analysis under the assumption that perturbations are not excessive (for example, a second order expansion was used in the derivation of (2.11)) [29]. In some cases this is valid only if the number of samples is very large, which suggests that a higher order expansion may be required in the derivation when considering a small number of samples. Therefore a re-evaluation of the assumptions made in deriving the error expressions for the pulse pair estimators may be necessary to be applied in turbulent weather environments if this work is to be extended further.

One of the assumptions made in evaluating the pulse pair estimates is that the Doppler return spectrum is symmetric. This may not be valid particularly in the turbulent weather situation. The analysis in Chapter III shows that the mean estimates can be seriously biased due to skewness in the weather spectrum as the spectrum is broadened even though the width bias error can be considered to be negligible. Degradation of estimation quality due to the bias term is less than 15% if WT_s is not larger than 0.15 as seen in Figure 27, but this condition may not always be satisfied. In the skewed spectrum case, the suggested poly-pulse pair method was demonstrated as useful in reducing bias errors of

mean estimates. It is also shown in Chapter III that the mode of the skewed spectrum and the pulse pair mean can differ very largely as the spectrum width increases. This may be a problem in some applications such as windshear detection where frequently the mode of a return spectrum may be a more informative statistic than the mean value.

It is anticipated that windshear can be detected by measurement of the windspeed gradient. From the results presented in Chapter IV, it is theoretically possible that windspeed gradient can be measured with a low PRF radar if the difference of mean windspeed between range cells is not larger than $(PRF \cdot \lambda)/4$. Low PRF does introduce an aliasing effect which prevents the measurement of high windspeed, but it is shown that the gradient information, i.e., the mean frequency difference, can be preserved and detected. The difficulties of decreased SNR due to aliasing also can be overcome by using the magnitude difference of return spectra between range cells. Therefore, Chapter IV demonstrates that the low PRF radar has a potential for the direct measurement of windspeed gradient. However, in a practical situation, this method may have some limitations. A very broad weather return spectrum can cause meaningless results because of seriously aliased weather signals. Also the total return signal power may be very small in dry weather conditions and a limited number of returns associated with low PRF radar may cause too low an SNR to be useful. Furthermore, in an airborne Doppler radar, the high clutter return level is a

serious problem and may preclude the use of low PRF radar since efficient clutter filtering is almost essential in these situations for the detection of windshear phenomena.

A new approach explained in Chapter V shows that windshear detection may be possible using a pattern recognition type technique by finding an "S" curve characteristic demonstrated here using the modified Prony method. From the results in Figure 45, it can be said that the very low order Prony model may make it possible to detect the windshear condition without any other preliminary processing. However, this new approach also has the limitation that some valuable weather information such as spectrum width can not be obtained without additional processing. Also as shown in Figure 44, where clutter and weather spectrum modes are very close together, identification of a weather return is an inherently difficult problem to solve. In these situations, the Prony method appears of limited use. Other more computationally complicated methods such as the Pisarenko harmonic decomposition method may be necessary.

Future work may include an evaluation of detection and false alarm rates by applying methods suggested here to data obtained in planned system flight tests. The thresholding method with use of the hazard index F-factor is simple, but it may be more susceptible to the mean velocity measurement error than the method of recognizing an S curve characteristic associated with microbursts. This pattern

recognition type technique may help eventually to build a more intelligent system for reliable windshear detection since typical microburst S curve signature information can be accumulated and stored for future reference in a correlation based detection processor.

APPENDICES

Appendix A

Rederivation of DFT Estimate Variances with Gaussian Phase Noise

Theoretical expressions for the variances of mean and width frequency estimate derived by Berger and Groginsky can be found in [33]. From these equations, the variance expressions for a narrow Gaussian spectrum without consideration of phase noise are given in [30], but rederivation should be made to analyze the phase noise effect. Therefore the autocorrelation function with phase noise derived in [49] can be rewritten as a series expansion form to obtain the return spectrum S(f), i.e.,

$$R(\tau) = Se^{-2\sigma^2} e^{-2\pi^2 w^2 \tau^2} \sum_{n=0}^{\infty} \frac{(2R_{\phi}(\tau))^n}{n!} + N\delta_{\tau,0}$$

where $R_{\phi}(\tau)$ represents the autocorrelation function of the phase noise model, ϕ [illegible]. With the assumption of Gaussian phase noise the spectrum can be easily obtained by Fourier transform. Ignoring negligible higher order terms, the spectrum can be approximated very accurately as

$$S(f)=Se^{-2\sigma^2}\left[\frac{1}{\sqrt{2\pi}\,w}e^{\frac{f^2}{2w^2}}+\frac{2\sigma^2}{\sqrt{2\pi}\,(w^2+\Delta f_c^2/2)^{\frac{1}{2}}}e^{\frac{f^2}{2(w^2+\Delta f_c^2/2)}}\right.$$

$$+\frac{2\sigma^4}{\sqrt{2\pi}\,(w^2+\Delta f_c^2)^{\frac{1}{2}}}e^{\frac{f^2}{2(w^2+\Delta f_c^2)}}+\frac{4\sigma^6}{3\sqrt{2\pi}\,(w^2+\frac{3}{2}\Delta f_c^2)^{\frac{1}{2}}}$$

$$\left.\cdot\, e^{\frac{f^2}{2(w^2+\frac{3}{2}\Delta f_c^2)}}\right]+NT_s$$

where NT_S represents a white noise power within the Nyquist bandwidth. By substituting this spectrum into the equations given in [33], the variance expressions including Gaussian phase noise are derived as

$$\mathrm{var}(\hat{f})=\frac{1}{MT_s^2}\left\{e^{-4\sigma^2}T_s\left[\frac{w}{4\sqrt{\pi}}+\frac{4\sigma^2w^2w_1^2}{\sqrt{2\pi}\,(w^2+w_1^2)^{3/2}}+\frac{\sigma^4w_1}{\sqrt{\pi}}\right.\right.$$

$$\left.+\frac{4\sigma^4w^2w_2^2}{\sqrt{2\pi}\,(w^2+w_2^2)^{3/2}}+\frac{8\sigma^6w^2w_3^2}{3\sqrt{2\pi}\,(w^2+w_3^2)^{3/2}}+\frac{8\sigma^6w_1^2w_2^2}{\sqrt{2\pi}\,(w_1^2+w_2^2)^{3/2}}\right]$$

$$\left.+e^{-2\sigma^2}2\left(\frac{N}{S}\right)T_s^2\left[w^2+2\sigma^2w_1^2+2\sigma^4w_2^2+\frac{4}{3}\sigma^6w_3^2\right]+\frac{1}{12}\left(\frac{N}{S}\right)^2\right\}\quad\text{and}$$

$$\mathrm{var}(\hat{w})=\frac{1}{4MW^2T_s}[\alpha_1+\alpha_2-\alpha_3]+\frac{1}{2MW^2}\left(\frac{N}{S}\right)[\alpha_4+\alpha_5-\alpha_6]+\frac{1}{MT_s^2}\left(\frac{N}{S}\right)^2\alpha_7$$

where

$$\alpha_1 = e^{-4\sigma^2}\left[\frac{3w^3}{8\sqrt{\pi}} + \frac{6\sqrt{2}\,\sigma^2}{\sqrt{\pi}}\,\frac{w^4 w_1^4}{(w^2+w_1^2)^{5/2}} + \frac{3\sigma^4}{2\sqrt{\pi}}w_1^3 + \frac{6\sqrt{2}\,\sigma^4}{\sqrt{\pi}}\,\frac{w^4 w_2^4}{(w^2+w_2^2)^{5/2}}\right.$$

$$\left. + \frac{4\sqrt{2}\,\sigma^6}{\sqrt{\pi}}\,\frac{w^4 w_3^4}{(w^2+w_3^2)^{5/2}} + \frac{12\sqrt{2}\,\sigma^6}{\sqrt{\pi}}\,\frac{w_1^4 w_2^4}{(w_1^2+w_2^2)^{5/2}}\right] ;$$

$$\alpha_2 = w^4 e^{-4\sigma^2}\left[\frac{1}{2\sqrt{\pi}\,w} + \frac{4\sigma^4}{2\sqrt{\pi}\,w_1} + \frac{4\sigma^2}{\sqrt{2\pi}}\,(w^2+w_1^2)^{-1/2} + \frac{4\sigma^4}{\sqrt{2\pi}}(w^2+w_2^2)^{-1/2}\right.$$

$$\left. + \frac{32\sigma^6}{3\sqrt{2\pi}}(w^2+w_3^2)^{-1/2}\right] ;$$

$$\alpha_3 = 2w^2 e^{-4\sigma^2}\left[\frac{w}{4\sqrt{\pi}} + \frac{\sigma^4}{\sqrt{\pi}}\,w_1 + \frac{4\sigma^2}{\sqrt{2\pi}}\,\frac{w^2 w_1^2}{(w^2+w_1^2)^{3/2}} + \frac{4\sigma^4}{\sqrt{2\pi}}\,\frac{w^2 w_2^2}{(w^2+w_2^2)^{3/2}}\right.$$

$$\left. + \frac{8\sigma^6}{3\sqrt{2\pi}}\,\frac{w^2 w_3^2}{(w^2+w_3^2)^{3/2}} + \frac{8\sigma^6}{\sqrt{2\pi}}\,\frac{w_1^2 w_2^2}{(w_1^2+w_2^2)^{3/2}}\right] ;$$

$$\alpha_4 = e^{-2\sigma^2}\left[\,3w^4 + 6\sigma^2 w_1^4 + 6\sigma^4 w_2^4 + 4\sigma^6 w_3^4\,\right] ;$$

$$\alpha_5 = w^4 ;$$

$$\alpha_6 = 2w^2 e^{-2\sigma^2} \left[w^2 + 2\sigma^2 w_1^2 + 2\sigma^4 w_2^2 + \frac{4}{3}\sigma^6 w_3^2 \right] \quad \text{and}$$

$$\alpha_7 = \frac{1}{320 w^2 T_s^2} + \frac{w^2 T_s^2}{4} - \frac{1}{24}$$

where

$$w_1^2 = w^2 + \frac{\Delta f_c^2}{2} \qquad w_2^2 = w^2 + \Delta f_c^2 \qquad w_3^2 = w^2 + \frac{3}{2}\Delta f_c^2 \quad .$$

Appendix B

NASA Simulation Parameters

****SIMULATION PARAMETERS*****	1.
	0.
A/C Distance to Touchdown (km)	7.
Aircraft Velocity (kts)	150.0
Glideslope Angle (deg)	3.
No. of Complete Scans	1.
Time Between Scans	5.
Roll Attitude (deg)	0.
Pitch Attitude (deg)	0.
Yaw Attitude (deg)	0.
Az Integration Range/2 (deg)	6.0
Az Integration Increment (deg)	.3
El Integration Range/2 (deg)	4.0
El Integration Increment (deg)	.2
Rng Integration Increment (m)	100.
Random Number Seed (0-1)	.224
Runway Number	26.
Right (1) or Left (2)	1.
	0.
****MICROBURST & CLUTTER******	0.
	0.
Along Track Offset from TD (km)	-2.
Cross Track Offset from TD (km)	0.
Rain Standard Deviation (m/s)	1.
Clutter Standard Deviation (m/s)	.5
Clutter Calc. Flag (1=ON,0=OFF)	1.
Discrete Calc. Flag (1=ON,0=OFF)	0.
Reflectivity Calc. Thres. (dBz)	-20.
Minimum Reflectivity (dBz)	-15.
Attenuation Code (0,1,2)	2.
	0.
****RADAR PARAMETERS**********	0.
	0.
Initial Radar Range (km)	1.
Number of Range Cells	40.
Antenna Az - if no scan (deg)	0.
Azimuth Scan Range/2 (deg)	0.
Azimuth Scan Increment (deg)	3.
Antenna Elevation (deg)	1.
Transmitted Power (watts)	2000.
Frequency (GHz)	9.3
Pulse Width (microsecs)	1.
Pulse Interval (microsecs)	268.6
Receiver Noise Figure (dB)	4.
Receiver Losses (db)	3.
Antenna Type (1 ,2 , or 3)	1.

Antenna Radius (m)	.381
Aperture Taper Parameter	.316
RMS Trans. Phase Jitter (deg)	.2
RMS Trans. Freq Jitter (Hz)	0.
	0.
****SIGNAL PROCESSING********	0.
	0.
Number of Pulses	512.
Number of A/D bits	12.
AGC Gain Factor	.6
Processing Threshold (dB)	4.
Clutter Filter Code (-2 to N)	0.
Clutter Filter Cutoff (m/s)	3.
No. of Bins for F-factor Avr.	5.

LIST OF REFERENCES

1. D. W. Burgess, "Single Doppler radar vortex recognition: part I - Mesocyclone signatures," in Preprints 17th Conf. Radar Meteorol., Amer. Meteorol. Soc., Boston, MA. 02108, pp. 97-103, Oct. 1976.

2. R. J. Doviak, D. Burgess, L. Lemon, and D. Sirmans, "Doppler velocity and reflectivity structure observed within a tornadic storm," J. Rech. Atmos., vol. VIII, nos. 1-2, pp. 235-243, Jan.-June 1974.

3. R. J. Doviak and C. T. Jobson, "Dual Doppler radar observations of clear air wind perturbations in the planetary boundary layer," J. Geophys. Res., vol. 84, no. c2, pp. 699-702, 1979.

4. D. W. Rice and K. H. Wu, "Quadrature sampling with high dynamic range," IEEE Trans. Aerosp. Electron. Syst., vol. AES-18, pp. 736-739, 1982.

5. J. McCarthy, J. W. Wilson and T. T. Fujita, "The joint airport weather studies (JAWS) project," Bull. Amer. Meteorol. Soc. pp. 15-22, 1982.

6. D. Sirman and B. Bumgarner, "Numerical comparison of five mean frequency estimators," J. Appl. Meteorol., vol. 14, pp. 991-1003, 1975.

7. R. F. Woodman, "Spectral moment estimation in MST radars," Radio Science, vol. 20, pp. 1185-1195, 1985.

8. K. S. Miller and M. M. Rochwarger, "A covariance approach to spectral moment estimation," IEEE Trans. Inform. Theory, vol. IT-18, pp. 588-596, 1972.

9. D. S. Zrnic, "Spectrum width estimates for weather echoes," IEEE Trans. Aerosp. Electron. Syst. vol. AES-15, pp. 613-619, 1979.

10. T. T. Fujita and F. Caracena, "An analysis of three weather-related aircraft accidents," Bull. Amer. Meteorol. Soc., vol. 58, pp. 1164-1181, 1977.

11. R. Bowles and R. Targ, "Windshear detection and avoidance: airborne systems perspective," 16th Congress of the International Council of the Aeronautical Sciences, Aug. 28-Sept. 2, 1988, Jerusalem.

12. B. M. Keel, "Adative clutter rejection filters for airborne Doppler weather radar applied to the detection of low altitude windshear," M.S. Thesis, Clemson University, 1989.

13. H. L. Van Trees, "Detection, estimation and modulation theory," Part I, John Wiley and Sons, 1968.

14. C. L. Britt, "An improved hazard index estimator," Tech. Memo. Research Triangle Institute, 1990.

15. R. S. Raven, "Requirements on master oscillators for coherent radar," Proc. IEEE, vol. 54, PP. 237-243, 1966.

16. S. Goldman, "Oscillator phase noise proves important to pulse Doppler radar systems," Microwave Systems News, pp. 88-100, Feb. 1984.

17. L. H. Janssen and G. A. Van der Spek, "The shape of Doppler spectra from precipitation," IEEE Trans. Aerosp. Electron. Syst., vol. AES-21, pp. 208-219, 1985.

18. S. Haykin et al., "Maximum entropy spectral analysis of radar clutter," Proc. IEEE, vol. 70, pp. 953-962, Sept. 1982.

19. C. Gibson and S. Haykin, "Radar performance studies of adaptive lattice clutter-suppression filters," IEE Proc., vol. 30, pp. 357-367, Aug. 1983.

20. J. Rutman, "Characterization of phase and frequency instabilities in precision frequency sources: fifteen years of progress," Proc. IEEE vol. 66, no. 9, Sept. 1978.

21. R. D. Weglein, "The coherence of a radar master oscillator," Proc. of the 40th Annu. Frequency Control Symp., pp. 379-384, 1986.

22. V. C. Vannicola and P. K. Varshney, "Modeling of frequency random walk instability and effects on spectral spreading," IEEE International Conf. on Communications, June 13-17, 1982.

23. V. C. Vannicola and P. K. Varshney, "Phase instability induced spectral spread in radar systems," Eascon 81, Washington D.C., Nov. 16-19, 1981

24. J. Rutman, "Relation between spectral purity and frequency stability," in Proc. 28th Ann. Frequency Control Symp., Atlantic City, NJ, May 29-31,1974.

25. V. Ya. Plekin, "Investigation of a tracking system for Doppler frequency measurements in the presence of frequency fluctuations of the tracking heterodyne," Telecomm. Radio Engineering, part 2, 21, no. 8, 1966.

26. D. Middleton, "The distribution of energy in randomly modulated waves," Phil. Mag. 1951.

27. J. A. Barnes et al., "Characterization of frequency stability," IEEE Trans. Instr. Meas. vol. IM-20, no. 2, pp. 105-120, May 1971.

28. R. J. Doviak and D. S. Zrnic, "Doppler radar and weather observations," Academic Press, 1984.

29. F. C. Benham, H. L. Groginsky, A. S. Soltes and G. Work, "Pulse pair estimation of Doppler spectrum parameters," Raytheon Co., Wayland, Mass., Final Rep., 1972.

30. D. S. Zrnic, "Spectral moment estimates from correlated pulse pairs," IEEE Trans. Aerosp. Electron. Syst., vol. AES-13, pp. 344-354, 1977.

31. E. Madelung, "Die mathematischen hilfsmittel des physikers," Berlin, J. Springer, 1936.

32. P. Linz, "An adaptive quadrature algorithm for Fourier cosine integrals," (unpublished) May 1972.

33. T. Berger and H. L. Groginsky, "Estimation of the spectral moments of pulse trains," presented at the Int. Conf. on Inform. Theory, Tel Aviv, Israel, 1973.

34. C. Karmel and N. Hilgendorf, "Local oscillator noise in microwave receivers," Conference on Military Microwaves, Brighton, England, 1986.

35. W. T. Davis, "The effects of clutter-rejection filtering on estimating weather spectrum parameters," M.S. Thesis, Clemson University, 1989.

36. L. Hennington, "Reducing the effects of Doppler radar ambiguities," 19th Conf. on Radar Meteorol., Am. Meteorol. Soc., PP. 216-218, 1980.

37. G. W. Snedecor, "Statistical methods," The Iowa State University Press, 1956.

38. R. G. Strauch,et al., "Improved Doppler velocity estimates by the poly-pulse pair method," 18th Conf. on Radar Meteorol., March 28-31, Atlanta, GA., 1978.

39. R. W. Ramirez, "The FFT fundamentals and concepts," Prentice-Hall, pp. 102-109, 1985.

40. J. J. Sitterle, "Estimation of spectral moments in small wavelength Doppler radar," M.S. Thesis, Clemson University, 1982.

41. L. J. Battan, "Radar observation of the atmosphere," Chicago, University of Chicago Press, 1973.

42. M. I. Skolnik, "Introduction to radar systems," McGraw-Hill, 1980.

43. H. A. Panofsky, "Atmospheric turbulence," Wiley-Interscience Publication, 1984.

44. A. V. Oppenheim, "Digital signal processing," Prentice-Hall, 1975.

45. B. M. Keel and E. G. Baxa, Jr., "Adaptive least square complex lattice clutter rejection filters applied to the radar detection of low altitude windshear," Proc. IEEE Int. Conf. Acoustics, Speech and Signal Processing, 1990.

46. S. L. Marple, Jr., "Digital spectral analysis with applications," New Jersey, Prentice-Hall, 1987.

47. S. L. Marple, Jr., "Spetral line analysis by Pisarenko and Prony methods," in Proc. IEEE Int. Conf. Acoustics, Speech and Signal Processing, 1979.

48. S. L. Marple, Jr., "Spectral line analysis via a fast Prony algorithm," in Proc. IEEE Int. Conf. Acoustics, Speech and Signal Processing, 1982.

49. J. Lee and E. G. Baxa, Jr., "Pulse pair spectral estimates in the presence of radar oscillator phase jitter," 21st Sutheastern Symposium on System Theory, Mar. 1989.

50. M. Michelson, W. W. Shrader and J. G. Wieler, "Terminal Doppler weather radar," Microwave Journal, Feb. 1990.

51. W. H. Heiss, D. L. McGrew and D. Sirmans, "NEXRAD: Next generation weather radar (WSR-88D)," Microwave Journal, Jan. 1990.

52. D. S. Zrnic, "Estimation of spectral moments for weather echoes," IEEE Trans. Geosci. Electrron. vol. GE-17, No. 4, Oct. 1979.

53. R. L. Mitchell, "Creating complex signal samples from a band-limited real signal," IEEE Trans. Aerosp. Electron. Syst., vol. AES-25, No. 3, pp. 425-427, 1985.

54. W. M. Waters and B. R. Jarrett, "Bandpass signal sampling and coherent detection," IEEE Trans. Aerosp. Electron. Syst., vol. AES-18, No. 4, pp. 731-736, 1982.

55. C. M. Rader, "A simple method for sampling in-phase and quadrature components," IEEE Trans. Aerosp. Electron. Syst., vol. AES-20, No. 6, pp. 821-824, 1984.